Synthesis and characterization of realistic molybdenum oxide based model systems in heterogeneous catalysis

vorgelegt von
Diplom Chemiker
Pablo Beato
aus Burgos (Spanien)

Fakultät II Mathematik- und Naturwissenschaften
der Technischen Universität Berlin
zur Erlangung des akademischen Grades

Doktor der Naturwissenschaften

-Dr. rer. nat.-

genehmigte Dissertation

Promotionsausschuss:

Vorsitzender:	Prof. Dr. rer. nat. R. Süssmuth
Gutachter:	Prof. Dr. rer. nat. M. Lerch
Gutachter:	Prof. Dr. rer. nat. R. Schlögl

Tag der mündlichen Prüfung: 05. Juli 2005

Berlin 2005
D83

Danksagung

Die vorliegende Arbeit entstand in der Zeit von September 2001 bis Dezember 2004 in der Anorganischen Abteilung des Fritz-Haber-Instituts, unter der Leitung von Herrn Professor Robert Schlögl. Der Erfolg dieser Arbeit wurde vor allem durch die Zusammenarbeit mit meinen Kollegen der Abteilung Anorganische Chemie möglich, bei denen ich mich ausdrücklich bedanken möchte.

Mein besonderer Dank gilt der gesamten Arbeitsgruppe Präparation, namentlich Almudena, Andreas, Annette, Bernd, Dirk, Gisela, Kilian, Olaf, Siegfried und Stefan, für die angenehme Arbeitsatmosphäre und die kontinuierliche Unterstützung.

Mein besonderer Dank gilt Jörg Wagatha von der Feinmechanik, für die vielen Stunden am Rechner, um den Reaktor so hinzubekommen, wie es eben sein musste.

Mein besonderer Dank gilt Ute Röper aus dem Sekretariat für die vielen Gespräche nach „Feierabend“, fern ab der Wissenschaft, die unbedingt notwendig waren.

Mein besonderer Dank gilt Gisela Weinberg von der Elektronenmikroskopie für die „schnellen Freitagsmessungen“.

Mein besonderer Dank gilt unseren fernöstlichen Gästen aus Malaysia, insbesondere Fazs, Ain, Dila und Sal, mit denen ich ein Büro geteilt habe und die mir „positive Energie“ übertragen haben.

Mein besonderer Dank gilt Herrn Prof. Schlögl für die interessante Aufgabenstellung, für die ständige Unterstützung und für den Glauben an meine Arbeit.

Die Arbeit ist meiner Familie, meiner Frau Elke und meinen Kindern Antonio und Mila gewidmet, denen gleichzeitig mein größter Dank gilt. Insbesondere für das große Verständnis das sie mir gegenüber aufgebracht haben, für die vielen Wochenenden und Abende an denen ich nicht bei Ihnen sein konnte.

Synthesis and characterization of realistic molybdenum oxide based model systems in heterogeneous catalysis

Dissertation vorgelegt von Pablo Beato

Abstract

Different synthetic approaches for the preparation of molybdenum oxide based thin film catalysts on silicon single crystals are investigated. The thin films should serve as realistic model systems which can be investigated as well by surface science as by bulk analytic methods. It is now generally accepted that the final properties of the catalyst will be largely affected by the synthetic procedure applied. The first chapters of the thesis are thus dealing with a detailed analysis of the different reaction steps during synthesis. As a basic requirement the films need to possess the chemical and structural complexity necessary for an active catalyst but at the same time stay thin and homogeneous enough to be suitable for the application of surface science analytics. An interesting novel synthesis route for the preparation of ultra thin films from aqueous transition metal solutions is described. The method comprises the dissolution of a spray dried mixture of polyoxometalates in a gelatin gel and subsequent spin-coating of the composite gel on a silicon substrate. After thermal treatment a smooth, homogeneous, 10 nm thick mixed oxide film is obtained. The film is tested in a self made quartz glass reactor for the selective oxidation of propene to acrolein and acrylic acid. The same reactor is then used for the investigation of the corresponding mixed polyoxometalate catalyst as a powder pellet. Additional, the reactor allows the investigation of the catalysts by *in situ* Raman spectroscopy. Thus catalytic and structure data is obtained from films and powders under the same reaction conditions. It shows that the film is able to convert propene to acrolein and acrylic acid fulfilling the activity requirement. Further a structural transformation of the catalysts during reaction at 673 K is observed which correlates to some extent with the catalytic activity. Under reaction conditions the transformation of the catalyst is reversible and only observable by in situ methods. The active structure seems to be composed of domains that can be derived easily from the Mo_5O_{14} structure. However, there must be additional factors governing the activity and selectivity, probably related to the dynamic surface structure. By applying surface science methods like *in situ* XPS to the presented model system it should be possible to get a realistic view of active complex metal oxide surfaces.

Synthese und Charakterisierung von realistischen auf Molybdänoxid basierenden Modelsystemen in der heterogenen Katalyse

Dissertation vorgelegt von Pablo Beato

Kurzzusammenfassung

In der vorliegenden Arbeit werden verschiedene Syntheseansätze zur Herstellung von auf Molybdänoxid basierenden Dünnschicht-Katalysatoren auf Silizium Einkristallen vorgestellt. Da bei der Katalysatorherstellung nicht nur das Endprodukt von Interesse ist sondern inzwischen allgemein akzeptiert ist, dass die Syntheseroute einen entscheidenden Einfluß auf die katalytische Aktivität ausübt, wird in den ersten Kapiteln der Arbeit detalliert der Syntheseweg untersucht. Die hergestellten dünnen Schichten sollen als realistische Modellsysteme dienen, um sowohl oberflächensensitive, als auch volumensensitive Charakterisierungsmethoden für deren Untersuchung anwenden zu können. Wichtig ist dabei, dass die hergestellten Filme die chemische und strukturelle Komplexität besitzen, die Voraussetzung für katalytische Aktivität ist. Andererseits, sollen die Filme dünn und homogen genug sein, um den Anforderungen der Oberflächenanalytik zu genügen. Es wird ein interessanter neuer Syntheseweg beschrieben, der es möglich macht, extrem dünne Schichten aus wässrigen Übergangsmetall-Lösungen herzustellen. Dabei wird ein bereits bekannter Mo-V-W-Mischoxidkatalysator als Pulver in einer Gelatinelösung gelöst und anschließend mittels eines sogenannten „Spin-coaters“ auf einen 10x10x0,7 mm großen Silizium Einkristall aufgebracht. Nach der thermischen Behandlung wird ein etwa 10 nm dünner homogener Film des Mischoxids auf dem Silizium erhalten. Der Film wird dann in einem eigens entwickelten Quarzglasreaktor hinsichtlich der selektiven Oxidation von Propen zu Acrolein und Acrylsäure untersucht. Der gleiche Reaktor wird benutzt, um den Filmkatalysator mit dem Pulverkatalysator zu vergleichen. Der Reaktor erlaubt eine *in situ* Charakterisierung des Katalysators mittels Raman Mikroskopie. Somit werden Katalysedaten und Strukturdaten von Film und Pulver und den gleichen Bedingungen erhalten. Es wird gezeigt, dass der hergestellte Film in der Lage ist aus Propen Acrolein und Acrylsäure zu machen und somit den Aktivitätsanforderungen genügt. Weiterhin wird gezeigt, dass sich der Katalysator bei 673 K strukturell umwandelt und diese Umwandlung mit einer partiell verbesserten Aktivität korreliert. Die strukturelle Umwandlung ist unter den gewählten Bedingungen reversibel und kann nur mit *in situ* Methoden beobachtet werden. Bei der aktiven Struktur handelt es sich vermutlich um Domänen, die sich von der Mo_5O_{14} Struktur ableiten lassen. Allerdings müssen noch weitere Faktoren einen Einfluß auf die Aktivität und Selektivität haben, die wahrscheinlich direkt mit der dynamischen Oberflächenstruktur zusammenhängen. Mit dem hergestellten Modell sollte es möglich, sein mittels oberflächensensitiver Methoden diese Faktoren zu bestimmen.

Contents

Chapter 4

General Introduction

Molybdenum oxides and molybdenum oxide based materials are of great technical interest. Besides the enormous importance in heterogeneous catalysis the ionic, electrochromic and photochromic properties of molybdenum oxides have received considerable attention because of potential applications in batteries, information displays and optical filters.

Closely related to the molybdenum oxides are the molybdenum polyoxometalates which have been found to be extremely versatile inorganic building blocks for the construction of functional materials. Polyoxomolybdates frequently serve as precursors for molybdenum oxide based catalysts, because they are cheap and can be dissolved in water.

In heterogeneous catalysis molybdenum oxides are technically used in a variety of important processes like selective oxidation of aldehydes and alkanes, oxidative dehydrogenation of alkenes, selective ammoxidation or metathesis reactions of alkenes. Catalytic selective oxidation reactions belong to the most important industrial processes and make one quarter of the gross profit of the world-wide catalytic performed reactions.

To understand the physico-chemical characteristics of a catalyst a detailed knowledge of the active structure is essential. However, heterogeneous catalysts represent a class of material of great complexity and the strategy of catalyst preparation in industry in part still remains to trial and error, leading to “mysterious” compositions and making a structure-activity analysis of the final catalyst almost impossible. Traces of many elements are present in most of the working molybdenum oxide catalysts in industry and in many cases it is still unclear whether these additional metals form active centres themselves, or act only as structural promoters for an active molybdenum oxide phase.

In industry most of the molybdenum oxide based catalysts are prepared using a water soluble ammonia molybdate precursor which is (co)precipitated or spray dried. After thermal treatment the resulting catalysts are complex polycrystalline materials with unpredictable participation of the different crystal phases and planes making them tremendously difficult to

analyse. For these “real” catalysts many of the surface science techniques cannot be used at all (AFM, STM, EELS, LEED) or not to their full potential (XPS, AES, SIMS). Therefore many experiments in heterogeneous catalysis research have been done on single crystals and single crystalline thin films which in contrast are easier to characterize in terms of surface geometric and electronic structure.

Both the industrial and the research materials represent the extremes of catalytic materials. To bridge this *materials gap* is therefore one of the major tasks for the preparative chemists in the field of heterogeneous catalysis.

The motivation for the thesis was the investigation of novel synthetic routes to prepare realistic catalytic model systems based on molybdenum oxides, which should preserve the chemical and structural complexity of real catalysts but at the same time stay accessible to both surface science and bulk analytic techniques and hence contribute to bridge the materials gap. A combination of metal-organic synthesis, sol-gel chemistry and inorganic aqueous solution chemistry was used to synthesize molybdenum oxide based powders and thin films. To get a detailed view of the interaction and structural development of the constituents of the catalyst *in situ* analytical methods during the preparation and the reaction of the catalyst were applied.

Chapter 1

Polyoxomolybdates via hydrolysis of molybdenum alkoxides - model catalysts for the selective oxidation of light alkenes

Parts of this chapter will be submitted for publication:
Pablo Beato, Thorsten Ressler, Olaf Timpe and Robert Schlögl "Polyoxomolybdates via hydrolysis of molybdenum alkoxides - model catalysts for the selective oxidation of light alkenes".

Introduction*

The enormous interest in polyoxometalates (POMs) in industrial as well as in academic research is reflected in the continuously increasing amount of publications over the past 50 years. A retrieval in the Chemical Abstracts resulted in 773 publications related to POMs in the year of 2003. The applications of POMs are primarily based on their redox properties, photochemical response, ionic charge, conductivity, magnetic properties and ionic weights.[1, 2] In heterogeneous catalysis POMs have received considerable attention as catalysts and suitable precursors for molybdenum oxide based selective oxidation catalysts.[3, 4] The POM is generally decomposed by a thermal treatment to generate an active oxide catalyst. The "real" structure of the active catalyst is governed by the structure of the precursor and the activation procedure applied. The overwhelming majority of the molybdenum containing heterogeneous catalysts described in the literature is prepared by (co)precipitation of an aqueous ammonium heptamolybdate $(NH_4)_6Mo_7O_{24}$ solution. Although this method has the advantage of easy handling, it is difficult to control the product purity due to the coexistence of different species at the time of precipitate formation.

**For the sake of clarity the tables referred to in this text are located at the end of the chapter.*

The inherent limitations of the aqueous precipitation chemistry with respect to phase purity and the generally small surface areas of the resulting catalysts have attracted chemists to seek alternative preparation methods, which allow better control of the structure, size, and morphology of the POM precursor. Hence, a number of attempts were made to develop sol-gel processes for the preparation of molybdenum oxide based catalysts.[5, 6]

The pioneer work of Jahr and Fuchs on the hydrolysis of amphoteric metal alkoxides in non-aqueous solutions revealed that in the presence of a base or an acid, polyanions with structures very similar to those obtained by aqueous precipitation chemistry were formed:[7]

$$\text{alkoxide} + \text{base/acid} + H_2O \rightarrow \text{POM} + \text{alcohol} \qquad (1)\,,$$

Though no spectroscopic analysis was performed, Fuchs and Jahr proposed the $Mo_7O_{24}^{6-}$ anion as the structural motif generated after hydrolysis of $[MoO_2(OEt)_2]_3*2NH_3$.[8] Errington *et al.* extended the work of Fuchs and Jahr and investigated in detail the hydrolysis of tungsten (oxo)alkoxides and mixtures with other (oxo)alkoxides (e.g. Ti, V, Zr, Nb, Ta) for the preparation of defined heteropolyoxoanions.[9] Those experiments revealed the great potential of the method with respect to phase purity and structural diversity. However, since the experiments by Fuchs and Jahr in 1967, molybdenum alkoxides have not been used in the synthesis of polyoxometalates and in contrast to the well studied aqueous solution chemistry of polyoxomolybdates, little is known about the hydrolysis behaviour of molybdenum alkoxides in organic solvents. The reason for the scarcely appearance of molybdenum alkoxides in the sol-gel literature is due to the lack of commercially available products and the rather difficult and low yield synthesis methods.

Nevertheless, the possibility of discovering novel catalytically relevant structures and the high purity of heteropolyoxoanions synthesized via the hydrolysis of mixed alkoxide systems, combined with the possibility to obtain large surface areas, inspired us to further investigate

the reactivity of molybdenum (oxo)alkoxides. In this chapter the preparation of highly crystalline POMs by addition of a polymerisation initiator (e.g. water or acetone) to an amine containing molybdenum oxoalkoxide solution at room temperature is described. The synthesized materials were used as precursors for the formation of active monometallic molybdenum oxide catalysts for the selective oxidation of propene to acrolein.

Experimental Section

Materials. All experimental procedures were carried out under inert gas atmosphere (Argon 5.0) or under vacuum conditions (< 10^{-3} mbar) using standard Schlenk techniques. The handling and storage of the products was realized in a Glovebox (H_2O < 1 ppm) operated with Argon 5.0. All solvents purchased were of highest purity, pre-dried (Merck SeccoSolv®) and stored over molecular sieves and under inert gas. Further drying was not performed. Before use the solvents were degassed. $MoOCl_4$ (puriss.) was purchased from Aldrich. Ammonium heptamolybdate (AHM) (p.a.) was purchased from Merck. Triethylamine was purchased from Merck distilled and stored over Molecular sieves under inert gas. $Mo[N(CH_3)_2]_4$ was synthesized as described in the literature.[10]

Synthesis of precursor solutions.

Preparation of alkoxide solutions via the amide route. $Mo[N(CH_3)_2]_4$ (5 mmol) was added in small portions to 50 ml of *t*-butanol under vigorous stirring at 298 K. The solution turned turquoise blue immediately and almost black after a minute. After ~10 minutes stirring the solution turns dark violet. This solution is designated as "*Mo*-solution". Dry synthetic air (200 ml) was bubbled slowly into the *Mo*-solution in 50 ml portions using a syringe. As the air was bubbled into the solution the colour turned into light yellow-brown. This solution is stable for several months and named "*Mox*-solution".

Preparation of alkoxide solution via metathesis reaction. A mixture of 19.10 ml *tert*-butanol and 27.90 ml of Et_3N was slowly added to a solution of 12.69 g $MoOCl_4$ in 250 ml of *n*-pentane. The reaction is exothermic and the formation of hydrogen chloride fumes was observed. After the addition of about 5 ml of the alcohol/amine mixture a dark blue to greenish precipitate formed. After completion of the reaction, the precipitate was filtered off and the *n*-pentane was removed from the remaining light yellow solution. After complete evaporation of the solvent a clear yellow liquid remained. Finally, the liquid was diluted with *tert*-butanol at a volume ratio of 1:10 which resulted in a solution that was stable for at least two months and is referred to as "*AmMox*-solution" in the following.

Hydrolysis experiments. (*Scheme 1*) The as-prepared alkoxide solution (*Mo*-solution) was hydrolysed with water (molar ratio alkoxide to water = 1:2) by adding portions of 5 µl via a micro syringe. A particulate sol was obtained which was filtered off and washed with acetone.

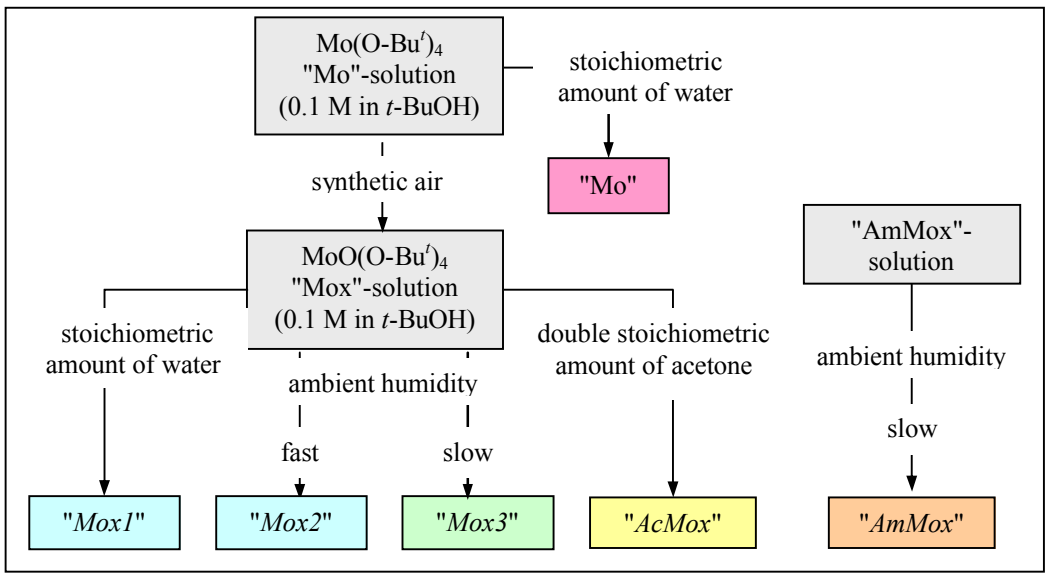

Scheme 1. Schematic overview of the preparation procedure and the subsequent sample assignment.

The resulting dark brown powder was named "*Mo*". Four different polymerisation methods were applied to the *Mox*-solution: (1) hydrolysis by addition of water (molar ratio oxoalkoxide to water = 1:2) via a micro syringe ("*Mox1*"), (2) hydrolysis via ambient

humidity by pouring the *Mox*-solution into a Petri dish ("*Mox2"*), (3) hydrolysis via ambient humidity over a period of 24 h by stirring the solution inside an open vessel ("*Mox3"*), (4) and non-hydrolytic condensation by addition of acetone (molar ratio oxoalkoxide to acetone = 1:4) via a micro syringe ("*AcMox"*).

The *AmMox*-solution was hydrolysed in the same way as for *Mox3*, via ambient humidity over a period of 24 h ("*AmMox"*). All samples precipitated as white to light ochre powders. *Mox3* and *AmMox* started to precipitate after 3 hours at ambient conditions both showing a light ochre colour. *Mox1* precipitated immediately after the addition of the first droplet as a white powder. *AcMox* started to precipitate precisely after the addition of half the amount of acetone. *Mox2* resulted in a few seconds in a white transparent gel, which transformed into a light ochre precipitate after about two minutes. The samples were filtered off, washed several times with acetone, and dried in a desiccator for at least 24 hours at room temperature.

Analytical equipment. Raman spectra were recorded with a DILOR LABRAM 1 spectrometer. A He-laser (632.8 nm, Melles Griot, 17 mW) was used for excitation. The laser light was focussed onto the sample using a 10x objective lens (Olympus) and the backscattered Raman lines were detected on a CCD camera (1024x298 pixel), which was Peltier-cooled to 243 K to reduce thermal noise. The entrance slit was set to 100 µm resulting in a spectral width of 1.5 cm^{-1}. A notch filter was applied to cut off the laser line and the Rayleigh scattering up to ~ 150 cm^{-1}. Each spectrum is the average of 3 accumulations with an integration time of 60 seconds. Optical filters were used to adjust the laser power at the sample to ~ 1 mW. Transmission IR-spectra were recorded with a Perkin-Elmer 2000 FTIR spectrometer. Samples were prepared as nujol mulls and placed between NaCl windows. 50 spectra were averaged each obtained at a resolution of 3 cm^{-1}. Powder X-ray diffraction (XRD) measurements were performed on a STOE STADI P diffractometer (Cu $K\alpha_1$; Ge 111 focused primary monochromator and a position sensitive detector) in a range of 5° - 90° 2θ with a step width of 0.01° 2θ and a measuring time of 10 sec/step. Structural refinement to the

experimental diffraction patterns was performed using the software TOPAS v 2.1 (Bruker AXS). SEM images were acquired using a HITACHI S 4000 FEG Microscope. The acceleration voltage was varied between 5 and 15 keV.

Temperature programmed reaction spectroscopy (TPRS) in 10 % propene and 10 % oxygen in helium was conducted in a tubular quartz reactor d_i = 5 mm. The sample (50 mg) was diluted with BN and SiC to improve heat transfer in the catalyst bed. The total gas flow was set to 100 ml/min. Prior to the TPRS runs the temperature was ramped at 5 K/min to 623 K in He and held for 1h before the feed was switched on. After one hour in the feed at 623 K the temperature was ramped to 773 K at 5 K/min and held for 1h. Product gases were analyzed by a Balzers quadrupole mass spectrometer: Water (m/e = 18), acrolein (m/e = 56), acrylic acid (m/e = 72), carbon dioxide (m/e = 44), C_2-carbonyl fragments (m/e = 43), isobutane (m/e = 43), pentane (m/e = 43), oxygen (m/e = 32), and propylene (m/e = 41). The signals are normalized to the He in the feed.

Results and Discussion

Raman and IR spectroscopy

The Raman spectra of polyoxomolybdates exhibit common characteristic intense Raman bands in the region between 920 cm^{-1} and 990 cm^{-1} indicative of stretching vibrations of terminal Mo-O bonds. The exact position of these bands is very sensitive to structural changes and has been used successfully in the literature for a reliable identification of polyoxomolybdate species both in solids and in aqueous solutions.[11-14]

Figure 1 depicts the Raman spectra of *Mox1* (*b*), *Mox2* (*c*), *Mox3* (*d*), *AcMox* (*e*), *AmMox* (*f*) and *Mo* (*g*); for comparison the spectrum of a commercial ammonium heptamolybdate (AHM) (*a*) is shown. The Raman spectrum of AHM is well known in the literature and the normal coordinate analysis agrees well with our experimental data (*Table 1*).[15, 16] The band for the symmetric stretching vibrations of the terminal Mo=O bonds in solid AHM are

reported to lie between 933 and 937 cm^{-1} and were found experimentally at 934 cm^{-1}. The same band is located at 935 cm^{-1} for *Mox1* and at 934 cm^{-1} for *Mox2*. Furthermore the Raman spectra of *Mox* (*1+2*) are almost identical to the spectral features of AHM in the range from 190 cm^{-1} to 1050 cm^{-1} (*Table 1*).

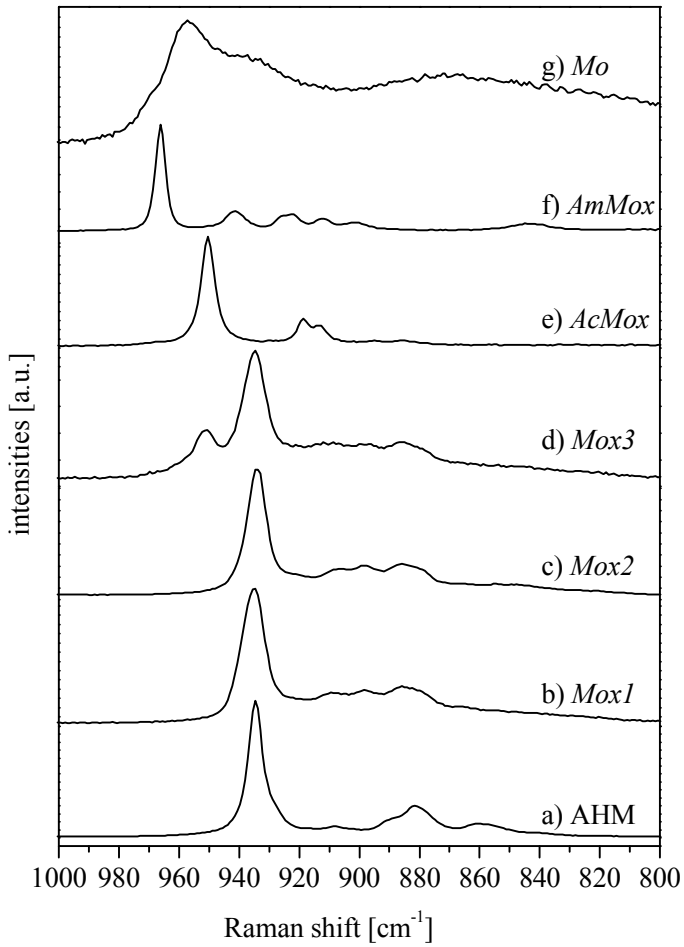

Figure 1. Raman spectra of the as prepared samples plus AHM for comparison: a) AHM, b) *Mox1*, c) *Mox2*, d) Mox3, e) *AcMox*, f) *AmMox*, g) *Mo* .

The similarity of the Raman spectra in *Figure 1* (*a-c*) indicates a close molecular structural relationship between the heptameric polyoxomolybdate units in AHM and the structural units in the *Mox (1+2)* samples. A comparison of the IR spectra (*Figure 3*) of AHM (*a*), *Mox1* (*b*) *and Mox2* (*c*) confirms the structural similarity of the three samples. The intense bands at 935 and 934 cm^{-1} in the Raman spectra are found as weak bands in the IR spectra located at 934 and 933 cm^{-1} for *Mox1* and *Mox2*. On the other hand, the IR spectra show broad and intense

absorption bands at around 880 and 900 cm^{-1}, whereas in the same region of the Raman spectra only various small bands are observed (*Table 1*). This inverse correlation between Raman and IR spectra holds for all the samples described here and is caused by the different intensities for asymmetric and symmetric stretching modes observed in IR and Raman. From the results of vibrational spectroscopy it is deduced that the structural units of the *Mox* (*1+2*) samples are indeed of the $(Mo_7O_{24})^{n-}$ type.

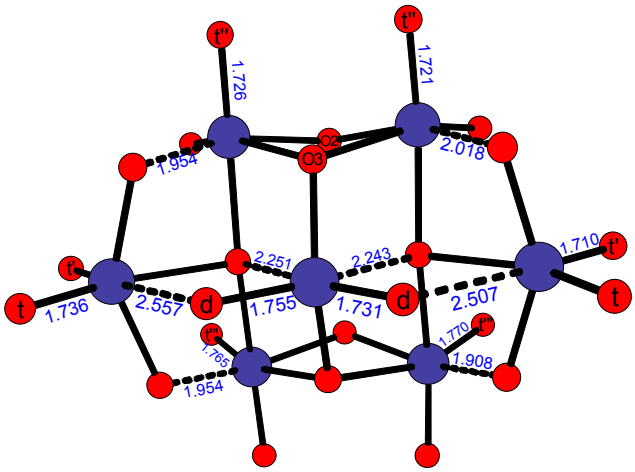

Figure 2. Structural model of the $(Mo_7O_{24})^{n-}$ structure, with bond length in Å. Atom designations are to compare with *Table 1*.[26]

Position and intensities of the Raman shifts of *Mox3* (*Figure 1d*) coincide with those in the spectra of the other *Mox* (*1+2*) samples except for an additional band at 950 cm^{-1}. The same applies to the band positions in the IR spectrum of *Mox3* (*Figure 3c*), which coincide well with the *Mox* (*1+2*) samples and AHM. However the extra band at 950 cm^{-1} in the Raman suggests the presence of a second polyoxoanion. Interestingly this band coincides in position with the strongest Raman band of *AcMox* (*Figure 1e*). As well the IR spectra of *Mox3* and *AcMox* correspond at 883, 899 and 925 cm^{-1}. An additional proof for the coexistence of the heptamolybdate and an additional structure in *Mox3* was obtained when the samples were investigated after three month again in order to detect possible ageing effects. Whereas the other samples showed only negligible differences in their Raman spectra, the aged *Mox3*

sample changed markedly (*Figure 4*). The band at 950 cm^{-1} increased and a doublet at 919 and 914 cm^{-1}, which is also observed for *AcMox*, gets visible.

As mentioned above the strongest band in the Raman spectrum of *AcMox* (*Figure 1e*) is located at 950 cm^{-1}. Further the above mentioned doublet at 919 and 914 cm^{-1} and two weak bands at 895 and 886 cm^{-1} are observed.

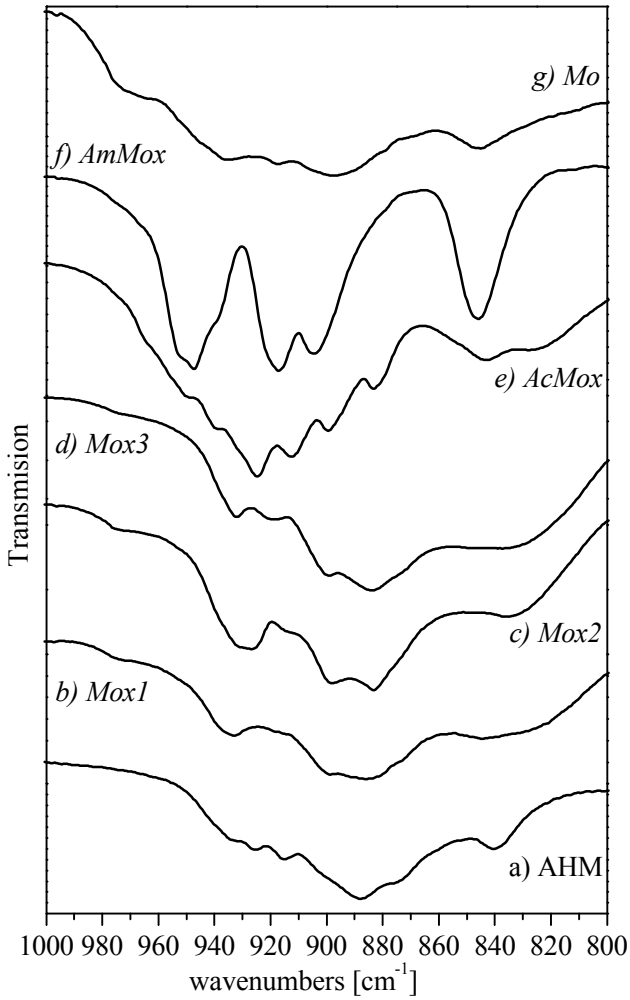

Figure 3. Infrared spectra of the prepared samples plus AHM for comparison (all Nujol mulls): a) AHM, b) *Mox1*, c) *Mox2*, d) *Mox3*, e) *AcMox*, f) *AmMox*, g) *Mo*.

The spectra of the so called trimolybdates, $M_2Mo_3O_{10}*H_2O$, where M = Na, K, Rb or NH_4, were found to fit best with the observed vibrational spectra of *AcMox*.[24] Relatively recently Kreusler *et al.* obtained for the first time single crystal X-ray and vibrational data of the trimolybdate $Rb_2Mo_3O_{10}*H_2O$. In well agreement with the experimental data (*Table 2*) they report Raman shifts at 949, 919, 909, 893 and 875 cm^{-1} and IR bands at 941, 924, 905 and 887

cm^{-1}.[25] A special feature of the Raman spectrum of the trimolybdates compared to other polyoxomolybdates is the presence of an intense band at around 600 cm^{-1} due to the relative large extent of threefold coordinated oxygen atoms (O-Mo_3) within the polymeric chain structure of the trimolybdate. This band is not only observed for *AcMox* (*Table 2*) but also present in the aged *Mox3* sample (*Figure 3*). From vibrational spectroscopy it is deduced that *Mox3* consists of a mixture of heptamolybdate and trimolybdate and that *AcMox* is exclusively composed of trimolybdate units.

The Raman spectrum of the *AmMox* sample (*Figure 1f*) exhibits the most intense band at 966 cm^{-1} and smaller bands at 941, 925, 923, 912, and 901 cm^{-1}. In the corresponding IR spectrum only a weak shoulder is detected at around 965 cm^{-1}. At 905 and 917 cm^{-1} an intense doublet is observed in the IR spectrum (*Figure 3d*) which is typical for molybdenum complexes and oligomers containing a *cis*-dioxo group.[19] The *cis*-dioxo group is a common feature in the structural chemistry of polyoxomolybdates and present in the spectra of all the samples presented in this work including AHM. Comparing the *AmMox* spectrum with the spectra described in the literature, a close similarity to the Raman and IR spectra described by Himeno *et al*. for γ-$[(CH_3)_3N(CH_2)_6N(CH_3)_3]_2Mo_8O_{26}*2H_2O$ was found (*Table 2*) and an attempt was made to correlate the XRD data of this compound with the literature data (*see below*).[14]

The vibrational spectra of the *Mo* sample (*Figure 1a, 3a*) differ significantly from all other samples. The Raman spectrum is characterized by a strong and broad band at 957 with a shoulder at 939 cm^{-1}, two maxima at around 872 and 820 cm^{-1}, and three bands at 281, 306 and 337 cm^{-1}. The band at 957 with the shoulder at 939 cm^{-1} is attributed to terminal Mo-O vibrations which typically occur in this region while broad Raman bands around 872 and 820 cm^{-1}, and a strong IR absorption band at around 721 cm^{-1} are characteristic for Mo-O-Mo bridging bonds.[17] The broadness of the observed Raman and IR bands indicates the absence of a well-crystallized polyoxomolybdate species.

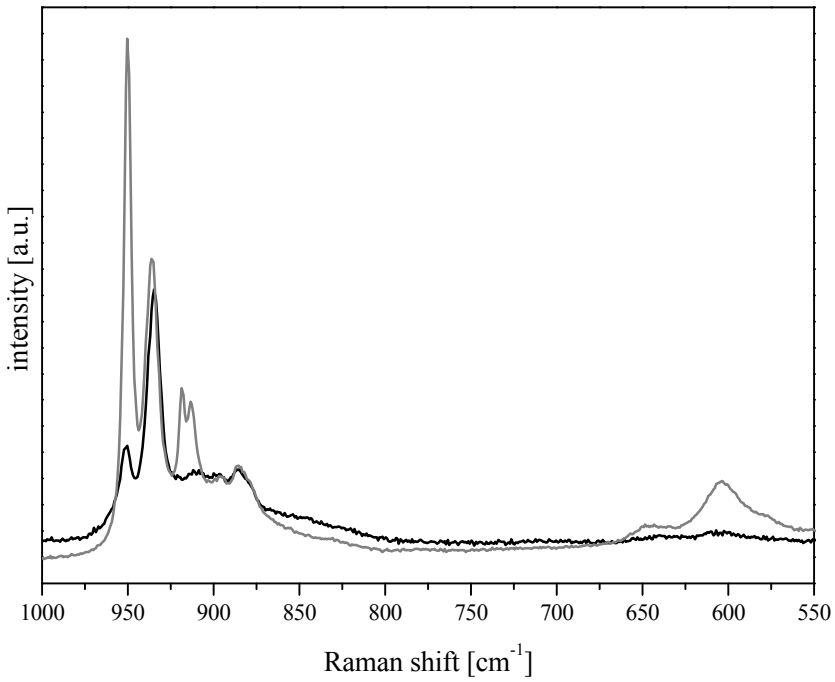

Figure 4. Raman spectra of *Mox3* as prepared (black line) and after three month (grey line).

X-ray diffraction

The XRD patterns of the synthesized samples and of AHM are shown in *Figure 5 (a-g)*. All patterns except for the *Mo* sample (*Figure 5g*) correspond to well-crystallized samples, in agreement with the vibrational spectra. The XRD patterns of *Mox1, Mox2* and *Mox3* are very similar to each other, but differ significantly from that of AHM. The patterns could be indexed with a triclinic unit cell, interestingly exhibiting lattice constants of similar dimension to those of *AmMox* (*Table 3*). However, indexing with a monoclinic unit cell comparable to that of *AmMox* was not possible. The good agreement between experimental data and a simulation obtained by the Pawley method indicates a single-phase material in the case of *Mox1+2* (*Figure 7e*).[27] It is likely that the presence of the bulky *tert*-butoxy groups in the crystal structure gives rise to a different arrangement of the heptameric units and consequently different unit cell parameters of *Mox1, Mox2* and *Mox3* compared to AHM. Although the XRD pattern of *AcMox* exhibits considerable differences compared to those of the *Mox-*

samples, it could also be indexed with a triclinic unit cell exhibiting slightly increased lattice constants (*Table 3*). *Mox1*, *Mox2*, *Mox3* and *AcMox* exhibit a decreasing crystallite size while the amount of strain for *Mox3* is relatively high and about three times that of *Mox2* (*Table 3*). It is interesting to note, that although the molecular conversion from *Mox3* to *AcMox,* that is to say the transformation from heptamolybdate to trimolybdate, is clearly recognized by Raman and IR spectroscopy, the crystal structure is not much affected by this transformation. This observation suggests that the transformation has occurred via condensation processes between neighbouring molecular entities and that the crystal structure is very much determined by the *tert*-butoxy groups and the amine functions representing a flexible *grid-box* for the polyoxometalate units.

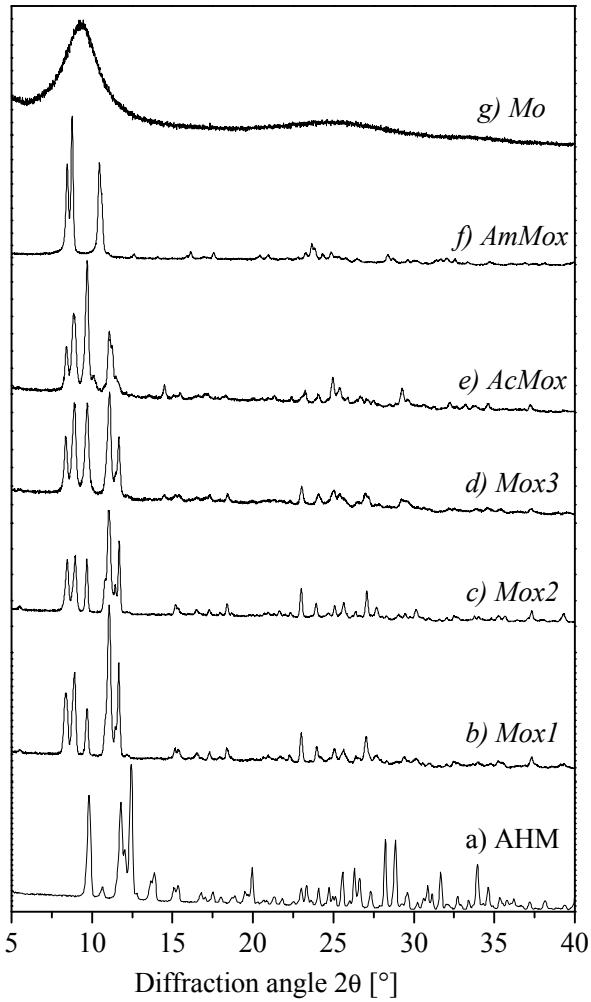

Figure 5. XRD pattern of the prepared samples plus AHM for comparison: a) AHM, b) *Mox1*, c) *Mox2*, d) Mox3, e) *AcMox*, f) *AmMox*, g) *Mo*.

The XRD pattern of *AmMox* could be indexed with a monoclinic unit cell (*Table 3*). A refinement of the corresponding hkl lines to the experimental pattern according to the Pawley method resulted in a very good agreement between simulation and experiment indicating a single-phase material (*Figure 7d*). The unit cell constants, crystallite size, and average strain are given in *Table 3*. From a comparison with polyoxomolybdates reported in the literature, it was found that the unit cell dimensions of *AmMox* agree well with the γ-octamolybdate described by Niven *et al.*.[20] A simulated XRD pattern of the octamolybdate is depicted in *Figure 7a*, while a schematic representation of a single octamolybdate unit and the arrangement of these units in the crystal structure are presented in *Figure 6*.

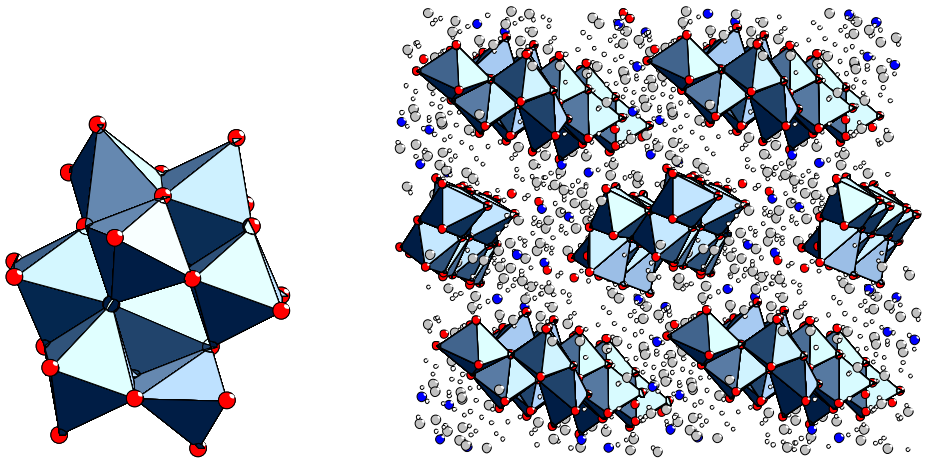

Figure 6. Schematic representation of a single γ-octamolybdate unit as described by Niven et al.[21] (left part) and the arrangement of these units in the crystal structure (right part).

Adjusting the unit cell parameters of the octamolybdate to those determined for *AmMox* (*Table 3*) resulted in the modified pattern shown in *Figure 7b*, which is in good qualitative agreement with the pattern of *AmMox*.

Hence, we propose that the arrangement of polyoxomolybdate units in the crystallographic structure of *AmMox* is analogous to that of the γ-octamolybdate with a different alkylamine and amount of solvent in the unit cell.

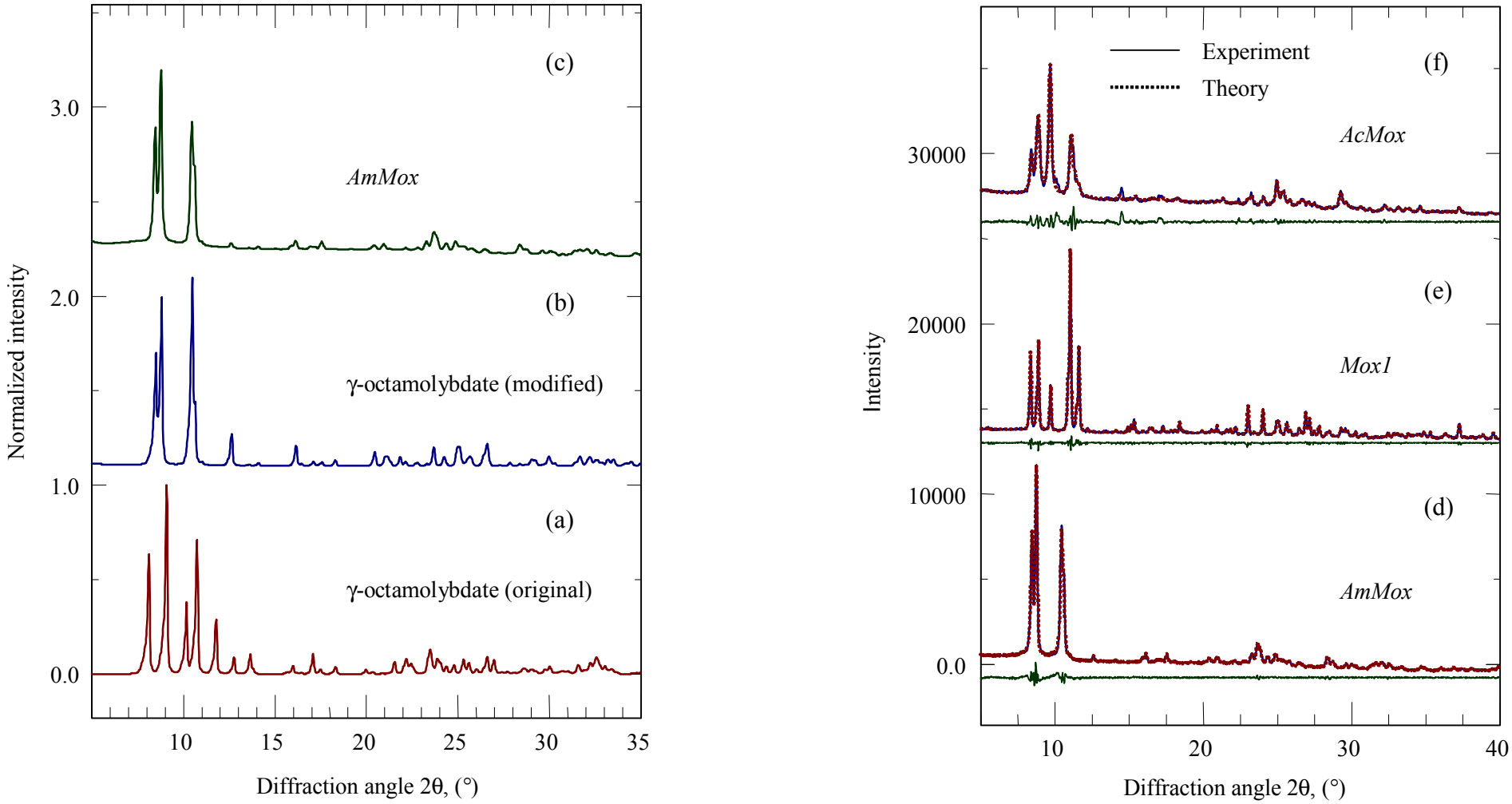

Figure 7. Model γ-octamolybdate (a), calculated γ-octamolybdate (b), experimental *AmMox* (c). *hkl (Pawley) fit to AmMox* (d), *Mox1* (e), *AcMox* (f).

Scanning electron microscopy (SEM)

The SEM images reveal the effects of the different rates of hydrolysis and condensation on the morphology of the samples. For *Mox1* (*Figure 8 a*) the dropwise addition of water leads to a quick hydrolysis and the formation of a mixture of small, round-edged crystals of ~1 µm size and bigger well-formed crystals (~5 µm). By spreading the *Mox*-solution onto the Petri dish a fast diffusion of water from air humidity through the solution results in a platelet crystal shape of *Mox2* (*Figure 8 b*), indicating a preferential growth of the heptamolybdate ions. For *Mox3* (*Figure 8 c*) the diffusion process is slowed down further by the reduced exposed liquid surface and two types of crystals were observed: small condensed platelets and fine needles. The effect of the addition of acetone to an alcoholic alkoxide solution is supposed to generate H_2O *in situ* via an aldol-condensation-elimination reaction.[22]

The result of this stepwise release of water is the formation of fine nano-shaped needles observed for *AcMox* (*Figure 8 d*). The needle shape is typical for trimolybdates as these are composed of polymeric chains of MoO_6 octahedra. Hence the SEM images support the results from vibrational spectroscopy indicating that *Mox3* is composed of a mixture of heptamolybdate and trimolybdate units, whereas *AcMox* consists of a regular arrangement of trimolybdate units only. In contrast to these distinct morphologies, *AmMox* (*Figure 8 e*) exhibits bigger condensed crystals exposing edges and small terraces. For Mo (*Figure 8 f*) no characteristic crystal morphology can be recognized.

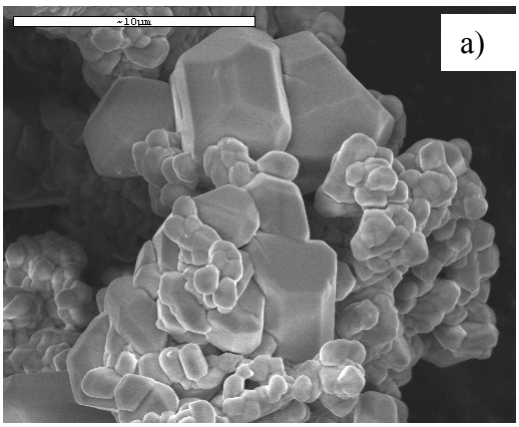

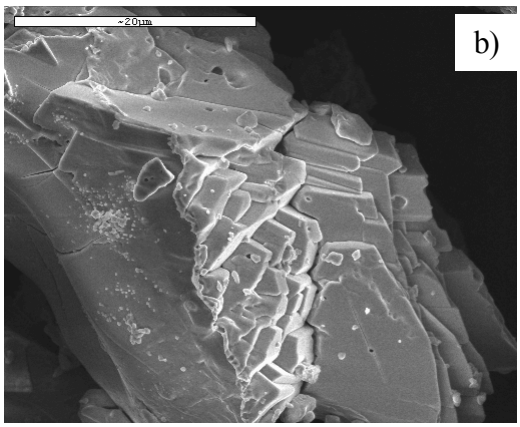

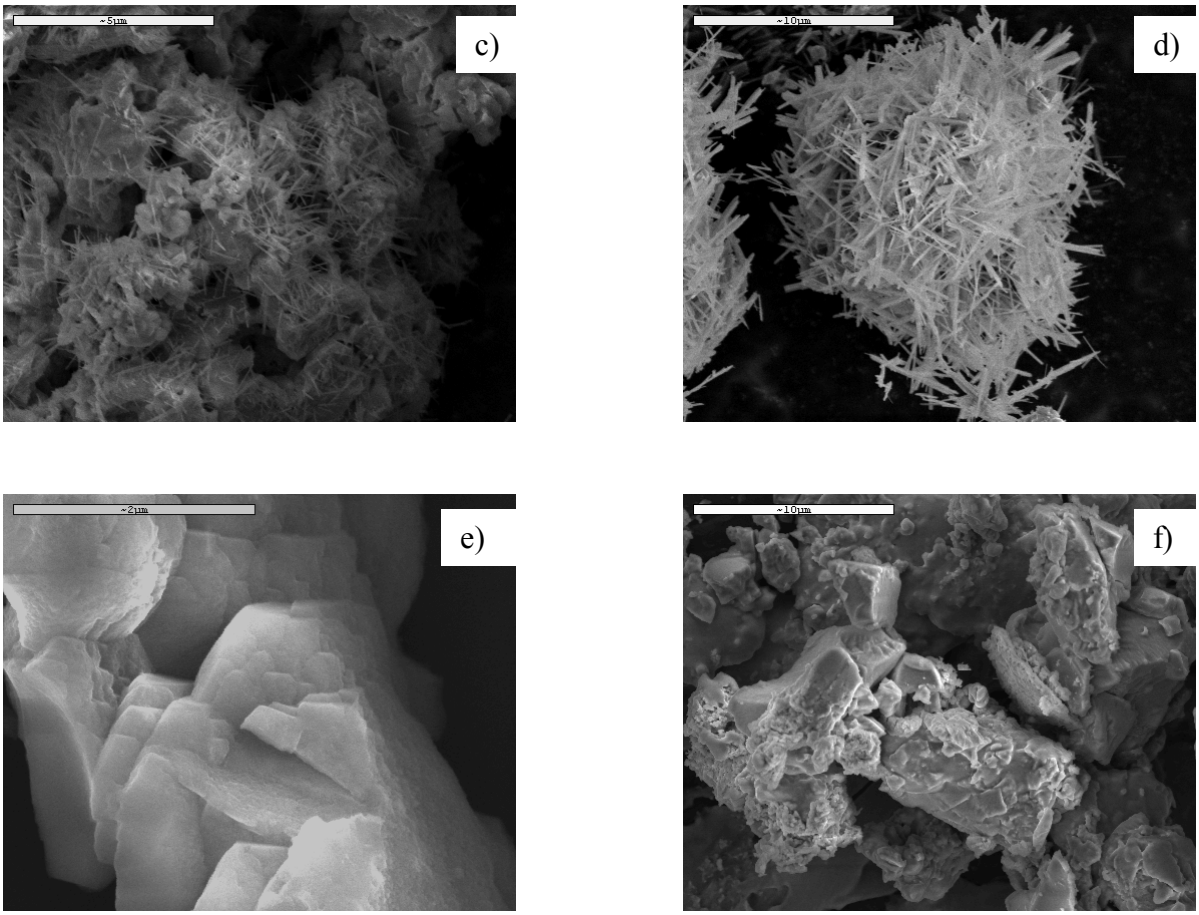

Figure 8. SEM images of the as prepared POM samples: a) *Mox 1*, b) *Mox 2*, c) *Mox3*, d) *AcMox,* e*)AmMox,* f*) Mo*.

Thermal decomposition and temperature programmed reaction spectroscopy (TPRS)

A detailed *in situ* XRD and X-ray absorption (XAS) study on the decomposition of AHM under different gas atmospheres and gas flows, by Wienold *et al.*, revealed that the transformation to molybdenum oxides takes place in four distinct steps.[23] The crystallinity of the intermediates was strongly affected by the partial pressure of the gas phase decomposition products. Surprisingly the structure of the solid intermediate products of the first three decomposition steps showed to be independent on the gas atmosphere and the heating ramp. In this three steps decomposition and evaporation of the ammonia and water ligands takes place inducing a polycondensation reaction of the cluster structure of AHM ions first to a XRD amorphous phase, then to poorly crystalline octamolybdate and finally to three-

dimensional hexagonal MoO_3. Restructuring of the hexagonal MoO_3 depends on the gas atmosphere during the last (fourth) step which starts at around 635 K for all experiments. Orthorhombic α-MoO_3 is the sole product when synthetic air is used while a mixture of Mo_4O_{11} and MoO_2 was detected under inert gas atmosphere.

A TG/DSC/MS analysis of the prepared samples in He using the same temperature ramp and flow conditions as in the following TPRS experiments and as used by Wienold *et al.* was performed (*Figure 9*). For *Mox2* (*Figure 9 a*) the decomposition behaviour agrees well with the decomposition observed for AHM by Wienold *et al.* (*Figure 9*), showing four distinct decomposition steps. Arnaud-Neu *et al.* have also prepared the heptamolybdate anion with dimethylamine as counterion, applying a different preparation route starting from MoO_3.[24] By sequential decomposition experiments in air they established the following decomposition steps (*eq. 2*):

$$\underset{\text{(rt-383 K)}}{\text{heptamolybdate}} \xrightarrow{397\ \text{K}} \underset{\text{(397-411 K)}}{\text{trimolybdate}} \xrightarrow{423\ \text{K}} \underset{\text{(423-523 K)}}{\text{octamolybdate}} \xrightarrow{653\ \text{K}} \alpha\text{-}MoO_3 \qquad (2)$$

Compared to the results of Wienold *et al.* the x-ray amorphous material was identified as a trimolybdate and the *hex.*-MoO_3 was not detected. However, the temperature intervals observed by Arnaud-Neu *et al.*, Wienold *et al.* and the experimental results in *Figure 9a* agree almost exactly. For *AmMox* the decomposition steps are not as pronounced as for the *Mox* sample (*Figure 9b*). The *AmMox* sample looses over a wide temperature range rather continuously about 25 % of its mass in form of ammonia, water and CO_2 and shows a distinct step at around 660 K.

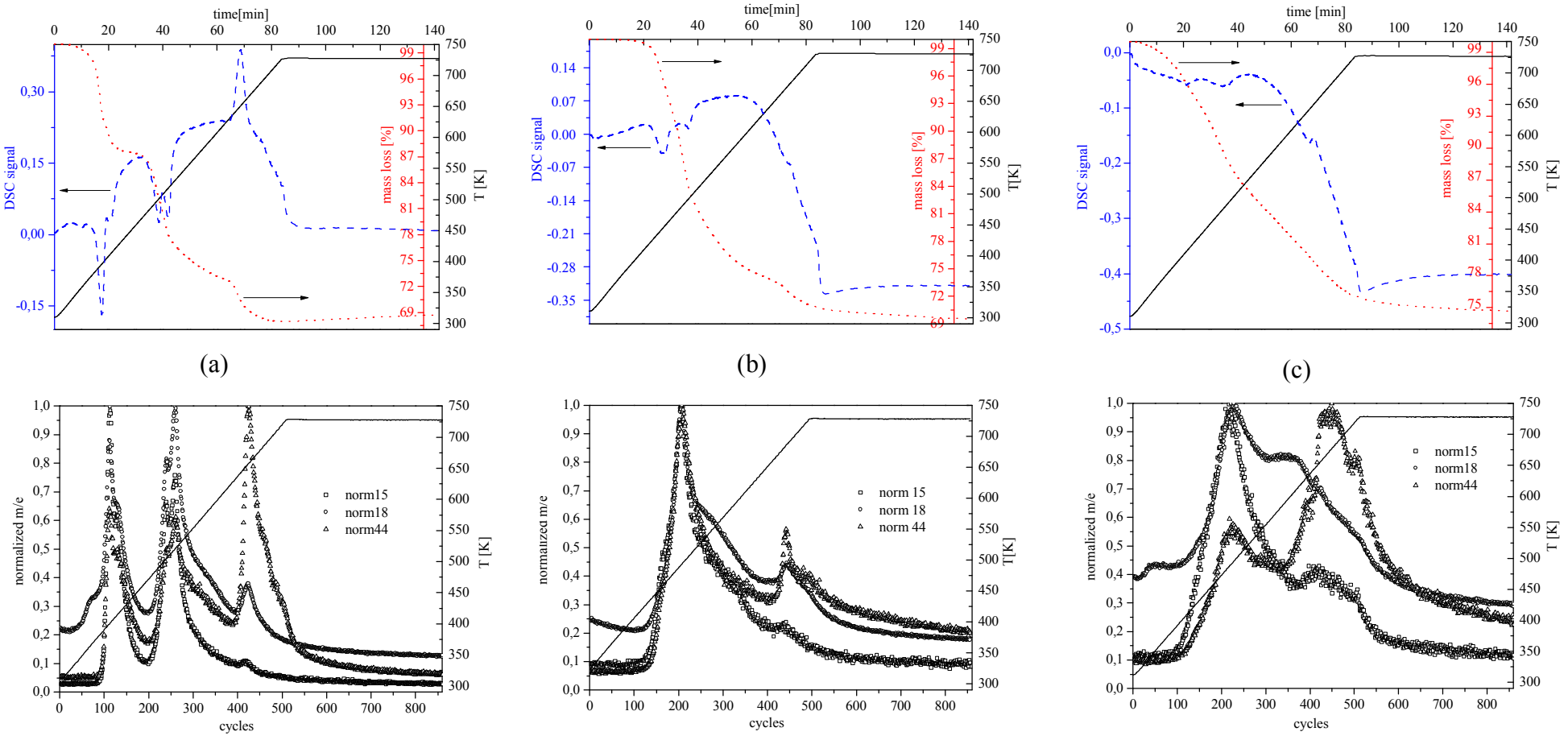

Figure 9. TG/DSC and corresponding MS data for *Mox2* (a), *AmMox* (b) and *Mo* (c). All samples were heated up to 725 K in 100% He with 5 K/min. The mass signals were individually normalized.

This is in line with the reaction sequence shown in *eq. 2* and the results of Wienold *et al.*, as *AmMox* is already an octamolybdate the polycondensation steps should not be observed for the *Mox* sample.

The *Mo* sample, being mostly amorphous, of course does not show any distinct decomposition step in the TG signal. However, at 650 K an exothermic DSC peak is observed indicating the formation of a crystalline molybdenum oxide. At the same temperature a huge amount of CO_2 is released. A direct comparison between the TG/DSC and the TPRS experiments is made in *Figure 10* exemplarily for the water release of the two samples *AmMox* and *Mox2*. Both experiments do nicely agree and can be used for direct comparison.

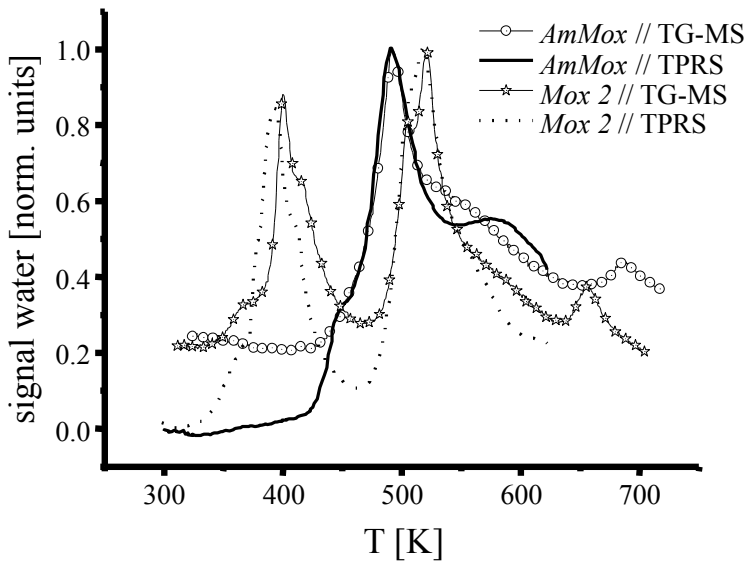

Figure 10. Comparison between MS-water signal (m/e = 18) obtained from TG-MS and TPRS experiments.

From 623 to 675 K a final exothermic decomposition step occurred for all samples related to a final mass loss of ~5% and coinciding with a mass signal m/e = 44 (CO_2). The occurrence of CO_2 during the last decomposition step indicates the oxidation of organic matter deriving from the former ligands. The oxidant in this case is the molybdenum for leak of ambient oxygen under inert gas conditions generating Mo(IV) sites. The TPRS experiments were thus adapted to investigate the last decomposition step under feed conditions.

Temperature programmed reaction spectroscopy is a suitable tool to detect the appearance of transient, catalytically active states.[21] In the following the data obtained for *Mox2*, *AmMox* and *Mo* will be discussed.

The results are divided into three experimental sections and condensed in *Figure 11*. In the ***First section*** samples were heated in inert atmosphere (RT to 623 K by 5 K/min) and the no additional features were observed with respect to the TG/DSC experiments (see *Figure 9*).

The source of all components detected therefore is the decomposition of the samples or the release of adsorbed species originating from solvents (*tert*-butoxy ligand, acetone and pentane). The detected TPRS traces are indicative of the ongoing structural rearrangement of the samples and in line with the TG/DSC findings. The following general conclusions were drawn:

- The samples release water, CO_2 and organic fragments (m/e = 43, m/e = 56 and m/e = 72) by several peaks.
- The reorganization of the samples is not a single step process.
- The sample being the less crystalline from the beginning (*Mo*) shows the less pronounced TPRS-peaks during decomposition. This can be understood in terms of less restructuring possibilities due to the amorphous parts of the sample which may further be enclosed by ligands and reaction products.

Second section: The temperature is first held at 623 K for one hour in He (not shown). After the 2 hours the feed (Σ100 ml/min = $10C_3H_6$ + $10O_2$ + 80He) was switched on and the temperature was still held at 623 K for one more hour (*Figure 11 a-c*). The response in the QMS-signals after the feed is introduced to the samples offers information on the effects the changed conditions may evoke in the sample material. Such response is likely to appear as a discrete peak when due to decomposition; whereas ongoing catalytically induced conversion of feed components in contact to the samples will appear as plateau like intensities.

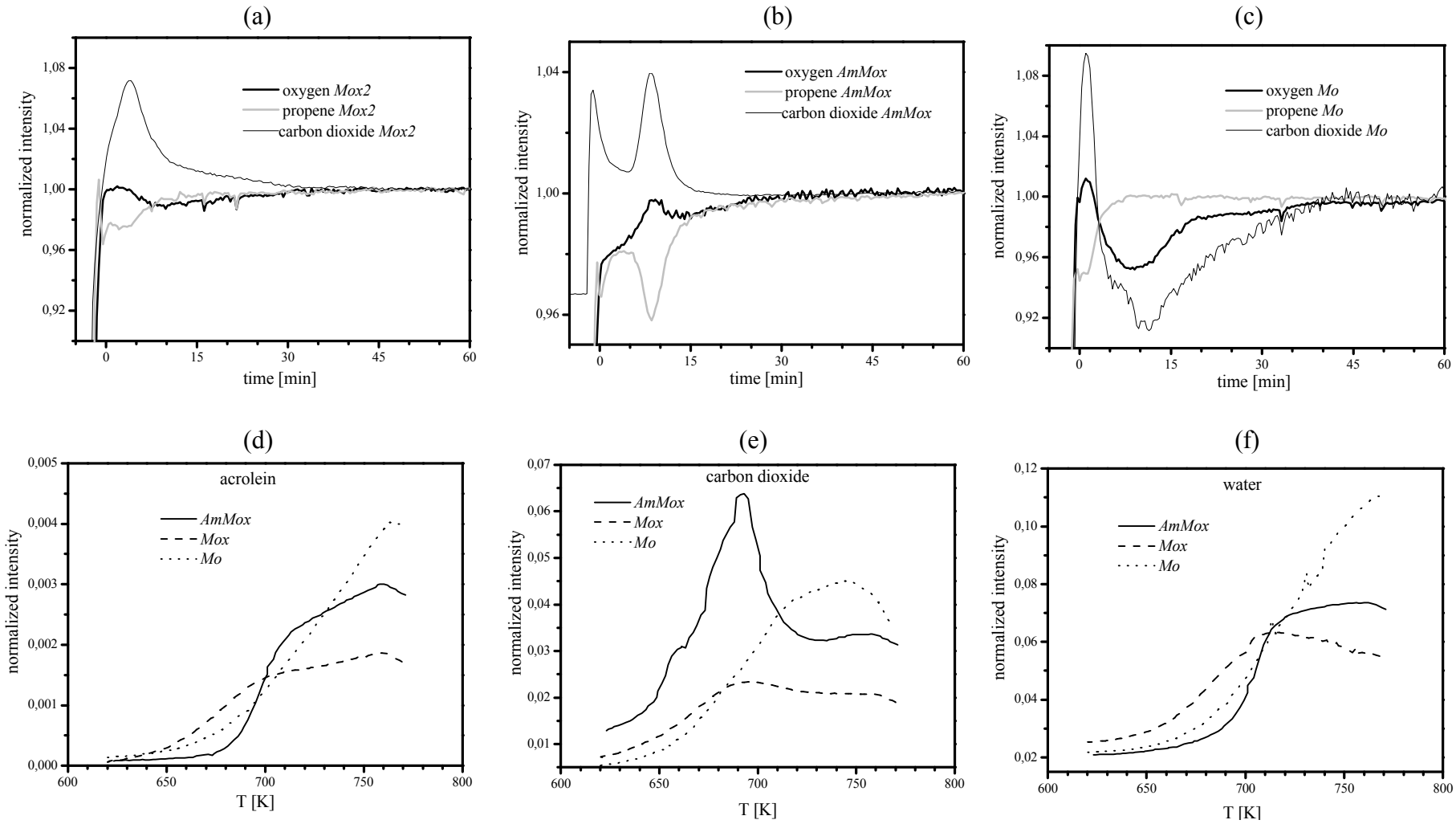

Figure 11. TPRS plots for second section when feed is switched on at constant temperature of 623 K (a-c). Plots for the third section where the temperature is increased with 5 K/min to 773 K (d = evolution of acrolein; e = evolution of carbon dioxide; f = evolution of water).

In response to the changed atmosphere peak maxima are detected for carbon dioxide and m/e = 43 for all samples; the course of both signals proceeds identical and only the carbon dioxide signal is displayed in *Figure 11 a-c*. The initial maxima in carbon dioxide and m/e = 43 correspond to a minimum in the propene signal. An analogues coincidence is missing in the signal for oxygen, which shows in the opposite, even a maximum corresponding to the maximum in carbon dioxide. This behaviour is indicative of a stoichiometric effect on the sample; most probably the sample is reduced by propene. The carbon dioxide maxima detected originates from feed propene in reaction with lattice oxygen. This reaction will deplete the feed concentration and evokes the coinciding maximum in oxygen.

AmMox behaves quite different from the other two samples and shows a doublet for CO_2 and m/e = 43 instead of a single peak. A sequential process should be the cause of the doublet observed. Probably the condensation process induces the formation of an intermediate, missing for the other samples. The TPRS traces for all three samples of the set give no hint for any catalytic action on the supplied feed components, all signals having rather stoichiometric background.

Third section (*Figure 11 d-f*): Heating in constant feed flow from 623 K to 773 K at 5 K/min. This part of the experiment is a TPRS run in a proper sense. A monotonic increase in signal intensity with temperature is probably linked to the temperature effect on the reaction pathways. In contrast, maxima or breaks are indicative of mechanistic changes, most probably due to an affected catalyst. Evaluated by this criterion, *AmMox* is again different from *Mox* and *Mo*. For *AmMox*, a pronounced maximum in the CO_2 production centred at 690 K is observed. *Mox* shows a very smooth maximum at around the same temperature. This suggests similar processes, in principle of the same nature: Both samples are transformed at the same temperature (and gas phase) - but *Mox* to a lessen extent. *Mo* shows the most monotonic course, indicative of a less affected/more stable catalyst. All three samples have a last

exothermic decomposition step beyond 623 K in common and get rid of remaining organic stuff originating from the ligands introduced during preparation. This last decomposition is related to the formation of the final (non molecular) Mo-oxide crystalline phases: α-MoO_3 under conditions of the TPRS runs, MoO_2 (mainly) in inert atmosphere as confirmed by XRD. The observed maxima in CO_2 below 700 K of the runs for *AmMox* and *Mo* may reflect the combustion of remaining organic matter from the samples. However, as the educt signal intensity for the fuel starts to be lowered from the same temperature point (*not shown*), one has to conclude a simultaneous onset of a catalytic promoted feed conversion. The maximum of CO_2 is most pronounced for *AmMox* and nearby missing for *Mo*. This intensity is likely to reflect the degree of order the samples have prior this event. The ongoing formation of Mo-oxide phases starts at about 630 K as established by means of TG/DSC and obviously is combined with the appearance of active sites. The onset for catalytic propylene conversion to the main product CO_2 is the same for all samples (~ 630 K), whereas the formation of acrolein starts for *Mox2* at 620 K and for *AmMox* at 680 K. Obviously, the onset temperature of active site formation is dominated by the formation of crystalline Mo-oxides and rather independent of the precursor structure, while the formation of selective sites is related to the structural "background" of the system .

The relaxation of the activity observed for the ongoing experiment at higher temperature (beyond 750 K) manifested in the main product signals (water, carbon dioxide) can be explained by the existence of transient oxide-phases existing as intermediates of higher catalytic potential than the final and thermodynamically favoured oxides (MoO_3, MoO_2). The suspected transient species are, in parallel, also very potent to catalyse the combustion of remaining ligand stuff. Following this interpretation, the formation of Mo-oxides is casual for the final ligand destruction and not the other way round.

AmMox. The onset of the rise in the products of partial oxidation at 680 K coincides with the diminution in carbon dioxide production (e.g. the rate of total combustion). Obviously, there

are competing reaction pathways. On an atomistic scale the changing abundance of concurring products might be understood as the existence of different (catalytic) centres which are not affected in the same way by the increasing temperature. *AmMox* is the only sample to produce detectable amounts of acrylic acid (not shown).

Mox. The evolution of all product signals with increasing temperature behaves similar, showing the smooth maximum around 690 K. Therefore we conclude that predominantly the total number of active centres is altered during TPRS, but the relative abundance of qualitatively different centres remains unchanged.

Mo. All signals are in accordance with simple kinetic relations and no affect on the catalyst is necessarily assumed.

Apparent activation energy. For the third section, the apparent activation energies (E_a) are calculated applying the simple Arrhenius law (*Figure 12, Table 4*).

The calculation is based on the linear line sections of the measured intensities for acrolein and water. For *AmMox* three linear sections, corresponding to three apparent activation energies were detected, whereas for *Mox2* and *Mo* only two linear sections were observed. *Table 4* summarizes the calculated activation energies in the corresponding temperature intervals for the three samples. It can be seen that the intervals for the two products agree well for all three samples. The following conclusions can be drawn from the obtained results:

- The small values for the high temperature interval indicate an increasing diffusion control with increasing temperature.
- The large values, especially for water for *AmMox* at lower temperature suggest a superimposed activation of the sample, *e.g.* the quantitative and qualitative generation of new centres. The different sequences observed for water for the *AmMox* sample can then be interpreted as activation → reaction → transport limitation with increasing temperature.

- In contrast at low temperatures the temperature dependence of acrolein for *AmMox* differs considerably from the observed dependence for water. An explanation for this behaviour at low temperatures could be the preferred generation of centres, which favour concurring reaction channels.
- The negative activation energy for water observed for *Mox2* at high temperatures indicates conversely to the scenario at lower temperatures a deactivation or rather destruction of active centres.

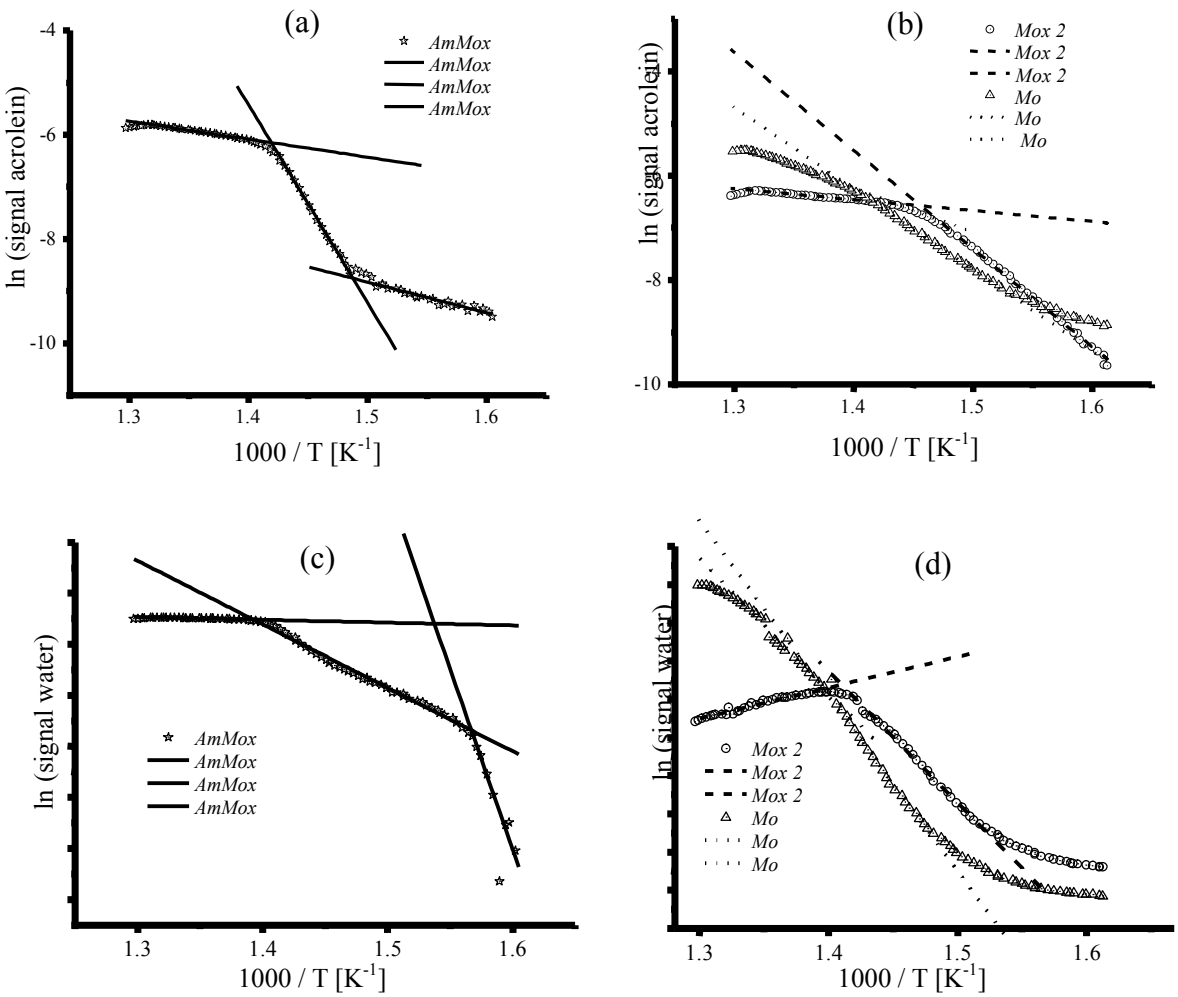

Figure 12. Arrhenius plots based on the signal for acrolein (a, b) and water (c, d) during Ramp from 623 K to 773 K at 5 K/min (*third section*).

After the TPRS experiment all samples were decomposed α-MoO_3 (proofed by XRD and Raman).

Conclusions

A versatile route to the formation of crystalline POMs via condensation of molybdenum oxoalkoxides is described. It has been shown that the added amine (dimethyl- vs. triethylamine) and hence the type of added counterion and the rate of hydrolysis strongly influence the morphology and the structure of the resulting POM. Further the nature of the alkoxy ligand and the polarity of the organic solvent, though not investigated in this study, are likely to be useful parameters for the synthesis of novel POM structures with new or enhanced properties. The introduction of synthetic air into the alkoxide solutions did not only oxidize the species in solution but also led to the structural arrangement of the polyoxoanions, necessary to obtain highly crystalline solids. This observation suggests that the presence of hydrogen bonds of the type -N-H---O=Mo- may be a structure-directing interaction. It is remarkable that the formation of the POMs occurs at room temperature and within seconds to minutes, in a self-assembly like process. By tuning the above mentioned parameters it should be possible to investigate spectroscopically the structure formation process and shed light on such self-assembled arrangements (*see chapter 2*).

TPRS experiments show the dependence of the catalytic behaviour on the various precursor structures. Evidently, the different microstructures of the materials prepared gave rise to very different catalytic properties. Although the *Mox*-samples transform during the heat treatment from heptamolybdate into octamolybdate units the catalytic behaviour of *AmMox*, which is octamolybdate from the beginning, and the *Mox*-samples is different from each other. This suggests that not only the nature of the polymolybdate is influencing the real structure of the

catalyst. The possibility to synthesize novel polyoxomolybdate model structures may help to understand the structural characteristics required for the preparation of molybdenum oxide based partial oxidation catalysts. The lack of a high yield synthesis method still prevents the use of molybdenum alkoxides as precursor for industrial relevant quantities of material. However, the alternative to synthesize high purity advanced materials *e.g.* thin films or nano-materials due to the possibility of an ordered (self-assembled) arrangement of POMs make molybdenum (oxo)alkoxides interesting precursors for the preparation of materials with novel optical, magnetic and/or electronic properties.

Table 1. Comparison between observed frequencies for *Mox* (*1+2*) samples and literature data for the heptamolybdate anion.

Description[21] (***see fig. 3***)	**AHM Raman** *this work*	**AHM IR** *this work*	**AHM Raman** Lyhamn[21]	**AHM IR** Lyhamn[21]	**AHM Raman** Hunnius[16]	***Mox1* Raman** *this work*	***Mox1* IR** *this work*	***Mox2* Raman** *this work*	***Mox2* IR** *this work*
Mo-O_t stretch; t', t'''	934 (10)	933 (sh)	965 955 950 938	940	934	935 (10)	971 (sh) 933 (m)	934 (10)	973 (sh) 932 (s)
Mo-O stretch; d		925 (w) 915 (w)	918	924	914		918 (sh)	920 (2)	919 (sh)
Mo-O_t stretch; t, t''	909 (1) 892 (1)	899 (sh) 888 (s)	895 880	900 882	907 902	909 (2) 898 (2)	898 (s) 886 (s)	906 (4) 898 (4)	899 (s) 884 (s)
Mo-O stretch + combinations with bendings	889 (1) 882 (2) 860 (1) 841 (0) 721 (0)	876 (sh) 851 (w) 840 (w) 792 (br)	865 852 745	872 841 770 720	889 880 861 839 715	885 (3) 879 (2) 866 (1) 715 (0)	874 (sh) 844 (br) 770 (w) 720 (s)	886 (4) 880 (3) 866 (2) 853 (2) 752 (1) 711 (1)	875 (sh) 850 (w) 837 (br) 719 (w) 703 (w)
Mo-O_3-Mo bendings	630 (0)	670 (br) 635 (br)	645	635	631	636 (0)	655 (br) 634 (br)	637 (3)	658 (br) 634 (br)
O_2-Mo-O_2 bendings	570 (0) 549 (0)	577 (s) 550 (sh)	550	555	574 547	573 (0) 550 (0)	585 (w) 565 (m) 544 (sh)	570 (1) 551 (2)	588 (w) 567 (s) 548 (sh)
torsion	480 (0) 460 (0) 444 (0)	480 (br) 462 (sh)	490 450	490 450	484 462 444	486 (0) 462 (0) 441 (0)	479 (sh) 458 (br)	483 (2) 462 (2) 443 (2)	482 (w) 462 (w)
O_t-Mo-O_2 bendings	411 (0) 393 (0) 371 (1) 364 (1)		405 395 378 370 360		411 362	411 (0) 401 (0) 368 (1) 359 (1)		409 (3) 402 (3) 371 (3) 361 (3)	
Bendings, "bridge stretchings" and torsions	337 (0) 308 (0) 262 (1) 244 (1) 224 (2)		340 304 260 222		335 308 249 221	338 (1) 302 (0) 251 (1) 218 (2)		340 (2) 304 (3) 250 (3) 219 (4)	

w = weak; m = medium;; v =strong; sh = shoulder; br = broad; numbers in brackets define the relative intensities of Raman Bands on a scale from 0 to 10.

Table 2. Experimental Raman and IR data for *Mox3*, *AcMox* and *AmMox* samples. Literature data is given for comparison.

Mox3 **IR** *this work*	***Mox3*** **Raman** *this work*	***AcMox*** **IR** *this work*	***AcMox*** **Raman** *this work*	**Trimoly IR** *Kreusler*[25]	**Trimoly Raman** *Kreusler*[25]	***AmMox*** **IR** *this work*	***AmMox*** **Raman** *this work*	**γ-octamoly IR** *Himeno*[27]	**γ-octamoly Raman** *Himeno*[27]
970 (w)	951 (6) 935 (10)	948 939	950 (10)	941	949	965 (sh) 952 (sh) 947 (s) 940 (sh)	966 (10) 941 (4)	946	963 943
928 (s) 914 (sh)	910 (5)	925 913	919 914	924 905	919 909	917 (vs) 905 (vs)	925 (4) 923 (4) 912 (4)	918 904	924 922 912
898 (s)	898 (5)	900	895		893		901 (4)		
884 (s) 834 (s) 770 (w) 722 (m) 668 (sh)	886 (5) 846 (4) 710 (3)	884 843 825 767 722	886	887 670	875	846 (s) 721 (s) 697 (s)	843 (3)	858 790 735 662	840
651 (br) 630 (sh)	641 (3)	652	648	659		659 (s)	659 (3)		
588 (w) 565 (m) 550 (br)	607 (4)	547 504	604 512	548	612 507	548 (m) 523 (m)	573 (3) 550 (3) 517 (3)	512	
		441		455			466 (3) 448 (3)	476	
	409 (3) 369 (4) 360 (4)		408 371		390 367		415 (3) 388 (3) 371 (3) 365 (4) 359 (3)		
	336 (4) 304 (3) 249 (4) 218 (5)		312 214		312 222		351 (3) 335 (3) 317 (3) 294 (3) 273 (3) 249 (3) 231 (4) 212 (4)		

w = weak; m = medium;; v =strong; sh = shoulder; br = broad; numbers in brackets define the relative intensities of Raman Bands on a scale from 0 to 10.

Table 3. Calculated unit cell constants, crystallite size, and average strain after refinement of an *hkl* pattern to the experimental diffraction patterns (*Figure 4*) using the software TOPAS v 2.1 (Bruker AXS).

Parameters	*Mox1*	*Mox2*	*Mox3*	*AcMox*	*AmMox*	OctaMo	AHM
Space group	P-1	P-1	P-1	P-1	P21/n	P21/n	P21/c
Cell volume (Å^3)	1943	1957	1928	1966	2455	2419	2858
a (Å)	18.01	18.13	17.98	18.24	11.48	12.42	8.39
b (Å)	11.48	11.49	11.45	11.51	12.61	12.90	36.17
c (Å)	11.14	11.16	11.10	11.18	17.41	15.74	10.47
α (°)	71.6	71.2	71.6	71.5	90	90	90
β (°)	113.9	113.6	113.9	114.3	103.1	106.4	116.0
γ (°)	109.3	109.7	109.4	109.9	90	90	90
Size (nm)	71	75	55	51	142	-	-
Strain (%)	0.44	0.23	0.61	0.53	0.88	-	-

Table 4. Apparent activation energies E_a [KJmol^{-1}], calculated for ramp (623 K to 773 K by 5 K/min) based on the signal for acrolein and water.

Sample	*Product*	*Temperature Range [K]*	*Ea [kJmol^{-1}]*
Amox	water	> 710	9.07
		640 – 710	207
		< 640	1178
	acrolein	> 705	28.6
		675 – 705	316
		< 660	49.0
Mox	water	> 715	- 13.5
		660 – 705	57.2
	acrolein	> 705	17.4
		625 – 690	156
Mo	water	> 710	7.01
		675 – 710	9.16
	acrolein	> 715	8.45
		660 – 705	15.5

References

[1] M. T. Pope, *Heteropoly and Isopoly Oxometalates*, Springer, Berlin, 1983.

[2] D. E. Katsoulis, *Chem. Rev.* **98** (1998) 359.

[3] G. Centi, F. Cavani, F. Trifiro, *Selective Oxidation by Heterogeneous Catalysis*, Kluwer, New York, 2001.

[4] N. Mizuno, M. Misono, *Chem. Rev.* **98** (1998) 199.

[5] J. Mendez-Vivar, A. Campero, J. Livage, C. Sanchez, *J. Non-Cryst. Solids* **121** (1990) 26.

[6] M. Tong, G. Dai, Y. Wu, X. He, W. Yan, D. Gao, V. Volkov, G. Zakharova, *J. Mater. Res.* **15** (2000) 2653.

[7] K. F. Jahr and J. Fuchs, *Chem. Ber.* **96** (1963) 2457.

[8] J. Fuchs, K. F. Jahr, A. Niebelung, *Chem. Ber.* **100** (1967) 2415.

[9] W. Clegg, M. R. J. Elsegood, R. J. Errington, J. Havelock, *J. Chem. Soc., Dalton Trans.* (**1996**) 681.

[10] D. C. Bradley and M. H. Chisholm, *J. Am. Chem. Soc.* **95** (1971) 1511.

[11] K.-H. Tytko, B. Schönfeld, *Z. Naturforsch.* **30b** (1975) 471.

[12] J. Aveston, E.W. Anacker, J. S. Johnson, *Inorg. Chem.* **3** (1964) 735.

[13] G. Johansson, L. Pettersson, N. Ingri, *Acta Chem. Scand. A* **33** (1979) 305.

[14] S. Himeno, H. Niiya, T. Ueda, *Bull. Chem. Soc. Jpn*. **70** (1997) 631.

[15] L. E. Lyhamn, S.J. Cyvin, *Z. Naturforsch.* **34a** (1979) 867.

[16] W. -D. Hunnius, Habilitationsschrift der freien Universität Berlin (1977).

[17] G. Busca, *J. Raman Spectrosc.* **33** (2002) 348.

[18] M. Dieterle, Technical University Berlin, PhD-Thesis (2001)

[19] M. T. Pope, *Prog. Inorg. Chem*. **39** (1991) 181.

[20] M. L. Niven, J. J. Cruywagen, J. B. B. Heyns, *J. Chem. Soc. Dalton Trans.* (**1991**) 2007.

[21] J. W. Niemantsverdriet, *Spectroscopy in Catalysis- An Introduction*, Wiley-VCH (2000).

[22] A. Vioux, *Chem. Mater.* **9** (1997) 2292.

[23] J. Wienold, R. E. Jentoft, T. Ressler, *Eur. J. Inorg. Chem.* (**2003**), 1058.

[24] F. Arnaud-Neu, M.-J. Schwing-Weill, *Bull. Soc. Chim.* **12** (1973) 3225.

[25] H.-U. Kreusler, A. Förster, J. Fuchs, *Z. Naturforsch*. **36b** (1980) 242.

[26] H. T. Evans, B. M. Gatehouse, P. Leverett, *J.Chem. Soc., Dalton Trans.* (**1975**) 505.

[27] G. S. Pawley, *J. Appl. Crystallogr.* **14** (1981) 357.

Chapter 2

Vibrational study of the initial steps of hydrolysis of molybdenum alkoxides by *in situ* Raman and infrared spectroscopy

Parts of this chapter will be submitted for publication:
Pablo Beato, Annette Trunschke, Robert Schlögl "Vibrational study of the initial steps of hydrolysis of molybdenum alkoxides by *in situ* Raman and infrared spectroscopy".

Introduction

The addition of alcohols to hydrocarbon solutions of $Mo(NMe_2)_4$ leads to an extensive series of compounds of general formula $[Mo(OR)_4]_n$.[1]

$$(1) \quad Mo[N(CH_3)]_4 + ROH \rightarrow Mo(OR)_4 + 4\,HN(CH_3)_2 \uparrow$$

When *tert*-butanol is used as alcohol component, $[Mo(O\text{-}t\text{-}Bu)_4]_n$ is formed. In contrast to primary and secondary alkoxides of molybdenum, the *tert*-butoxide appears to be monomeric (n = 1), in the solid state. This was deduced from mass spectrometry giving a parent peak of m/e = 388.[1] However, the solid state structure of $Mo(O\text{-}t\text{-}Bu)_4$ has not been determined so far due to the difficulties to isolate and conserve the compound in a pure form. The isolation problems are due to the thermal instability which is probably related to the inherent strong tendency of molybdenum to form terminal Mo=O ("molybdenyl") double bonds.[2] The structure of $Mo(O\text{-}t\text{-}Bu)_4$ in solution is not clear at all, though the cryoscopically determined molecular weight (450 ± 20) indicates a tendency towards dimerisation.[1] Inconsistent results

were found for the magnetic properties of the compound. While Chisholm *et al.* measured for Mo(O-*t*-Bu)$_4$ an intermediate magnetic moment of μ_{eff} = 1.38 μ_B in toluene and of μ_{eff} = 1.37 – 1.40 μ_B in the solid state, Stoffelbach *et al.* investigated the compound by NMR and EPR spectroscopy and could not detect any paramagnetic contribution.[3] For the ^{1}H-NMR spectrum of Mo(O-*t*-Bu)$_4$ in C_6H_6 they observed a singulet at δ = 1.55, indicating that all methyl groups were equivalent. As far as the author knows besides the two above cited reports the compound has not been subject of further investigation. In *chapter 1* the preparation of alkylamine polyoxomolybdates via hydrolysis of an amine containing molybdenum *tert*-butoxide solution in *tert*-butanol is described (*see first chapter*). The observed hydrolysis reaction occurred remarkably slowly taking 2-3 hours until precipitation started. As the hydrolysis of transition metal alkoxides usually occurs very fast the system seemed to be an ideal model to study the initial stages of the reaction via in situ methods. Vibrational spectra of metal alkoxides have revealed to be quite complicated; in contrary, for polyoxometalates vibrational spectroscopy represents a reliable, straightforward and quick method. In this chapter the observations during the hydrolysis and condensation of a molybdenum alkoxide in the presence of an amine are investigated by Raman and infrared spectroscopy. Though it was not possible to determine the crystal structures of the formed intermediates the results allow some basic considerations concerning the structural transformations during the hydrolysis of molybdenum (IV) alkoxides.

Experimental

Materials. All experimental procedures, if not otherwise stated, were carried out under inert gas atmosphere (Argon 5.0) or under vacuum conditions (< 10^{-3} mbar) using standard Schlenk techniques. The handling and storage of the products was realized in a glove-box operated with Argon 5.0 (H_2O < 1ppm). All solvents purchased were of highest purity, pre-dried (*Merck SeccoSolv*®) and stored over molecular sieves under inert gas. Further drying was not

performed. However, before use the solvents were degassed. $Mo[N(CH_3)_2]_4$ was synthesized as described in the literature.[4]

Preparation of alkoxide solution and subsequent experimental steps *(see also Scheme 1)*. $Mo[N(CH_3)_2]_4$ (5 mmol) was added in small portions to 50 ml of *t*-butanol under vigorous stirring at 298 K. The solution turned turquoise blue immediately and almost black after a minute. After ~10 minutes stirring the solution turns dark violet. This solution is designated as "*Mo-solution*". Dry synthetic air (200 ml) was bubbled slowly into the *Mo-solution* in 50 ml portions using a syringe. As the air was bubbled into the solution the colour turned into light yellow-brown. This solution is stable for several months and named "*Mox-solution*". Finally the hydrolysis was performed by exposure of the *Mox-solution* to ambient humidity after removing the reactor cap under vigorous stirring. This solution is named "*HydroMox-solution*", until precipitation occurs.

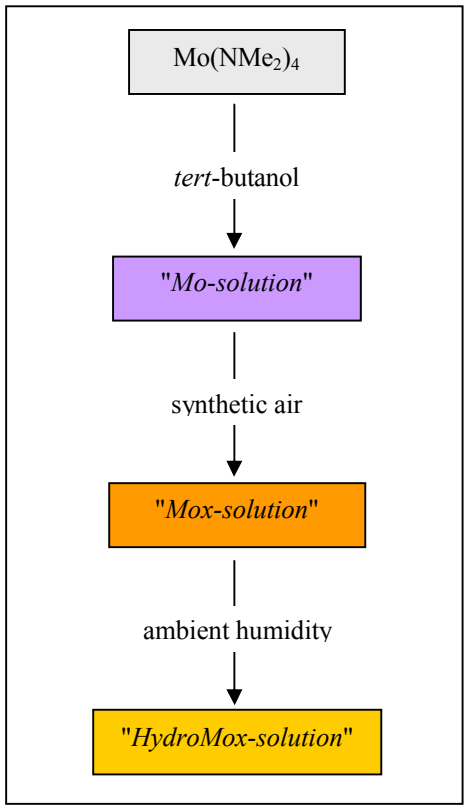

Scheme 1: Schematical representation of the experimental procedure and the designation of the investigated solutions.

Analytical equipment. Raman spectra were recorded with a DILOR LABRAM 1 spectrometer. A He/Ne-laser (632.8 nm, Melles Griot, 17 mW) was used for excitation. For the *in situ* experiments the laser beam was directed through the glass reaction vessel and focused into the solution by a 10x objective (Olympus). The backscattered Raman lines were detected on a CCD camera (1024x298 pixel), which was Peltier-cooled to 243 K to reduce thermal noise. The entrance slit was set to 200 µm resulting in a spectral width of 2.5 cm^{-1}. A notch filter was applied to cut off the laser line and the Rayleigh scattering up to ~ 150 cm^{-1}. Each spectrum is the average of 3

accumulations with an integration time of 60 seconds. Spectra were recorded continuously over a period of three hours. Transmission IR-spectra were recorded with a *Perkin-Elmer 2000 FTIR spectrometer*. A small quantity of the *Mox-solution* was filled in a sealable KBr cuvette (0.1 mm) inside the glove-box and then exposed to ambient humidity during spectra acquisition. After each measurement the cuvette was sealed again and agitated in order to homogenize the reaction mixture.

Results and Discussion

The experimental procedure and the designated names for the prepared solutions (*see also experimental part*) that will be discussed in the following text are given schematically in *Scheme 1*. The general structural theory for metal alkoxide polymers developed by Bradley predicts the smallest possible structural unit consistent with all the metal atoms attaining a higher co-ordination number.[5] Usually the oligomerization of alkoxides occurs via alkoxy bridges (μO-R), whereby the steric demand of the R group determines the degree of oligomerization. For molybdenum and tungsten oxoalkoxides an additional linkage mechanism has been observed, that consists in the formation of oxobridges between two metal centres, *e.g.* (M=O---M) (*Figure 1*).[6] Chisholm suggested that for Mo(O-*t*-Bu)$_4$ a dimer with two bridging alkoxy groups could satisfy the tendency of molybdenum to expand its covalency by attaining a co-ordination number of five. An example for this structural arrangement represents the well characterized solid state

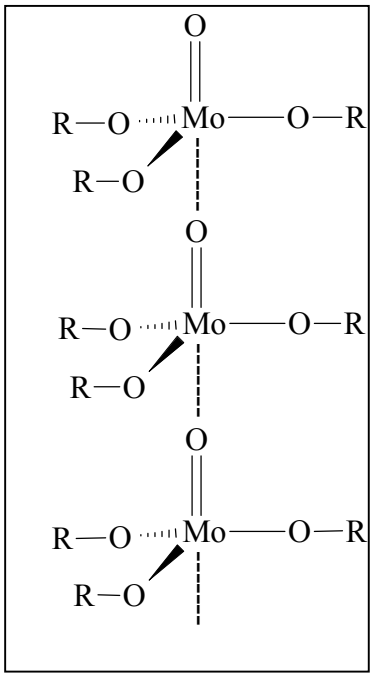

Figure 1. Chain-like arrangement typically observed for molybdenum oxoalkoxides.

structure of $Mo_2(O\text{-}i\text{-}Pr)_8$. In this structure molybdenum adopts a trigonal bipyramidal co-ordination with C_{2h} symmetry for the Mo_2O_8 frame.[7]

Specific aspects of the vibrational spectra of tert-butanol.

When analyzing the vibrational spectra of metal alkoxides, vibrations related to the alkoxy ligands and vibrations originating from the metal-oxygen frame can be discussed separately. However, care should be taken due to the possibility of coupling between both. In our case the situation is complicated since the bands due to the solvent *tert*-butanol are very close to the bands of the alkoxy ligands. In the following discussion, the observed vibrational modes of the alkoxy ligands will be examined in close connection to the band assignments given for *tert*-butanol. Surprisingly, the vibrational assignments for *tert*-butanol found in the literature were remarkably inconsistent. Only very recently a fairly complete vibrational assignment of *tert*-butanol by IR and Raman was done by Kipkemboi *et al.*.[8] A comprehensive assignment of the vibrational features is also given in the paper by Suwa *et al.*, who determined the molecular structure of *tert*-butanol by gas electron diffraction and compared the obtained results with theoretical calculations.[9]

From the reaction in *eq. 1* dimethylamine is released. Therefore, it had to be checked if the vibrational bands due to dissolved $HN(CH_3)_2$ would interfere the vibrational pattern derived from the metal-oxygen vibrations. In the spectral region between 200 and 1000 cm^{-1}, where characteristic metal oxygen and ligand vibrations occur, dimethylamine absorptions are relatively weak. The strongest IR absorption in the gas phase occurs at 730 cm^{-1} and is assigned to the N-H bending mode.[10, 11] The absorption is probably shifted to lower wavenumbers due to hydrogen bonding in the solution. As a result the band falls into the very broad absorption at 650 cm^{-1} assigned the OH---O out of plane (o.o.p.) deformation vibrations of *tert*-butanol and consequently these two bands are difficult to separate from each other. A similar observation was made for the C-N stretching mode at around 925 cm^{-1}, which falls

into the broad absorption of the CH_3 rocking mode of *tert*-butanol at 917 cm^{-1}. We have prepared a mixture of dimethylamine and *tert*-butanol by bubbling 5 minutes gaseous dimethylamine into the alcohol and could not detect any shoulder probably due to the low intensity of the bands of dimethylamine. In the Raman spectrum only the C-N stretching mode should have intensity high enough to be detected but again the band coincides with the CH_3 rocking mode of *tert*-butanol at 917 cm^{-1} and was not detected in the mixture of amine and alcohol. The only proof for the presence of dimethylamine in the solution was the detection of bands at 2835 cm^{-1} due to overtones of the CH_3 symmetric (1412 cm^{-1}) and antisymmetric (1441 cm^{-1}) deformation modes and the band at 2795 cm^{-1} due to the CH_3 symmetric stretching mode.

Vibrational analysis of the Mo-solution.

An approach similar to the presented here was carried out by Lynch *et al.* by comparing the IR spectra of tetra-*tert*-butoxides of group IV transition metals (Ti, Zr, Hf). They found four common characteristic absorptions for all *tert*-butoxides at around 1190, 1010, 900 and 785 cm^{-1}, and assigned these bands to the normal vibrations of the *tert*-butoxy groups.[12]

Table 1. Literature infrared data on solid tetra-tert-butoxides.

$Ti(OR)_4$ [*Lynch1*[12]]	$Zr(OR)_4$ [*Lynch*[12]]	$Hf(OR)_4$ [*Lynch*[12]]	$Cr(OR)_4$ [*Bradley*[13]]	$Mo(OR)_4$ [*Chisholm*[1]]
1190	1186	1190	1162 (s)	1171 (vs)
1008	1002	1015	1025 (w)	1025 (m)
			928 (vs)	994 (sh) 923 (vs)
909	901	904	906 (w)	902 (vs)
797				
783	785	787	784 (m)	785 (s) 774 (s)
744				
597	548	565 544	623 (m)	575 (s)
476 416	479	490 456	471 (w)	474 (m)
374	357	355	354 (w)	379 (m)

In *Table 1* we have compiled the results of Lynch and added the IR data of Cr(O-*t*-Bu)$_4$ and Mo(O-*t*-Bu)$_4$. [1, 13] The tungsten compound is not known to date. From *Table 1* it is obvious, that the characteristic absorptions found by Lynch can be observed as well for the chromium and molybdenum alkoxide. In *Table 2* we have summarized the experimentally observed bands during the different stages of our investigation together with the tentative assignment. *Figure 2* displays the IR spectra of the *Mo-solution* and pure *tert*-butanol, respectively, together with the calculated first and second derivatives. For the sake of clearness the relevant region from 1100 to 700 cm^{-1} is selected. Unfortunately the absorption of the KBr windows became to strong for a further assignment below 500 cm^{-1}.

Table 2. Experimental infrared and Raman data together with the tentative assignment.

tentative assignment	*tert*-butanol		*Mo-solution*	*Mox-solution*		*HydroMox-solution*	
	IR	Raman	IR	IR	Raman	IR	Raman
$\delta_{rk}(CH_3)$	1023 (m)	1028 (m)	1023 (solv.)	1023 (solv.)	1028 (solv.)	1023 (solv.)	1028 (solv.)
ν(Mo=O)			984 (sh,m)	975 (br,w)	994 (vs)	978 (m)	
ν(Mo=O)			968 (sh,vw)		967 (w)	968 (m)	971 (s)
ν(Mo=O)			953 (vs)	944 (s)	949 (sh)	947 (w)	948 (sh)
ν(Mo=O)			941 (s)	936 (s)	939 (vw)	939 (w)	
$\delta_{rk}(CH_3)$	916 (vs)	917 (s)	916 (solv.)	916 (solv.)	917 (solv.)	916 (solv.)	917 (solv.)
ν_{as}(Mo-O-Mo)			892 (m)	891 (s)	890 (m)	891 (m)	890 (w)
ν(Mo=O---Mo)		819 (vw)	828 (w, br)	828 (w, br)	816 (vw)	826 (w, br)	821 (vw)
$\nu_s(C_3C\text{-}O)$			781 (s)	786 (sh,m)		787 (s)	788 (s)
			767 (sh,m)	776 (s)	779 (sh)	776 (w)	776 (w)
$\nu_s(C_3C\text{-}O)$	750 (m)	753 (10)	750 (solv.)	750 (solv.)	753 (solv.)	750 (solv.)	753 (solv.)
δ(O–H) o.o.p.	648 (br)		648 (solv.)	648 (solv.)		648 (solv.)	
ν_s(Mo-OR)			586 (m,br)		583 (sh,w)	592 (m,br)	583 (s)
				554 (m)	554(s)		554 (sh,w)
δ(C_3C) (skeletal)		480			480 (solv.)		480 (solv.)
		430			430 (solv.)		430 (solv.)
		350			350 (solv.)		350 (solv.)
					287		275
					231		213

The characteristic IR band reported at around 1010 cm^{-1}, and observed for Cr(O-*t*-Bu)$_4$ and Mo(O-*t*-Bu)$_4$ at 1025 cm^{-1} was assigned by Lynch to the antisymmetric stretching vibrations of the C_3C-O bond. Various authors, however, assigned the antisymmetric stretching vibrations of the C-O bond in alkoxides to completely different bands. [14-18] The position of this band coincides nearly exactly with a band of *tert*-butanol located at 1023 cm^{-1}.

Kipkemboi *et al.* did not cover this range in their IR measurements, but they assigned the corresponding band in the Raman spectrum at 1024 cm^{-1} to a rocking mode of the methyl groups.[8] Although this band is quite intense in the IR spectrum of *tert*-butanol no assignment has been offered in the literature. In monographs dealing with vibrational spectroscopy, metal alkoxides appear rather scarcely but it is stated, that the band between 1000 and 1030 cm^{-1} should generally be assigned to the stretching mode of the RC-O bond.[19, 20]

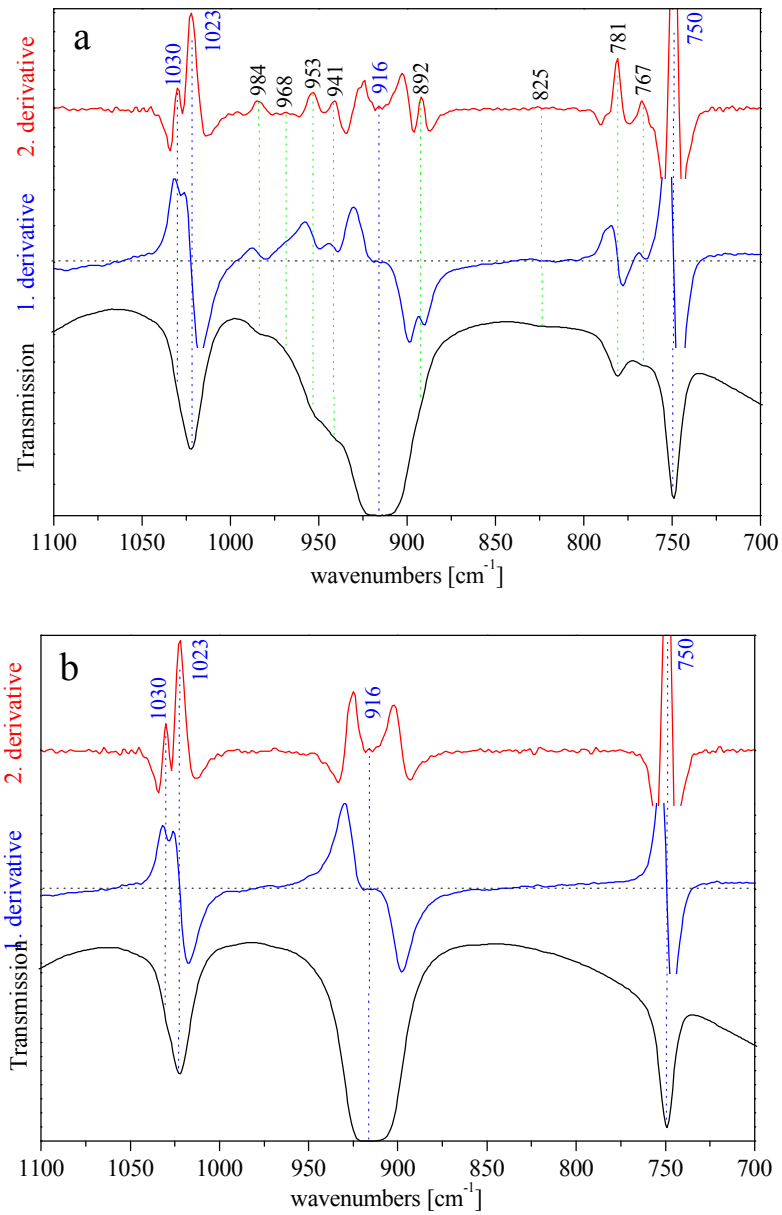

Figure 2. Selected spectral area of the infrared spectrum and the calculated first and second derivatives of (a) *Mo-solution*, (b) *tert*-butanol.

However, in the primary literature cited by these textbooks, mainly alkoxy ligands with primary carbon atoms bonded to the oxygen were considered.[15, 16, 18, 21]

It is known, that the antisymmetric stretching vibration of the C-O group in alcohols depends very much on whether a primary (1075 – 1000 cm^{-1}), secondary (1120 – 1090 cm^{-1}) or tertiary alcohol (1210 – 1100 cm^{-1}) is considered.[22, 23] This effect should be valid for alkoxides as well. It has been argued that there is some π-backbonding from the oxygen p- to the empty metal d-orbitals, leading to considerable double bond character of the M-O bond. This, as a consequence, should weaken the C-O bond due to the electron pulling effect of the oxygen on the carbon atom. For this reason the C-O stretching frequency was supposed to be shifted to lower wavenumbers from the alcohol to the alkoxide.[16] However, in order to interact with each other, the oxygen p-orbital and the metal d-orbital have to be orientated in the same plane. If this is not possible due to steric hindrance, the effect should be reversed and the positive inductive effect of the *tert*-butyl group will lead to a short carbon-oxygen bond, which should be observed at higher frequency than in the parent alcohol. This effect is observed, for sodium *tert*-butoxide, where π-bonding can not occur due to the absence of metal d-orbitals and where the C-O bond length is 138.9 pm which is shorter than the C-O bond length in *tert*-butanol (144.6 pm).[9, 24] Having in mind the above mentioned points, a band position at 1020 cm^{-1} might be assigned to the C-O bond of a methoxy group - as found experimentally and theoretically for the methoxy groups in $Mo(OCH_3)_6$ [18] - but it is hard to believe that the frequency for the C_3C-O antisymmetric stretching vibrations is shifted more than 150 cm^{-1} to lower wavenumbers. In fact, it seems more probable that the antisymmetric stretching mode of the C_3C-O bond lies much higher corresponding to the band of *tert*-butanol at around ~1200 cm^{-1}.[8, 22, 25] Due to the high intensity and the broadness of this band in *tert*-butanol the shifted band for the alkoxy groups could not be detected. However, as will be described below, it was possible to observe the shifted symmetric stretching frequency of the C_3C-O vibrations.

By a comparison with a series of compounds containing a *tert*-butyl group (*e.g. tert*-butyl hydroperoxide, di-*tert*-butyl peroxide, 1,5-di-*tert*-butyl phenol, *etc.*) a band around 1020 cm^{-1} was found in all of them independent of the tertiary C-atom being bonded to an oxygen atom or not. This comparison encouraged the author to favour the assignment done by Kipkemboi *et al.* attributing the band observed at 1023 cm^{-1} for *tert*-butanol to a rocking mode of the methyl groups.[8]

Interestingly, bands between 920-1000 cm^{-1} occur for both, the solid reference Mo(O-*t*-Bu)$_4$ and the *Mo-solution*. Bands in this region are usually assigned to the stretching modes of Mo=O terminal bonds and none of the other described homoleptic alkoxides in *Table 1*, except for the reported Cr(O-*t*-Bu)$_4$ absorb in this range. For the solid Mo(O-*t*-Bu)$_4$ Chisholm found a shoulder at 994 cm^{-1} and a very strong band at 923 cm^{-1}. For the chromium compound Alyea *et al.* observed a very strong band at 928 cm^{-1} but did not assign this band. Instead they attributed the band at 623 cm^{-1} to the ν_3 (t_2) Cr-O stretching mode of the tetrahedral CrO_4 skeleton.[13] From the present knowledge on the vibrational modes of *tert*-butoxy alkoxides and of *tert*-butanol, no reason was found to attribute the bands between 920 and 1000 cm^{-1} observed for Mo(O-*t*-Bu)$_4$ and Cr(O-*t*-Bu)$_4$ to the *tert*-butoxy groups. Of course, a coupling between the metal-oxygen frame and the ligand vibrations cannot be excluded.

For the *Mo-solution* four bands between 930 and 1000 cm^{-1} are observed [984 (m), 968 (vw), 950 (vs), 944 (sh, s)]. The high intensities of the latter bands, suggest an assignment to stretching vibrations of Mo=O terminal bonds. However, it seems quite improbably that all four bands come from a single species since for a monooxo compound we would expect one and for a dioxo compound two bands.

The IR absorption observed around 905 cm^{-1} for the solid *tert*-butyl alkoxides in *Table 1* corresponds to the intense band at 916 cm^{-1} for *tert*-butanol. The same band is found at 917 cm^{-1} in the Raman spectrum of the alcohol. This band is assigned concordantly in the literature to a rocking mode of the methyl groups.[8, 9, 22, 25] For the *Mo-solution* a pronounced

band located at 892 cm^{-1} was found. The band changes in intensity during the reaction with oxygen (*see below*). As there is no reason why the methyl group should be affected by the reaction with oxygen, an alternative assignment of this band had to be found. Since the band can not belong to a doublet originating from a *cis*-$Mo=O_2$ vibration because the splitting (Δ = 50 cm^{-1}) would be too large, the vibration must be due to a single Mo-O bond. Jezowska-Trzebiatowska *et al.* performed calculations and experimental studies on several monomeric, dimeric and tetrameric oxomolybdenum(V)-complexes and came to the conclusion, that the stretching vibrations of linear single bridged Mo_2O_3 oxomolybdate(V) dimers absorbs at about 880 cm^{-1}.[26] It will be shown in the following that this structure is present in all the solutions described in this study.

A broad and very weak band is observed around 825 cm^{-1}, that has no counterpart in the solid $Mo(O\text{-}t\text{-}Bu)_4$. As mentioned above it has been found, that molybdenum alkoxides tend to interact via the terminal molybdenyl bonds to form bridging bonds of the type (Mo=O---Mo) resulting in a chainlike arrangement (*Figure 1*). Several authors associate a broad absorption between 800-850 cm^{-1} with this type of interaction.[27, 28, 29]

The characteristic absorption at 785 cm^{-1} is attributed by Lynch to a symmetric skeletal vibration of the *tert*-butoxy groups. The band is found at 781 cm^{-1} for the *Mo-solution* and at 785 cm^{-1} for solid $Mo(O\text{-}t\text{-}Bu)_4$. Generally bands between 700-800 cm^{-1} are ascribed to Mo-O-Mo bridging bonds. However, for *tert*-butanol a band of medium intensity at 750 cm^{-1} in the IR and a very strong line at 753 cm^{-1} in the Raman spectrum were observed. Kipkemboi assigns the intense Raman line to the in-phase C_3C-O stretching mode.[8] The symmetric nature of the vibration is strongly supported by the observed relative intensities in the IR and Raman spectra. Tanabe also assigned the Raman line at 753 cm^{-1} for *tert*-butanol to the C-O stretching mode.[30] He observed a linewidths broadening with increasing alcohol concentration and attributes this behaviour to the higher amount of hydrogen bonding. Suwa came to the same conclusion after comparing his calculations with the experimental spectrum

of *tert*-butyl methyl ether.[9] As outlined above, the C-O bond of the *tert*-butoxy group in Mo(O-*t*-Bu)$_4$ can be stronger than in the corresponding alcohol due to sterical and inductive effects. Consequently, it seems to be justified to assign the band at 781 and 785 cm^{-1} in the *Mo-solution* and for solid Mo(O-*t*-Bu)$_4$, respectively, to the symmetric vibration of the C_3C-O bond. As the exact position of this band should be sensitive to the alkoxy-ligand co-ordination, the second band for the *Mo-solution* at 767 cm^{-1}, slightly shifted to lower wavenumbers might be an indication for the presence of a different, weaker C-O bond *e.g.* μ_2-OR. A similar pattern has been observed in the IR spectrum of MoO(O-*t*-Bu)$_4$ at 790 and 775 cm^{-1}.[31]

Nearly all vibrational studies on (oxo)alkoxides agree in assigning the bands between 540 and 600 cm^{-1} to the symmetric stretching vibrations of the Mo-OR bond. For solid Mo(O-*t*-Bu)$_4$ the Mo-OR frequency is located at 575 cm^{-1} (*Table 1*). For the Mo-solution this band is observed at 586 cm^{-1} (*Table 2*) showing a broad and asymmetric shape indicating an unresolved splitting, although this is difficult to determine due to broad background of the band centred at 648 cm^{-1} originating from the OH---O out of plane (o.o.p.) deformation vibrations of *tert*-butanol.[25]

As a preliminary resume the vibrational analysis of the Mo-solution indicates that at least two if not three different species coexist, in their majority monomers, which partly form chains via Mo=O---Mo bridges (*Figure 1*). Other species are present in the form of [Mo_2O_3] dimers, interconnected by singly bridging oxygens (Mo-O-Mo). It could not be proved without doubt, if species with *cis*-Mo=O_2 groups are present, though the positions and a splitting of $\Delta \sim 30$ cm^{-1} of the two bands at 984 and 953 cm^{-1} is typical for *cis*-Mo=O_2 groups.

It should be emphasized that (oxo)alkoxides generally show a markedly dynamic behaviour in solution whereby the alkoxy ligands are readily exchanged intramolecular and/or - if working in alcoholic solution - with the solvent. Clegg et al. applied variable-temperature ^{1}H NMR and observed an equilibrium between monomeric and dimeric structures for WO(OR)$_4$ in solution,

where R = Me, Et, *i*-Pr, *cyclo*-C_6H_{11}, OC_6H_3i-Pr_2-2,6.[32] For smaller R groups, the equilibrium is shifted nearly entirely towards the dimers but for a large R (*e.g.* *t*-Bu), the monomers predominate. Unfortunately they did not measure temperature dependent spectra for $WO(O\text{-}t\text{-}Bu)_4$, but they recorded ^{183}W NMR for all compounds and found the largest line broadening for the *tert*-butoxy derivate. They stated that the line broadening and the specific chemical shift (δ_W) indicate a dynamic structural interconversion between square pyramidal and trigonal bipyramidal coordination of the central Mo atom.

FTIR and Raman spectra of the Mox-solution.

When dry air (150 ml) is bubbled into the *Mo-solution*, the solution brightens and the colour changes from dark purple to yellow-brown. Further addition of dry air does not cause any change in spectra of the resulting *Mox-solution*. For the *Mox-solution* both IR and Raman spectra are available and displayed in *Figure 3*. Additional, the Raman spectrum of pure *tert*-butanol is plotted for comparison. The four band pattern between 930 and 1000 cm^{-1} observed in the IR spectrum of the *Mo-solution* is still present in the *Mox-solution*. However, all four bands have shifted to lower wavenumbers. The two strong bands are now located at 935 and 944 cm^{-1} and the band at higher wavenumbers has shifted and lost in intensity to give a broad band centred at 975 cm^{-1}. The broadness and the shape of the band indicates that actually several bands are present (see below). From the second derivative of the corresponding Raman spectrum, we can resolve two bands at 967 and 949 cm^{-1}. The band at 936 cm^{-1} in the IR can only be recognized in the second derivative of the Raman spectrum as a small shoulder at 939 cm^{-1}. In contrast to the IR spectrum, the Raman spectrum shows an intense band at 994 cm^{-1}. There are in principle two possibilities to explain the absence of this band in the IR: either the structure element that contains the high-lying molybdenyl band has a symmetry centre, or the corresponding band in the IR is simply too weak to be observed.

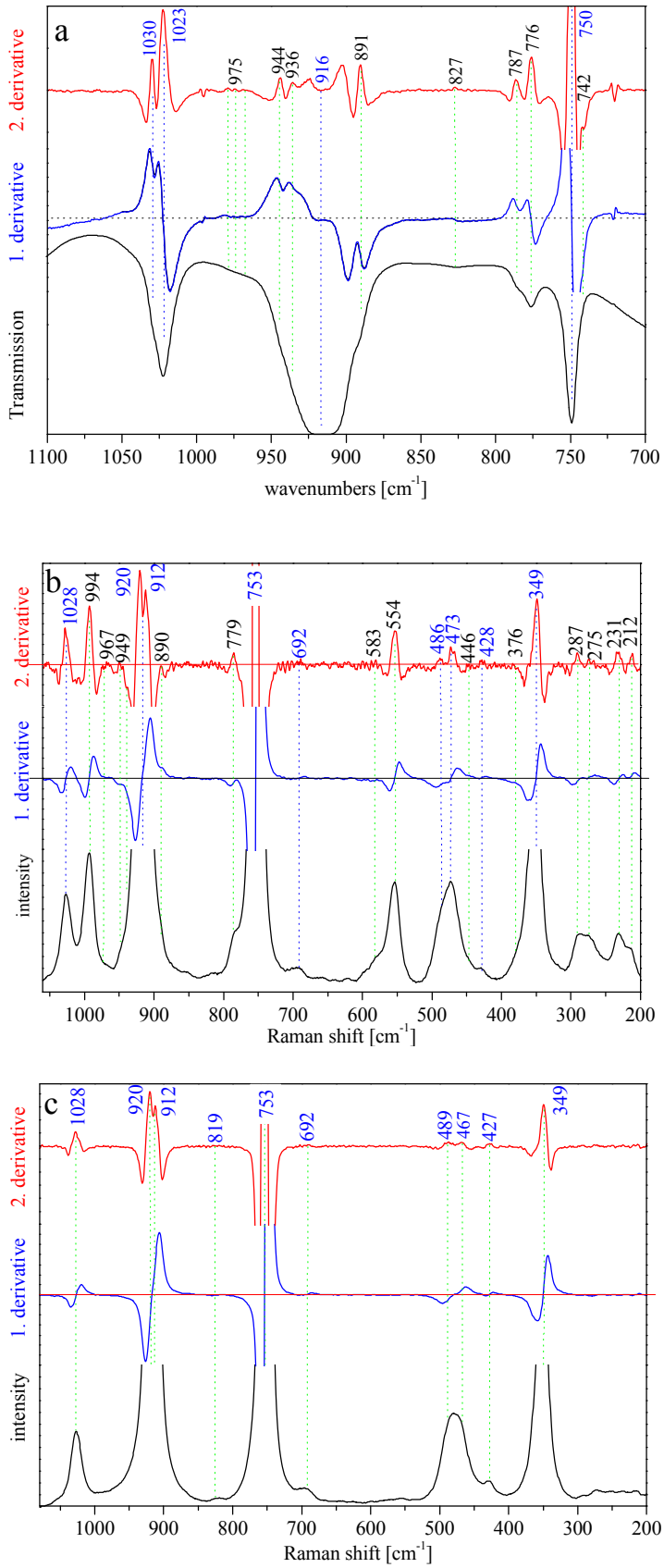

Figure 3. Selected areas of the vibrational spectra of the *Mox-solution* together with its first and second derivatives. (a) Infrared spectrum; (b) Raman spectrum; (c) Raman spectrum of *tert*-butanol.

As we have described above, monomeric Mo(V)-complexes are relatively rare due to the high tendency of d^1 ions to form dimers via Mo-O-Mo bridges (band at 890 cm^{-1}). Assuming the singly bridged Mo_2O_3 group represented in *Figure 8*, the Mo=O groups can be orientated *trans* or *syn* relative to each other. In the *trans* form this group has C_{2h} symmetry, with the centre of symmetry lying on the bridging oxygen atom. The band at 994 cm^{-1} is then assigned to the Raman active A_g mode, whereas one of the two bands centred at 975 cm^{-1} could be assigned to the IR active asymmetric stretching mode (A_u).[33]

An increasing intensity of the band assigned to the linear Mo-O-Mo bridges at 890 cm^{-1} is observed, indicating that the fraction of $[Mo_2O_3]$ was increased in solution. Further the weak and broad band at 827 cm^{-1} has somewhat increased in intensity as well. Regarding the dynamic behaviour of metal alkoxides in solution, it might be possible that fast interconversion between the Mo=O---O and the Mo-O-Mo bridges occurs (*Figure 4*)

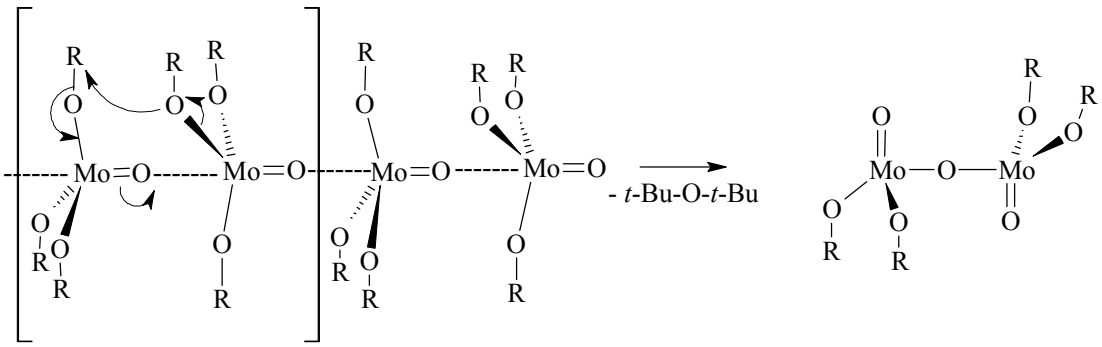

Figure 4. Possible interconversion mechanism for molybdenum oxoalkoxides in solution.

The band for the C_3C-O symmetric stretching mode has slightly shifted to lower wavenumbers and is now located at 776 cm^{-1} in the IR and at 779 cm^{-1} in the Raman spectrum. The shift to lower wavenumbers is interpreted in terms of the steric hindrance and electronic repulsions induced by the covalence expansion of the Mo-centres. Obviously, the weak shoulder at 787 cm^{-1} in the IR corresponds to a consecutive product, as this band grows during hydrolysis. As expected, the electronic repulsions induced by the covalence expansion

is even more pronounced for the band at 586 cm^{-1} assigned to symmetric stretching vibrations of the Mo-OR bond, which has shifted about 30 cm^{-1} to lower energies and is observed with higher intensity than before at 554 cm^{-1}. In the Raman spectrum the band is observed at 554 cm^{-1} as well.

For the *Mox-solution,* the addition of oxygen to the *Mo-solution* leads to additional Mo(VI) centres, which are characterized by a covalence expansion attaining an octahedral like ligand sphere. At the same time Mo(V) centres in the form of dimeric $[Mo_2O_3]$ species and probably some monomeric species containing a *cis*-$Mo{=}O_2$ group (*e.g.* 968, 936 cm^{-1}) have been formed.

In situ FTIR and Raman spectra during hydrolysis – the HydroMox-solution.

During the hydrolysis reaction Raman and IR spectra were recorded continuously. For the IR spectra the areas where changes occur were selected and magnified (*Figure 6 a-d*), while for the Raman spectra the whole spectral range is show because the changes are more readily seen (*Figure 5*).

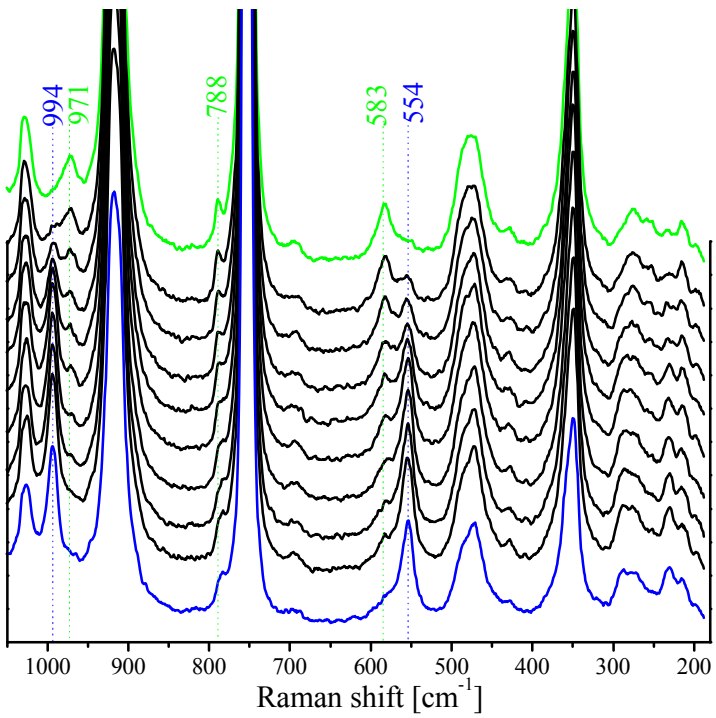

Figure 5. In situ Raman spectra during hydrolysis reaction (from bottom to top).

The spectra for the final *HydroMox* solution are shown in *Figure 7 a, b* together with its first and second derivatives. *Figure 8*, displays the IR difference spectrum between *HydroMox* and *Mox-solution*. The positive y-axis of *Figure 8* shows the bands that were present in the *Mox-solution*, while the negative y-axis gives direct information on the shifts and new bands in the *HydroMox*-solution. Obviously the overall intensity especially of the terminal Mo=O bonds has decreased during hydrolysis. This is exactly what one would expect during a polymerization process.

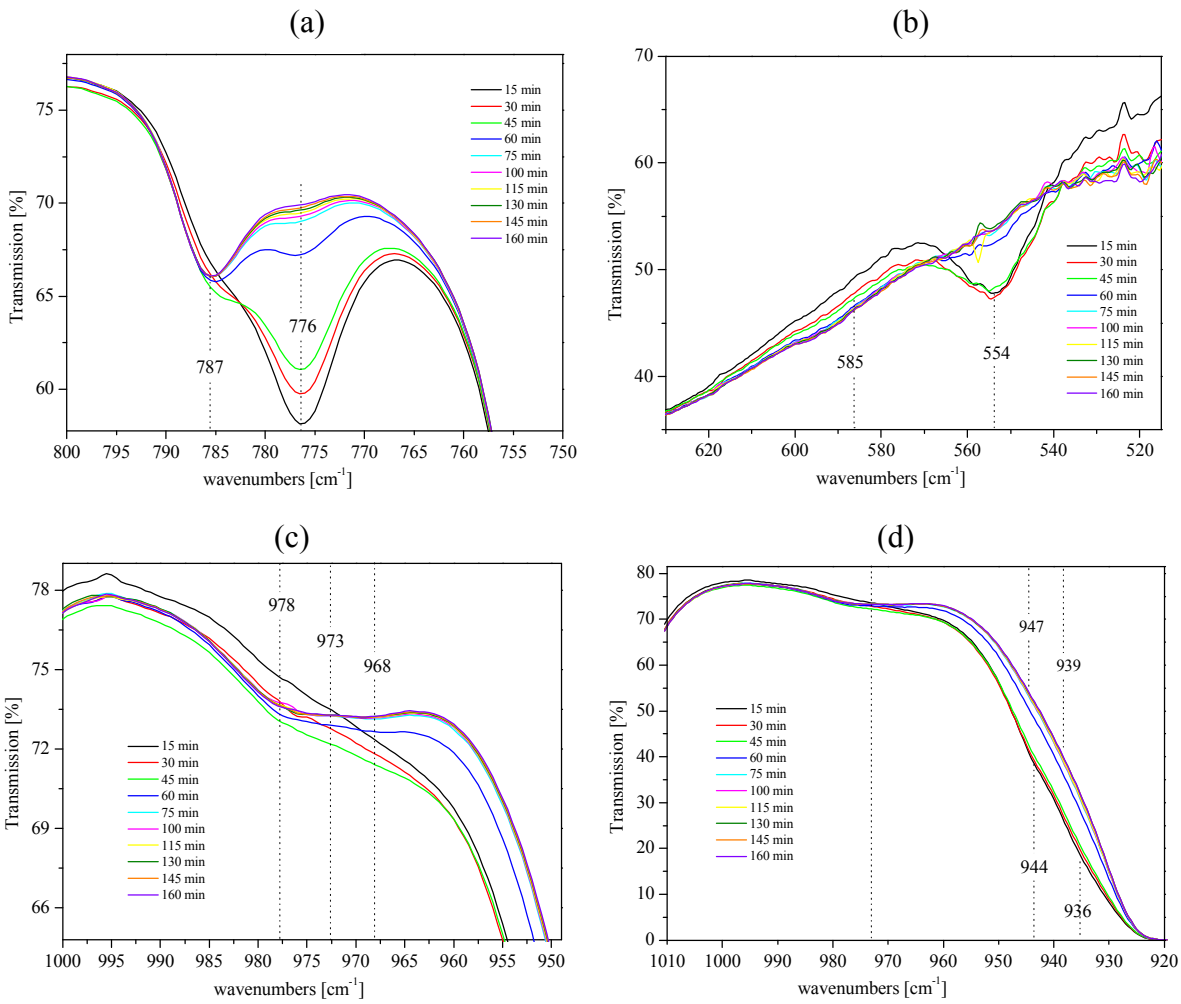

Figure 6 a-d. Selected spectral areas of the in situ infrared spectra during hydrolysis.

The sharp band at 776 cm^{-1}, originating from the stretching vibrations of the C_3C-O bonds of the *tert*-butoxy ligands, shrinks to result in a weak shoulder of the newly formed band at 786 cm^{-1} (*Figure 6 a*). The persisting shoulder demonstrates that until this stage of the reaction the hydrolysis is not complete. However, as expected most of the C-O bonds were broken as recognized by the disappearance of the band at 554 cm^{-1} (*Figures 6 b* and *5*). In both IR and Raman spectra new bands at higher wavenumbers, namely at about 592 cm^{-1} in the IR, and 583 cm^{-1} in the Raman appear.

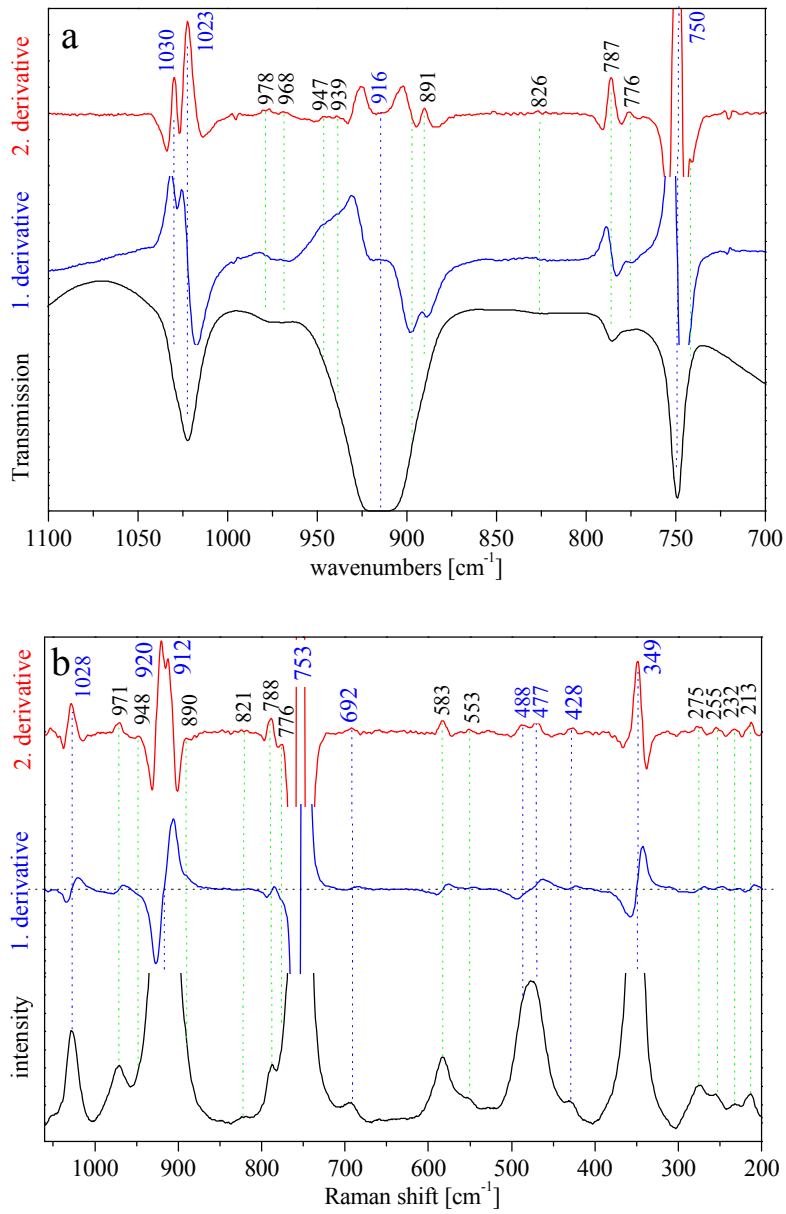

Figure 7. Selected areas of the vibrational spectra of the *HydroMox-solution* together with its first and second derivatives. (a) Infrared spectrum; (b) Raman spectrum.

According to the literature on polymolybdates in aqueous solutions the bands around 600 cm^{-1} are assigned to the symmetric Mo-O-Mo stretches while the newly formed band at 786 cm^{-1} in the IR and at 788 cm^{-1} in the Raman is not proper for polymolybdates and tentatively assigned to the asymmetric Mo-O-Mo stretching vibrations of a dimeric $[Mo_2O_4]$ species with μ_2-oxo bridges.[34, 35, 36]

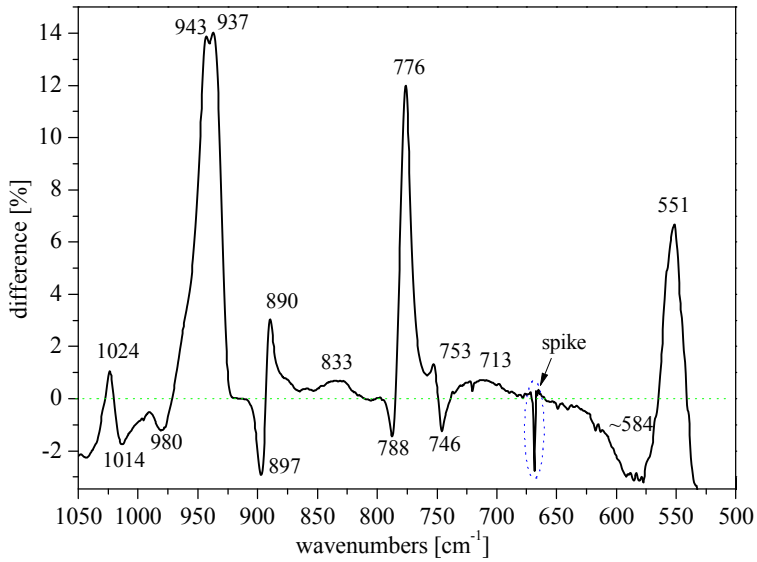

Figure 8. Diference spectrum between *HydroMox*- and *Mox-solution*. Positive y-axis represents bands that disappeared from the *Mox-solution*. Negative y-axis represents newly formed bands or intensities of the *HydroMox-solution*.

The two bands between 800 and 900 cm^{-1}, which were correlated to the singly bridging interactions, loose slightly in intensity, indicating that the ongoing hydrolysis is favouring new type of bonds between the monomers.

In the IR spectra the highest terminal Mo=O stretching modes do not change much in position but the broad band centred at 975 cm^{-1} has now resolved to give two bands at 978 and 968 cm^{-1} (*Figure 6 c*). The two bands at 944 and 936 cm^{-1} loose much in intensity and are both slightly shifted to higher energy (*Figure 6 d and Figure 8*). In the Raman spectra the band at 994 cm^{-1} is replaced continuously by a band at 971 cm^{-1} (*Figure 5*). At the same time the weak shoulder observed at 939 cm^{-1} has vanished leaving the somewhat broadened band at

948 cm^{-1}. Taking into account that most of the alkoxy groups have been hydrolysed a subsequent condensation process is inevitable. The high frequency bands due to the terminal Mo=O bonds must consequently form part of some higher polycondensates. The previous hydrolysis experiments (*first chapter*) have shown that slow hydrolysis via ambient humidity or via acetone condensation favours the formation of the so called trimolybdate $[Mo_3O_{10}]^{2-}$, with the most intense absorption frequencies found at 949 cm^{-1} in the Raman and at 941 cm^{-1} in the IR spectrum.[37]

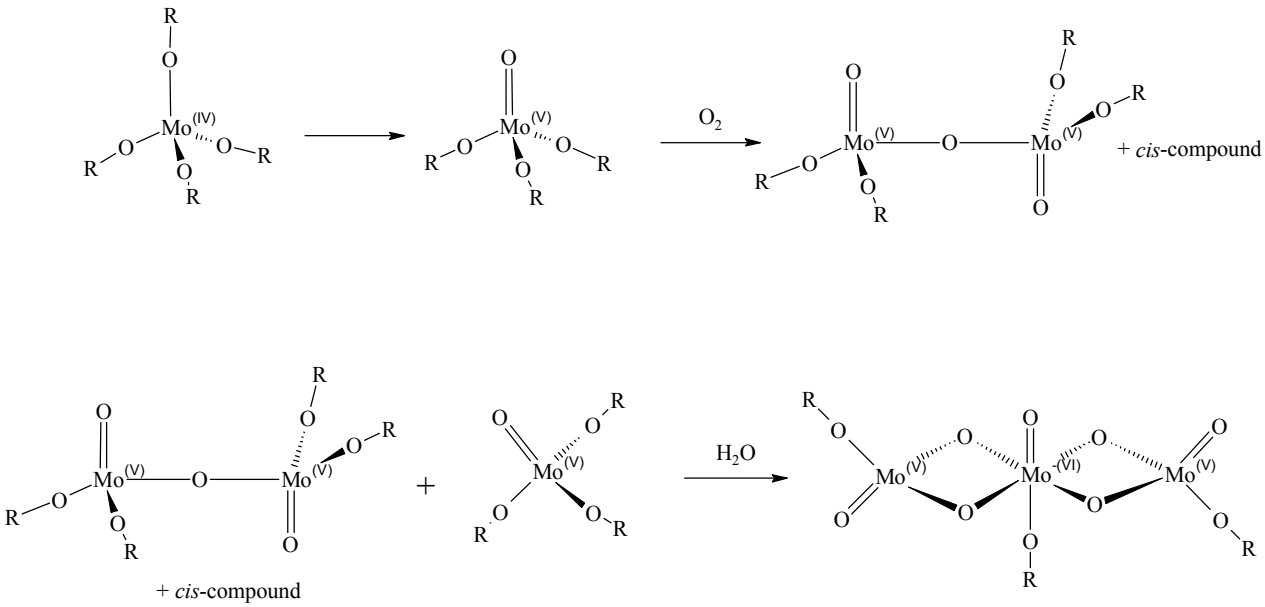

Figure 9. Schematic representation of the possible formation mechanism of polyoxometalates via hydrolysis of alkoxides.

The spectra of the *HydroMox-solution* give evidence that the trimolybdate species is already formed before precipitation occurs (see also *Figure 6* band shift to 897 cm^{-1}). Interestingly the structure of the trimolybdate is composed of chains of MoO_6-octahedra, while the reaction product of the fast hydrolysis, the heptamolybdate ion $[Mo_7O_{24}]^{6-}$, is composed of a three dimensional arrangement of octahedra. A decisive factor during the growth of

polyoxometalates seems to be the velocity of the condensation process and the availability of reactive monomers. Based on the obtained results we propose a mechanistic model for the formation of polyoxometalates from the described solution process (*Figure 9*). The mechanism proposed is compatible with the proposed "*addition mechanism*" by Tytko and Glemser (*Figure 10*) occurring during the acidification of aqueous metal ion solutions.[38] In the *addition mechanism* the formation of primary aggregation products proceeds via the addition of a tetrahedral MO_4 species (HMO_4^-, H_2MO_4) to the edge of another tetrahedral MO_4 unit (MO_4^{2-}, HMO_4^-, H_2MO_4) to form an octahedra with an edge sharing tetrahedra (*Figure 10*). By further addition of MO_4 tetrahedra to an octahedral edge or to the corners of two adjacent octahedra (larger polyoxometalate already formed) a large number of polyoxometalate species can be built up. The product of *Figure 9* can alternatively serve as a starting point for the addition mechanism shown in *Figure 10*.

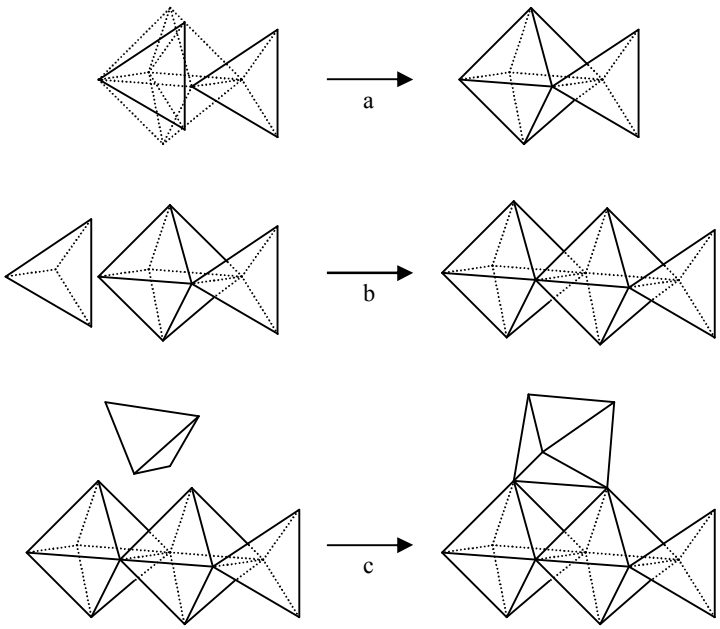

Figure 10. The addition mechanism after Tytko and Glemser.

Conclusions

The existing vibrational data on transition metal alkoxides has been critically revised. An attempt was made to give a new view of the complex behaviour of these compounds in solution. The vibrational data presented does not serve for an unequivocally structure determination, but it reveals some structural characteristics, that may serve in future experiments as an endorsement. The proposed weaker Mo-O bonding due to steric hindrance impeding the formation of π-backbonding and the absence of metal-metal bonds could be a reason for the thermal instability and the related problems during isolation of $Mo(O\text{-}t\text{-}Bu)_4$. By selectively blocking reaction sites at the monomeric species and controlling the polymerization velocity it could be possible to direct the growth and obtain new types of polyoxometalates.

References

[1] M. H. Chisholm, W. W. Reichert, P. Thornton, *J. Am. Chem. Soc.* **100** (1978) 2744.

[2] M. I. Yanovskaya, I. E. Obvintseva, V. G. Kessler, B. Sh. Galyamov, S. I. Kucheiko, R. R. Shifrina, N. Ya. Turova, *J. Non-Cryst. Solids* **124** (1990) 155.

[3] F. Stoffelbach, D. Saurenz, R. Poli, *Eur. J. Inorg. Chem.* (**2001**) 2699.

[4] D. C. Bradley and M. H. Chisholm, *J. Am. Chem. Soc.* **95** (1971) 1511.

[5] D. C. Bradley, *Nature* **182** (1958) 1211.

[6] N. Ya. Turova, E. P. Turevskaya, M. I. Yanovskaya, A. I. Yanovsky, V. K. Kessler, D. E. Tcheboukov, *Polyhedron* **17** (1998) 899.

[7] M. H. Chisholm, F. A. Cotton, M. W. Extine, W. Reichert, *Inorg. Chem.* **17** (1978) 2944.

[8] P. K. Kipkemboi, P. C. Kiprono, J. Sanga, *Bull. Chem. Soc. Ethiop.* **17** (2003) 211.

[9] A. Suwa, H. Ohta, S. Konaka, *J. Mol. Struct.* **172** (1988) 275.

[10] G. Gamer, H. Wolff, *Spectrochim. Acta* **29A** (1973) 129.

[11] K. Hamada, H. Morishita, *Z. Phys. Chem.* **97** (1975) 295.

[12] C. T. Lynch, K. S. Mazdiyasni, J. S. Smith, W. J. Crawford, *Anal. Chem.* **36** (1964) 2332.

[13] E. C. Alyea, J. S. Basi, D. C. Bradley, M. H. Chisholm, *J. Chem. Soc. (A)* (**1971**) 772.

[14] D. L. Guertin, S. E. Wiberley, W. H. Bauer, J. Goldenson, *J. Phys. Chem.* **60** (1956) 1018.

[15] H. Kriegsmann, K. Licht, *Z. Elektrochem.* **62** (1958) 1163.

[16] C. G. Barraclough, D. C. Bradley, J. Lewis, I. M. Thomas, *J. Chem. Soc.* (**1961**) 2601.

[17] K. Witke, A. Lachowicz, W. Brüser, D. Zeigan, *Z. Anorg. Allg. Chem.* **465** (1980) 193.

[18] G. Tatzel, M. Gruene, J. Weidlein, *Z. Anorg. Allg. Chem.* **533** (1986) 83.

[19] K. Nakamoto, *Infrared and Raman Spectra of Inorganic and Coordination Compounds, 5th Edition*, John Wiley & Sons (**1997**).

[20] D. M. Adams, *Metal-Ligand and Related Vibrations: A critical survey of the infrared and Raman spectra of metallic and organometallic compounds*, Edward Arnold (Publishers) Ltd London (**1967**).

[21] D. C. Bradley, A. H. Westlake, Nature **191** (1961) 273.

[22] H. Günzler, H. Böck, *IR-Spektroskopie - Eine Einführung*, Verlag Chemie, Weinheim (1988).

[23] H. Zeiss, M. Tsutsui, *J. Amer. Chem. Soc.* **75** (1953) 897.

[24] H. Nekola, F. Olbrich, U. Behrens, *Z. Anorg. Allg. Chem.* **628** (2002) 2067.

[25] N. B. Colthup, *Introduction to Infrared and Raman Spectroscopy*, Academic Press (1990).

[26] B. Jezowska-Trzebiatowska, M. F. Rudolf, L. Natkaniec, H. Sabat, *Inorg. Chem*. **13** (1974) 617.

[27] O. A. Rajan, A. Chakravorty, *Inorg. Chem.* **20** (1981) 660.

[28] J. M. Berg, R. H. Holm, *Inorg. Chem.* **22** (1983) 1768.

[29] S. Bhattacharjee, R. Bhattacharyya, *J. Chem. Soc. Dalton Trans.* (**1993**) 1151.

[30] K. Tanabe, *Spectrochim. Acta* **40A** (1984) 437.

[31] M. H. Chisholm, K. Folting, J. C. Huffman, C. C. Kirkpatrick, *Inorg. Chem.* **23** (1984) 1021.

[32] W. Clegg, R. J. Errington, P. Kraxner, C. Redshaw, *J. Chem. Soc. Dalton Trans.* (**1992**) 1431.

[33] F. A. Cotton, *J. Less. Comm. Metals* **36** (1974) 13.

[34] J. Avenston, E. W. Anacker, J. S. Johnson, *Inorg. Chem.* **3** (1964) 735.

[35] G. Johansson, L. Pettersson, N. Ingri, *Acta Chem. Scan. A* **33** (1979) 305.

[36] K. Y. Simon Ng, E. Gulari, *Polyhedron* **3** (1984) 1001.

[37] H.-U. Kreusler, A. Förster, J. Fuchs, *Z. Naturforsch*. **36b** (1980) 242.

[38] K.-H. Tytko, O. Glemser, *Adv. Inor. Chem. Radiochem.* **19** (1976) 239.

Chapter 3

Raman and electron microscopic characterization of a nanostructured α-MoO_3 thin film

Parts of this chapter will be submitted for publication:
Pablo Beato, Jakob B. Wagner, Gisela Weinberg, Achim Klein-Hoffmann and Robert Schlögl
"Raman and electron microscopic characterization of a nanostructured α-MoO_3 thin film".

Introduction

The partial oxidation of light alkanes *e.g.* propane to higher valuable chemicals *e.g.* acrolein and/or acrylic acid is technically performed over multi metal oxides (MMO). Although much effort has been made to understand the working mechanism of MMO's, the complexity of such systems has prevented up to now unequivocal proofs for the existing theories. It is obvious that *in situ* analytical methods are indispensable to obtain such proofs. One concern is that most of the research on MMO's was conducted with bulk analytical techniques (XRD, EXAFS, IR, Raman, etc.) because charging effects and surface roughness of real powder catalysts make the reliable analysis by surface science methods very difficult. However, a combination of surface sensitive and bulk sensitive methods is necessary to fully characterize and understand such complex catalytic systems.

One of the current research targets in heterogeneous catalysis therefore comprises the preparation of adequate models ranging from pure molybdenum to complex mixed metal oxides which should preserve as much as possible of the structural complexity of real catalysts but at the same time stay accessible to both surface science and bulk analytic

techniques. A major requirement is the control over the lattice defects which are likely to be of key relevance for determining the lattice oxygen delivery.

A promising strategy to meet these requirements is to deposit a thin film or nanoparticles of the metal oxide on an inert, conducting substrate, such as silicon.[1] If the film or the particles are homogeneous in composition and thin or small enough respectively, charging even of non-conducting oxides can be minimized and surface science techniques like *in situ* XPS can be applied. Spin-coating of solutions containing metal ions represents a straight forward method for the preparation of thin films. A further advantage over physical preparation methods such as pulsed laser deposition, CVD or sputtering is the similarity of the chemistry occurring during spin-coating to that of the powder synthesis. In this way the structural complexity typical for real catalysts is transferred to the model system. However, the high surface tension and low vapor pressure of water inhibits the use of aqueous solutions for the preparation of dense and closed thin films. Instead of aqueous solutions, sol-gel procedures employing alcoholic media are typically used for wet chemical thin film deposition.

Metal alkoxides are popular precursors for the synthesis of metal oxides and particularly used in many sol-gel processes. In a *chapter 1* the synthesis and characterization of novel highly crystalline molybdenum polyoxomolybdates by the hydrolysis of molybdenum oxoalkoxide solutions in the presence of an amine was described.[2] This chapter describes the formation of thin films by spin-coating the same solutions on Si [100] single crystals. First the formation of a nanostructured mesoporous polyoxomolybdate film is observed, which is subsequently decomposed to generate a nanostructured α-MoO_3 thin film.

The films were analyzed by confocal Raman microscopy, scanning electron microscopy (SEM) and high resolution transmission electron microscopy (HRTEM).

Experimental

Silicon [100] wafers (p-type doped with boron (15 mOhm x cm) from Silchem®) were cut into pieces of 10.0 x 10.0 x 0.7 mm. The cleaning procedure for the Si-wafers consisted in successive ultrasonic cleaning in chloroform, acetone, ethanol and bi-distilled water. After wet cleaning the Si-wafers were oxidized in air at 800°C to generate a thin SiO_2 film of about 5 nm thickness. The preparation of the alkoxide solutions is described in detail in *chapter 1*. Spin-coating of the solutions was performed in air at 4000 rpm. After drying at 40°C for 12 h the films were calcined at 723 K inside a quartz tube under flowing synthetic air (50ml/min).

Raman spectra were recorded with a DILOR LABRAM 1 spectrometer. A He-laser (632.8 nm, Melles Griot, 17 mW) was used for excitation. The laser light was focussed onto the sample using a 100x long distance objective lens (Olympus) and the backscattered Raman lines were detected on a CCD camera (1024x298 pixel), which was Peltier-cooled to 243 K to reduce thermal noise. The confocal hole was set to 300 µm and the entrance slit to 100 µm, resulting in a spectral width of 2 cm^{-1}. A notch filter was applied to cut off the laser line and the Rayleigh scattering up to ~ 150 cm^{-1}. Each spectrum is the average of 3 accumulations with an integration time of 60 seconds. Optical filters were used to adjust the laser power at the sample to ~ 1 mW.

For TEM the sample material was separated using a wire saw in 3 mm x 0.5 mm dimension. After gluing the sample face to face with epoxy G1 the mechanical thinning process was carried out by a Tripod polisher.[3] The samples were lapped from both sides by diamond-lapping foils from 30 µm up to 1 µm grain size to achieve a sample thickness of 20 µm. For better handling a copper aperture with a 2 mm hole was centred glued with epoxy onto the sample. The ion mill used in this study was a Fischione 1010. The following conditions were chosen for both ion guns: a milling angle of 5^o relative to the surface, 5 kV gun voltage, 8 mA gun current, a sample oscillation angle of 90^o. The gas used for etching process was argon. After 4 hours etching time the electron transparency was achieved.

The samples were studied in a Philips CM 200 FEG TEM operated at 200 kV and equipped with a Gatan Image Filter and a CCD camera. Scanning electron microscopy (SEM) images were acquired with an S 4000 FEG microscope (Hitachi) operated in secondary electron (SE) mode. The acceleration voltage was set to 5 kV.

Results and Discussion

The SEM micrographs (*Figure 1*) illustrate the microstructure of the as prepared film. Small particles of sub 50 nm size are randomly distributed and interconnected in a chain like arrangement forming a network. Due to this alignment pores of different sizes, ranging from 10 nm to 1 µm, are formed.

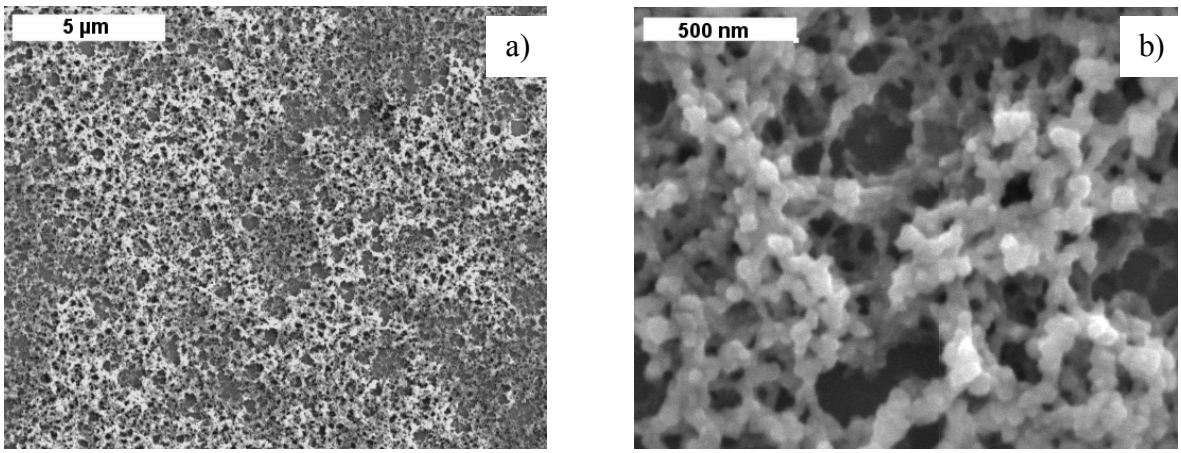

Figure 1. SEM images of the as prepared film. Overview of the porous structure (a). Detailed view on the three dimensional network of octamolybdate units (b).

In *Figure 2* the Raman spectrum of the as prepared film is shown together with the spectrum of a bare silicon wafer and the difference spectrum of both. The characteristic Raman bands for molybdenum polyoxometalates are located in the range between 600 and 1050 cm^{-1}. The exact positions of the bands can be used to determine the condensation degree and the structure of the polyanions.[4, 5]

In addition to the Raman spectrum of the bare Si [100] wafer, an intense band at 965 cm^{-1} with a shoulder at 958 cm^{-1} can be recognized for the as prepared film. Further, a medium-sized band at 944 cm^{-1} and two broad and weaker bands are centered at 914 and 833 cm^{-1}. The bands at 965, 958 and 944 cm^{-1} are characteristic for terminal Mo=O bonds of polyoxomolybdates. From the positions of the molybdenyl bands at 965 and 958 cm^{-1} the formation of different types of octamolybdate ions - probably α- and γ-$Mo_8O_{26}^{4-}$ - are suggested, whereas the band at 943 cm^{-1}, though slightly too high in energy, is assigned to the heptamolybdate ion ($Mo_7O_{24}^{6-}$).[6, 7, 8]

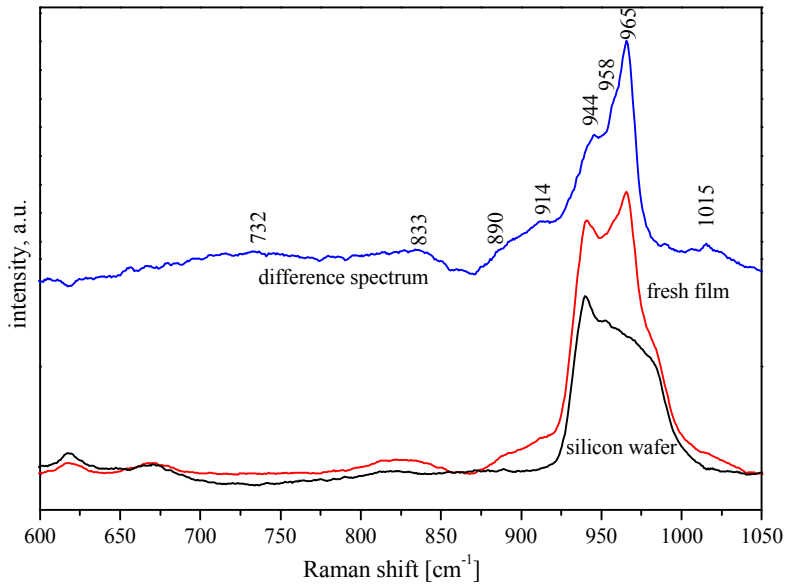

Figure 2. Raman spectra of the as prepared film (red), the bare oxidized Si [100] wafer (black) and the difference spectrum (blue) of both after normalization to the Si band 520 cm^{-1}.

The formation of heptamolybdate and octamolybdate species on silica surfaces has been described several times in the literature and is supposed to depend critically on the surface acid-base properties of the silica.[9,10,11] At this point it is interesting to mention that the fast hydrolysis of the same solution in the absence of the silicon/silica substrate yielded a heptameric $(Mo_7O_{24})^{6-}$ polyoxomolybdate.[2] The interaction between the silica and the alkoxide solution seems to be responsible for the equilibrium displacement and the subsequent formation of the octamolybdate. The broad and structured band around 915 cm^{-1} is

assigned to unresolved Mo-O stretching vibrations of the polymolybdates, whereas the flat band at around 830 cm^{-1} is too low for hepta- and octamolybdates and is in the characteristic range of bridging Mo-O-Mo bonds, typically observed for molybdenum oxides. This could be an indication for the presence of polymeric MoO_x. The corresponding stretching vibrations for the terminal Mo=O bonds of this polymeric species could provoke the band at 1015 cm^{-1}. Such species have been described by Xie *et al.* on ZrO_2.[26]

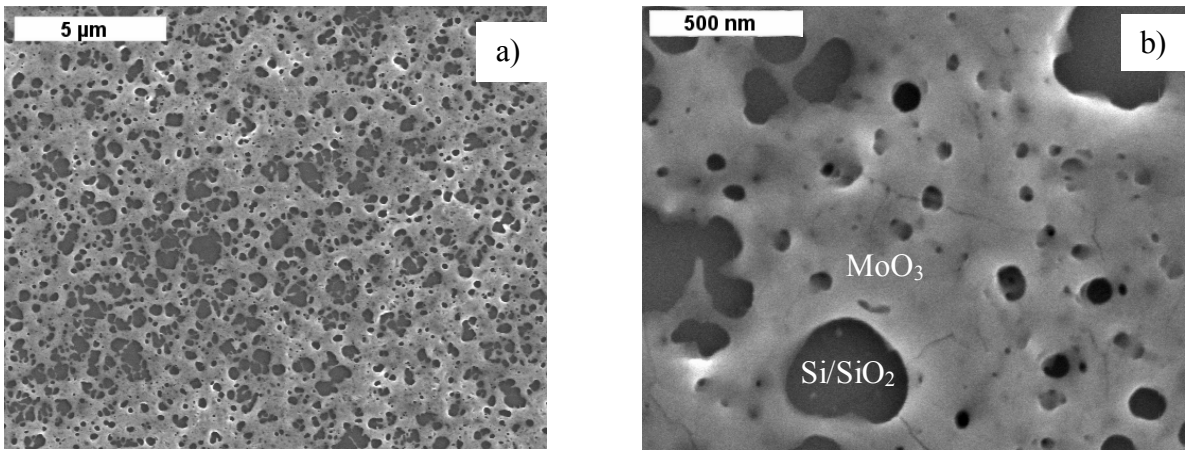

Figure 3. SEM images of the at 723 K in air calcined film. Overview of the spread α-MoO_3 film (a). Detailed image showing the densified morphology of the film (b).

After calcination at 723 K in air, the SEM images reveal that during the thermal treatment a spreading and densification of the small particles has occurred (*Figure 3*). At closer observation, the film appears very smooth at the surface but riddled with different sized holes, suggesting that a surface melting of the network structure occurred during calcination (*Figure 3b*). Melting at such low temperatures seems improbable as polyoxometalates are usually transformed to oxides by successive loss of ligands and a subsequent polycondensation process.[12] Nevertheless, the overlap of highly exothermic processes like the combustion of organics, condensation, crystallization and surface minimization of the particles might have induced a surface melting process.

The Raman spectrum of the calcined film is comparable to that of the well known structure of orthorhombic α-MoO_3, showing the typical band positions at 666, 820 and 995 cm^{-1} (*Figure*

4a).[13] However, the relative band intensities indicate a deviation from the α-MoO_3 structure (*Figure 4b*). Moreover, an additional band at 1006 cm^{-1} is clearly visible, besides the line of the Si substrate.

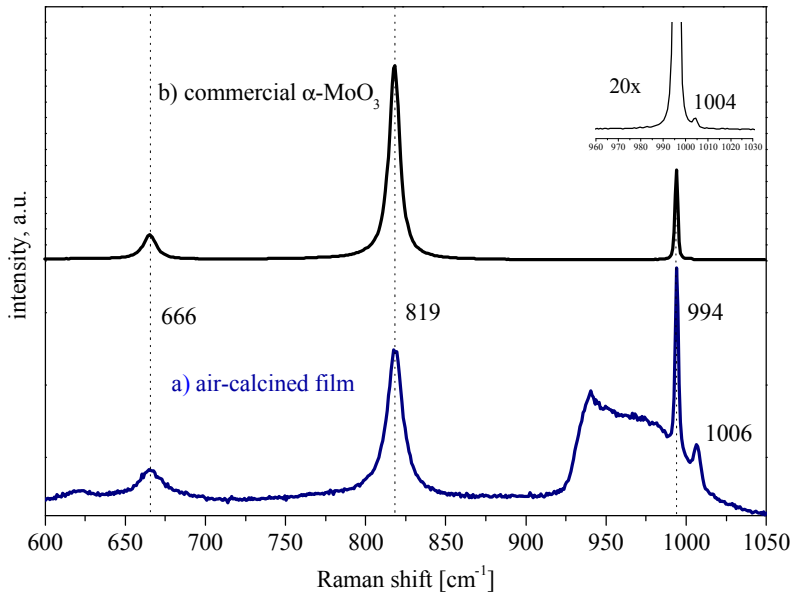

Figure 4. Raman spectrum of the air-calcined film (a).Characteristic Raman Spectrum of ordinary crystalline orthorhombic α-MoO_3 (b). Inlet shows the 20x magnified (in y direction) spectrum of 3b in the range from 960 to 1030 cm^{-1}, in order to detect the band at 1004 cm^{-1}.

Orthorhombic α-MoO_3 has a layered structure of which each layer can be described as a double half-layer of corner sharing tetrahedra chains, running along the c axis (*Figure 5*). The typically observed morphology of α-MoO_3 crystals is closely related to the arrangement of the constituting polyhedra (*Figure 5*). The crystals grow along the tetrahedra chains in c direction and across the ac plane, forming layers which are stacked in direction of the b-axis, thus resulting in platelet-like, elongated crystals with exposed plane ratios (010)/(100) > 1 and (010)/(001) >>>1.[7]

For vibrational considerations it is useful to distinguish the three inequivalent oxygen atoms present in the structure of α-MoO_3 (*Figure 5*): terminal Mo=O (O1), two-fold bridged Mo-O-Mo (O2) and three-fold bridged O-Mo_3 (O3) . The associated stretching vibrations correspond to the observed Raman shifts at 995 (O1), 820 (O2) and 666 cm^{-1} (O3). The band intensity (I)

ratios typically observed for polycrystalline α-MoO_3 are approximately 0.5(I_{995}) : (I_{820}) : 0.2(I_{666}).

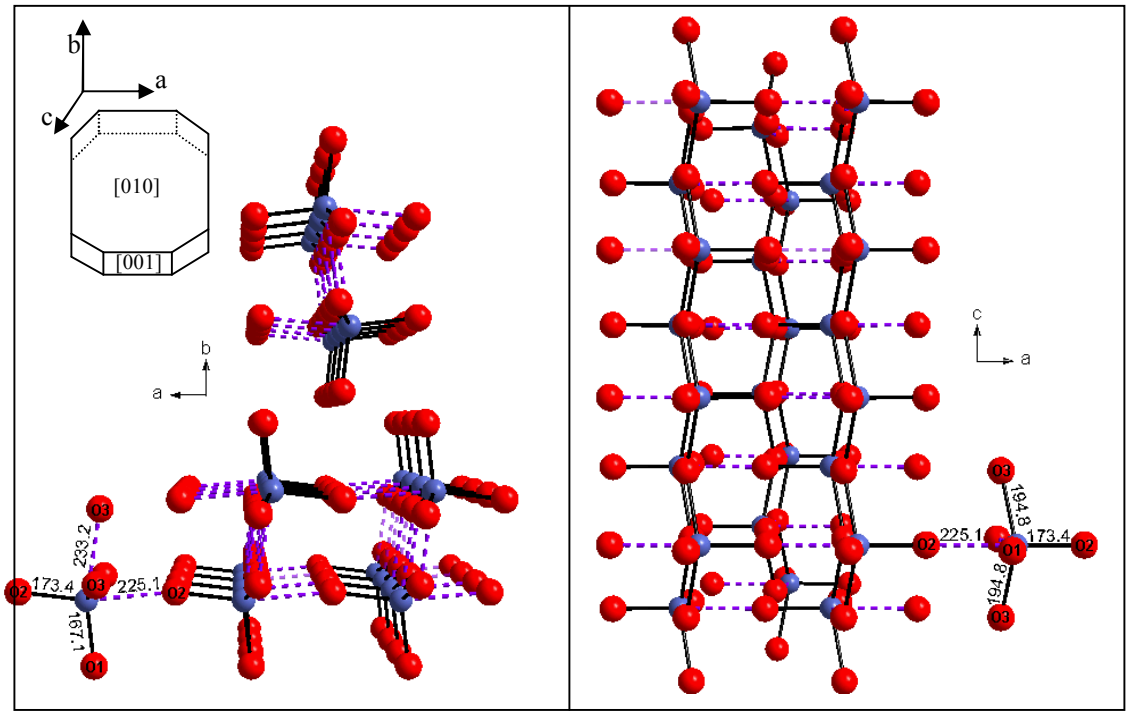

Figure 5. Different planes of the crystal structure of α-MoO_3. View along the (001) plane (left). View on the basal (010) plane. Bond lengths are given in pm. Oxygen atoms are given in red and molybdenum atoms in blue color. Dashed lines represent long distance bonds. Top left: schematic representation of the typically observed crystal morphology of α-MoO_3.

For the calcined film the band intensity at 995 cm^{-1} is extremely high and nearly doubles the intensity for the bridging Mo-O-Mo bonds at 820 cm^{-1}. On the other hand the band intensity at 1006 cm^{-1} is in the range normally observed for the band at 995 cm^{-1}.

A band between 1000 and 1010 cm^{-1} has been observed occasionally for crystalline α-MoO_3 but it is usually only recognized if the spectra are highly magnified (*Figure 4 inlet*). The origin of this band has been assigned differently by various authors and is still under debate. Py and Maschke observed a very weak Raman band at 1002 cm^{-1} for α-MoO_3 single crystals and explained it as an IR active crystal mode resulting from the longitudinal-transversal splitting of the (Mo=O) B_u mode of a single α-MoO_3 layer.[14] Mestl *et al.* found a band around 1006 cm^{-1} for ball-milled α-MoO_3 and assigned it to newly formed Mo=O bonds, due

to the generation of oxygen vacancies (defects) during the mechanical treatment.[15] Stencel *et al.* observed an unusual high I_{995}:I_{820} ratio for supported molybdenum oxide on large surface area silica.[16] They argue that such high intensity of the band at 997 cm^{-1} cannot origin from bulk crystalline α-MoO_3 and hence correlate the band to highly dispersed MoO_x-species. However they did not detect any band above 1000 cm^{-1}. Marchi *et al.* prepared two supported MoO_x/SiO_2 samples with different loadings of Mo. For a 5 wt% Mo sample they observed a high I_{995}:I_{820} ratio and for a 1.6 wt% Mo sample they detected only the band at 995 cm^{-1} without any band around 800 cm^{-1}.[17] They assigned the single band at 995 cm^{-1} to a monomeric octahedral surface species. Wachs *et al.* investigated molybdenum surface oxide species on various supports under dehydrated conditions and conclude that dehydration shortens the terminal Mo=O bond due to the absence of hydrogen bonding and consequently shifts the vibration to above 1000 cm^{-1}.[18, 19, 20] For the samples analyzed by Wachs, the high energy band was only observed when no crystalline α-MoO_3 was present due to the low Mo loading. More recently Gaigneaux *et al.* prepared molybdenum oxide thin films on Si [100] wafers by spin-coating peroxo-polymolybdic solutions.[21] The preparation method and the thermal treatment were very similar to ours. In fact they observed equal intensities for bridging (820 cm^{-1}) and terminal (995 cm^{-1}) bands. Though they did not discuss the unusual Raman intensities, they deduced from the shape and the relative intensities of the XRD reflections a rather small crystallite size (~100 nm) and an unusual morphology with higher relative amounts of lateral faces.

As molybdenum oxides are of great interest in many fields of applications we found quite a lot of literature on Raman spectroscopic investigations. However, to the best of our knowledge there is no report on a α-MoO_3 Raman spectrum showing such high relative intensities for I_{995} and I_{1006} as presented in this work in *Figure 4*.

In order to elucidate the question whether the microstructure of the material, and in particular defects in the α-MoO_3 structure, are responsible for the band at 1006 cm^{-1}, HRTEM on cross-

sections of the calcined films were performed (*Figure 6*). The two HRTEM images shown in *Figure 6b* and *6c* are representative of the two types of areas and their corresponding structural characteristics mainly observed for the calcined films.

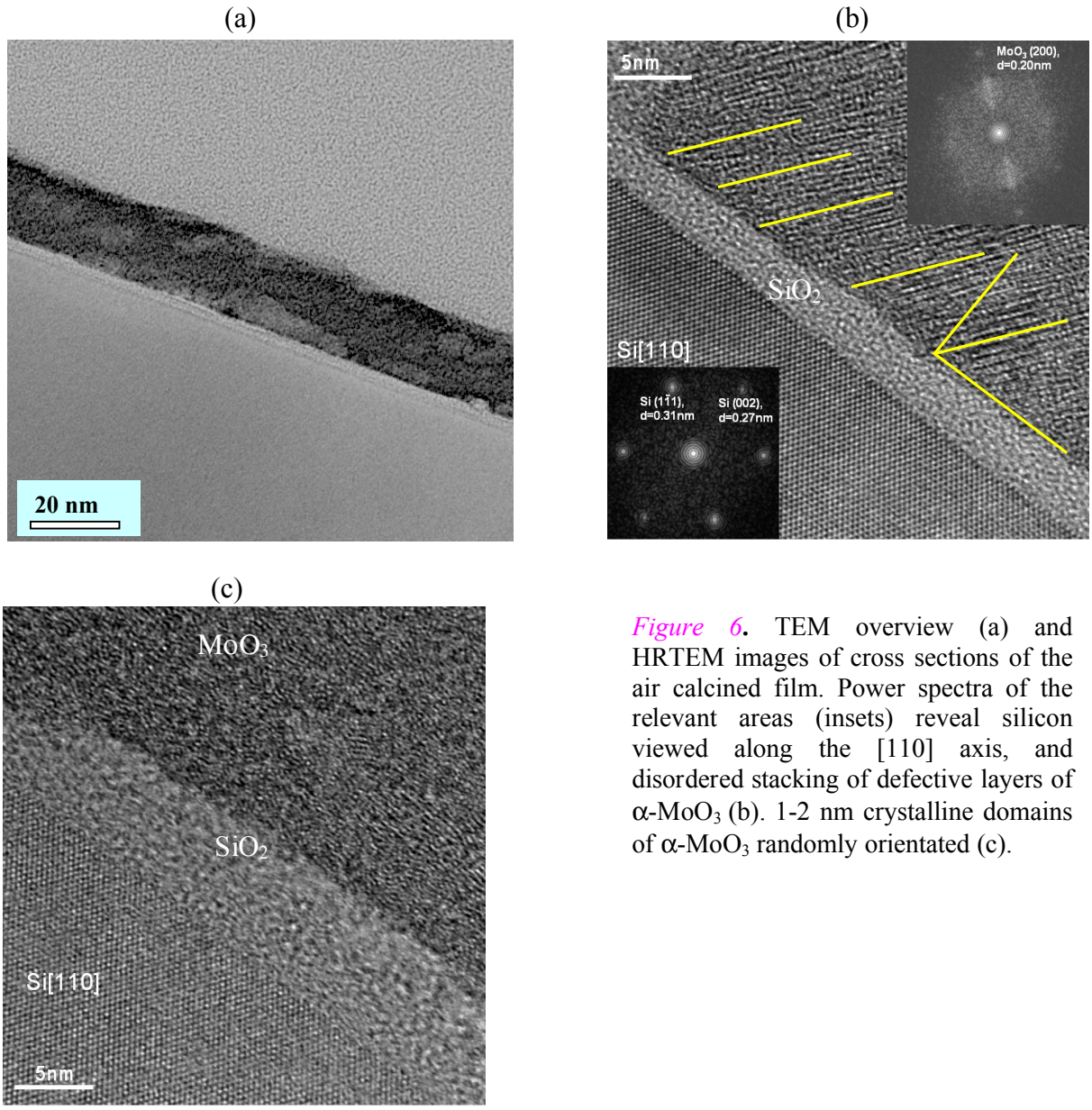

Figure 6. TEM overview (a) and HRTEM images of cross sections of the air calcined film. Power spectra of the relevant areas (insets) reveal silicon viewed along the [110] axis, and disordered stacking of defective layers of α-MoO_3 (b). 1-2 nm crystalline domains of α-MoO_3 randomly orientated (c).

Generally three different layers can be identified (*Figure 6b*): the well ordered single crystalline Si [110], a thin and amorphous SiO_2 layer (3-5 nm) and the top molybdenum oxide layer of about 20 nm (*Figure 6a*). One type of areas consist of a disordered stacking of molybdenum oxide at angles between 20° and 60° parallel to the surface (*Figure 6b*). The lattice fringe separation corresponds in general to the (200) planes of α-MoO_3 as seen in the

Fourier Transform (*inlet Figure 6a*). However, the lattice fringes reveal irregularities indicating highly defective states of the crystalline material. The other type of areas is characterized by the microstructure shown in *Figure 6c*. The image reveals a dense arrangement of randomly oriented 2-3 nm crystalline domains.

As already described above, for α-MoO_3 crystals the (001) faces are the least exposed. From *Figure 3* one can see that the two short molybdenum oxygen bonds are lying parallel to the (001) plane. It is known from α-MoO_3 single crystal Raman data that the band at 995 cm^{-1} is highly polarized and that the polarizability is anisotropic, *i.e.* the electrons forming the bond are more easily displaced by an electric field applied along the bond axis than one across this direction.[22] In other words, if a laser beam interacts with α-MoO_3 perpendicular to the (001) plane, the electric field is parallel to the terminal Mo=O bonds and the induced dipole moment is largest. The discussed thin film on the one hand has areas of very small crystalline domains without any preferential growth and thus equal amounts of exposed faces and on the other hand small areas are present, where the (001) planes are exposed to the surface. Both facts together are the reason for the unusual and unique high intensity of the 995 cm^{-1} band.

Consequently, we assign the band at 1006 cm^{-1} to terminal Mo=O bonds from highly distorted and coordinatively unsaturated molybdenum centers, as a result of the nanometer crystallite size. This seems reasonable as we were not working under dehydrated conditions. Hence, even if a monolayer or monomeric surface species would have been present, it should not have been detected due to hydration. In principle the band at 1006 cm^{-1} can be described as a defect band similar to what Mestl *et al*. have achieved by mechanical treatment.[15]

Within this context it is worth mentioning that for 2-3 nm sized $Ce_{1-x}Zr_xO_2$-nanoparticles a band at 1003 cm^{-1} was observed whereas in the bulk Raman spectrum of the corresponding oxide this band was absent.[23] In another, very recent investigation, a band at 1002 cm^{-1} was detected for crystalline magnetite nanoparticles of about 15 nm size.[24] Again this band is not

present in the bulk spectrum of magnetite. It is likely that the origin of the band at around 1000 cm^{-1} is in all three cases the same, namely the nanometer crystallite size leading to a high ratio of distorted, coordinatively unsaturated metal centers with strong terminal oxo-bonds.

Conclusions

Defective, short Mo-O bonds on the surface generate basic, nucleophilic oxygens sites which are necessary for C-H bond activation, thus leading to reactive catalysts. The synthetic control of defects is therefore a key requirement for the generation of active catalysts. We have shown that the formation of polyoxomolybdate thin films on a silicon substrate by spin coating of alkoxides solutions represents a possibility to mimic and transfer the "real" catalyst preparation chemistry to flat substrates. The thermal treatment of the polyoxomolybdate film results in the decomposition of the ligands (NH_3, H_2O, CO_2) followed by a polycondensation process leading to highly defective α-MoO_3. Regarding this concept preliminary experiments have shown that the films prepared in this study can be used as active catalysts in the partial oxidation of alkenes. The formation of a defective nanostructured oxide thin film on a conducting substrate will permit the investigation of structure-activity relationships by combining *in situ* bulk and surface analytic methods.

Moreover the formation of nanostructured mesoporous polyoxometalate films on silicon is an interesting subject itself and should be investigated in more detail.[25] The vast variety of polyoxometalates and their unique redox, magnetic, photochemical and conductivity properties make them ideal candidates for nano-engineered materials.

References

[1] J.W. Niemantsverdriet, A.F.P. Engelen, A.M. de Jong, W. Wieldraaijer, G.J. Kramer, A*ppl. Surf. Sci.* **84** (1995) 339.

[2] Pablo Beato, *PhD thesis*, TU Berlin 2005 (Chapter 1). *See also* P. Beato, T. Ressler, O. Timpe, R. Schlögl, will be submitted to *Chem. Eur. J.*

[3] R. Anderson, S. J. Klepeis, *MRS Symposium Proceedings* **480** (1997) 193.

[4] S. Himeno, H. Niija, T. Ueda, *Bull. Chem. Soc. Jpn.* **70** (1997**)** 631.

[5] K. H. Tytko, B. Schönfeld, *Z. Naturforsch.* **30 b** (1975) 471.

[6] J. Fuchs, I. Brüdgam, *Z. Naturforsch.* **32 b** (1977) 853.

[7] M. L. Niven, J. J. Cruywagen, J. B. B. Heyns, J. Chem. Soc. Dalton Trans. (1991) 2007.

[8] A. J. Bridgeman, *J. Phys. Chem. A* **106** (2002) 12151.

[9] C. C. Williams, J. G. Ekerdt, J.-M. J. Jehng, F. D. Hardcastle, A. M. Turek, I. E. Wachs, *J. Phys. Chem.* **95** (1991**)** 8781.

[10] T. Ono, M. Anpo, Y. Kubokawa, *J. Phys. Chem.* **90** (1986) 4780.

[11] B. L. Mojet, L. Coulier, J. van Grondelle, J. W. Niemantsverdriet, R. A. Van Santen, *Catal. Lett.* **96** (2004) 1.

[12] J. Wienold, R. E. Jentoft, T. Ressler, Eur. *J. Inorg. Chem.* (2003), 1058.

[13] M. A. Py, P. E. Schmid, J. T. Vallin, *Il Nuovo Cimento* **38B** (1977) 271.

[14] M. A. Py, K. Maschke, *Physica* **105B** (1981) 370.

[15] G. Mestl, T. K. K. Sirinivasan, H. Knözinger, *Langmuir* **11** (1995) 3795.

[16] J. M. Stencel, J. R. Diehl, J. R. D'Este, L. E. Makovsky, L. Rodrigo, K. Marcinkowska, A. Adnot, P. C. Roberge, S. Kaliaguine, *J. Phys. Chem.* **90** (1986**)** 4739.

[17] A. J. Marchi, E. J. Lede, F. G. Requejo, M. Renteria, S. Irusta, E. A. Lombardo, E. E. Miro, *Catal. Lett.* **48** (1997) 47.

[18] I. E. Wachs, *Catal. Today* **27** (1996) 437.

[19] J. M. Jehng, H. Hu, X. Gao, I. E. Wachs, *Catal. Today* **28** (1996) 335.

[20] B. M. Weckhuysen, I. E. Wachs, *Handbook of Surfaces and Interfaces of Materials, Vol. 1* (2001) 613.

[21] E. M. Gaigneaux, K. Fukui, Y. Iwasawa, *Thin Solid Films* **374** (2000) 49.

[22] G.-A. Nazri, C. Julien, *Solid State Ionics* **53-56** (1992) 376.

[23] A. S. Deshpande, N. Pinna, P. Beato, M. Antonietti, M. Niederberger *Chem. Mater.* **16** (2004) 2599.

[24] N. Pinna, S. Granvarov, P. Bonville, P. Beato, M. Antonietti, M. Niederberger, *accepted in Chem. Mater.*

[25] "*Polyoxometalate Chemistry From Topology via Self-Assembly to Applications"*, ed. M. T. Pope, A. Müller, Kluwer Academic Publishers (2001).

[26] S. Xie, K. Chen, A. T. Bell, E. Iglesia, *J. Phys. Chem. B* **104** (2000) 10059.

Chapter 4

Complex catalysts on flat substrates - Bridging the materials gap in heterogeneous catalysis

Parts of this chapter will be submitted for publication:
Pablo Beato, Annette Trunschke, Siegfried Engelschalt, Jakob B. Wagner, Gisela Weinberg, and Robert Schlögl "Complex catalysts on flat substrates – Bridging the materials gap in heterogeneous catalysis".

Introduction

Heterogeneous catalysis is a research area where engineering, chemistry and physics meet. A problem arising from the fusion of disciplines is the fact that research is conducted frequently in separate channels of investigation leading to a mismatch of knowledge. Thus, surface scientists restrain their efforts mainly on single crystals under high vacuum conditions, whereas chemists

are often confined to industrial complex systems. This has led to the so called *pressure* and *materials gap* rendering the transfer of knowledge very difficult. In the last years efforts have been undertaken to design new experiments such as high pressure *in situ* XPS which make the investigation of samples by surface science methods under more realistic conditions possible.[1] A major drawback is the supply of adequate samples to investigate, because charging effects and surface roughness of real powder catalysts make the reliable analysis by surface science methods very difficult. Therefore, we have tried to prepare new model materials that preserve as much as possible of the structural complexity of real catalysts but at the same time stay accessible to both surface science and bulk analytical techniques. A promising strategy to meet these requirements is to deposit a thin film or nanoparticles on an inert, conducting substrate, such as silicon.[2] In a second step the structural and catalytic properties of the model catalyst have to be compared with the same catalyst in its real state, which is usually a powder pellet. If the thin film model is able to catalytically mimic the complex powder catalyst, the model can be used to investigate the structural and electronic surface properties by surface science methods, ideally under *in situ* conditions. The obtained knowledge can then be transferred much easier to complex catalysts such as multi metal oxides (MMO). This would be of tremendous importance since there is a great need for a better understanding of the working mechanisms of complex MMO's used for the partial oxidation of light alkanes.

In the following a new synthesis method for smooth thin films of MMO's is presented and an attempt is made to show the high potential of such complex model systems in heterogeneous catalysis. We have selected the partial oxidation of propene on a Mo-V-W mixed oxide catalyst as a test system for three reasons: (1) the catalyst has been proven to be highly active for the selective oxidation of alkenes and acrolein; (2) the powder synthesis conditions have been investigated in detail over the last years in our department and (3) the elemental composition is close to that of the industrial catalysts for acrolein selective oxidation to acrylic acid.

Experimental

Silicon [100] wafers (p-type doped with boron [15 mOhm x cm] from Silchem®) were cut into pieces of 10.0 x 10.0 x 0.7 mm. The cleaning procedure for the Si-wafers consisted in successive ultrasonic cleaning in chloroform, acetone, ethanol and bi-distilled water. After wet cleaning the Si-wafers were oxidized at 800°C in air to generate a thin SiO_2 film of about 5 nm thickness. The Mo-V-W mixed oxide powder catalyst (relative atom ratio = 0.68:0.23:0.09) has been prepared according to the method described by Knobl *et al.* via spray-drying of mixed solutions of ammonium heptamolybdate (AHM; Merck, p.a.), ammonium metatungstate (AMT; Fluka; purum, >85% WO_3 gravimetric), and vanadyl oxalate of the respective transition metal concentrations.[3]

The thin film catalysts were prepared via a gelatin-polyoxometalate composite gel by dissolving 1wt% of the spray dried powder in a 1wt% gelatin (Sigma®, Type A, ~300 Bloom) water gel at 60°C. The obtained sol was subsequently filtered through a micro-filter (Ø = 0.2 µm) and cooled down to 37°C before spin-coating at 5000 rpm on the silicon [100] substrate. The as prepared thin films were dried over night at 37°C and then pre-calcined for 3 h at 573 K in static air (heating ramp 2K/min). The pure spray dried polyoxometalate powder was calcined for 2 h at 623 K in air (5 K/min). For the catalytic tests the spray dried powder was pressed into a pellet (8 mg, Ø = 5 mm, 25 bar) and countersunk in a specially prepared silicon wafer, containing a cavity of the precise pellet size (*Figure 1b*).

A new type of quartz glass micro-reactor was built which allows to investigate the powder and thin film catalysts under the same reaction conditions by *in situ* Raman spectroscopy (*Figure 1*). The reactor consists of a stack of three quartz plates. The middle plate is micro-structured carrying the catalyst, the reaction channels and grooves for thermocouples (Ø = 0.5 mm). The catalyst can be mounted in the reactor as a thin foil, or as a coated carrier plate. Removable heating elements are located in cut-outs of the base plate (*Figure 1b*).

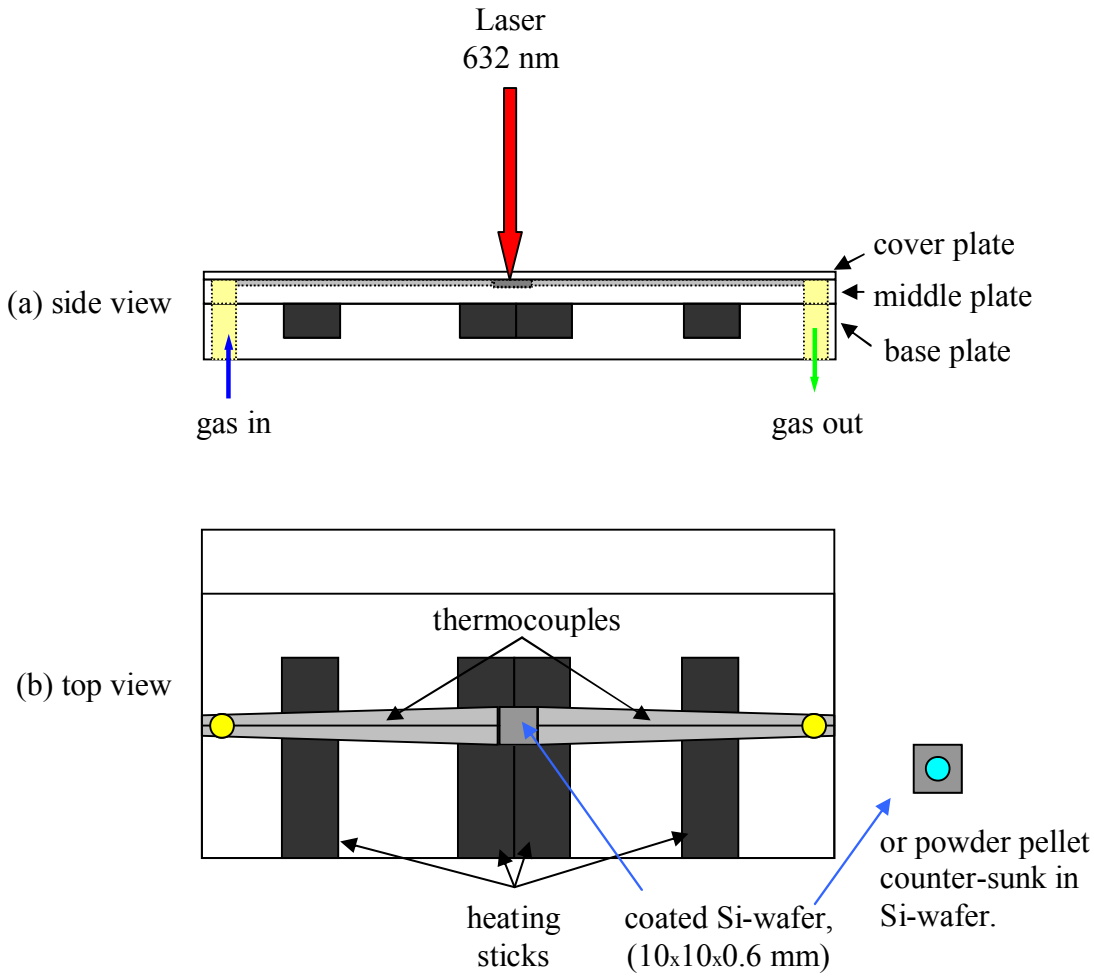

Figure 1. Schematic drawing of the self made quartz plate micro-reactor, which was used for the thin films and powder pellets; (a) side view showing the three plates and the incident laser beam; (b) top view showing the gas channel and the catalyst wafer.

A Labram system from Yobin Yvon equipped with a confocal microscope (Olympus) and a He/Ne laser (15mW) was used for the Raman investigation. The parameters used for spectra acquisition of the thin films were: 50x long distance objective (NA = 0.75, Olympus), slit 500 µm, confocal hole 200 µm, integration time 300 seconds with 3 averages. For the powder pellets the confocal hole was set to 500 µm and the integration time could be reduced to 120 seconds. Filters were used to reduce the laser power at the sample to ~ 1mW (measured by power meter). The educt gas compositions and flows were controlled by mass flow controllers (Bronkhorst). Propene (Messer, 99.95%) and oxygen (Westfalen, 99.999%) were used as

reactants and He (Westfalen, 99.999%) as an inert diluent. The total flow of reactants was 1 ml/min consisting of 10 vol% propene and 20 vol% O_2 balanced by He.

Part of the gas outlet from the micro-reactor was fed into a proton-transfer-reaction mass spectrometer (PTR-MS, IONICON ANALYTIK) used for reaction product analysis. This system is based on the principle of chemical ionization using H_3O^+ as the proton donator combined with the swarm technique of the flow tube type. It is especially suitable for a qualitative and quantitative product analysis at ppb level.[4, 5] In order to be able to directly compare the results of different measurements, the amount of propene fed into the PTR-MS was adjusted to 7 ppm before reaction.

Results and Discussion

Preparation of a smooth mixed oxide thin film via an inorganic-organic hybrid gel.

Industrial mixed oxide catalysts are mostly prepared via co-precipitation from aqueous solution or by wet impregnation, and it is now widely accepted that the exact conditions during the synthesis of complex oxide catalysts can play a decisive role for the final properties of the catalyst.[10] Therefore, it is obvious that the preparation method of a realistic model system for complex oxide catalysts must be selected very carefully.

The high surface tension and low vapor pressure of water inhibits the use of aqueous solutions for the preparation of dense and closed thin films. Inspired by the fabrication of photographic paper we have developed a new method to prepare smooth mixed oxide films by suspending the spray dried catalyst powders in gelatin gels. The gelatin method has the advantage that one can use the original spray dried powder catalyst for the thin film preparation, thereby avoiding deviations from the original synthesis method.

Only few reports dealing with the interaction between gelatin and inorganic material have been found in the literature. Apart from the photographic process most work has been conducted in the field of biomineralization.[6, 7] Recently Coradin *et al.* reported on the synthesis of silica-

gelatin nano-composite material.[8] To the best of our knowledge no investigations concerning the use of gelatin for the preparation of inorganic oxide thin films have been reported so far.

As a biopolymer gelatin is very sensitive to changes in temperature and pH. By simply increasing the temperature a few degrees Kelvin above a critical value the three dimensional ordered helical structure of gelatin transforms to randomly orientated coils. The delicate behavior of gelatin gels towards external parameter variation, forces the experimenter to strictly keep the experimental conditions constant if reliable results are to be obtained. On the other hand it is exactly this sensitive behavior and the possibility to chemically modify gelatin that offers a great synthetic potential. By changing the relative amounts of gelatin to reactant at variable temperatures, a great variety of different morphologies within the same system can be obtained.

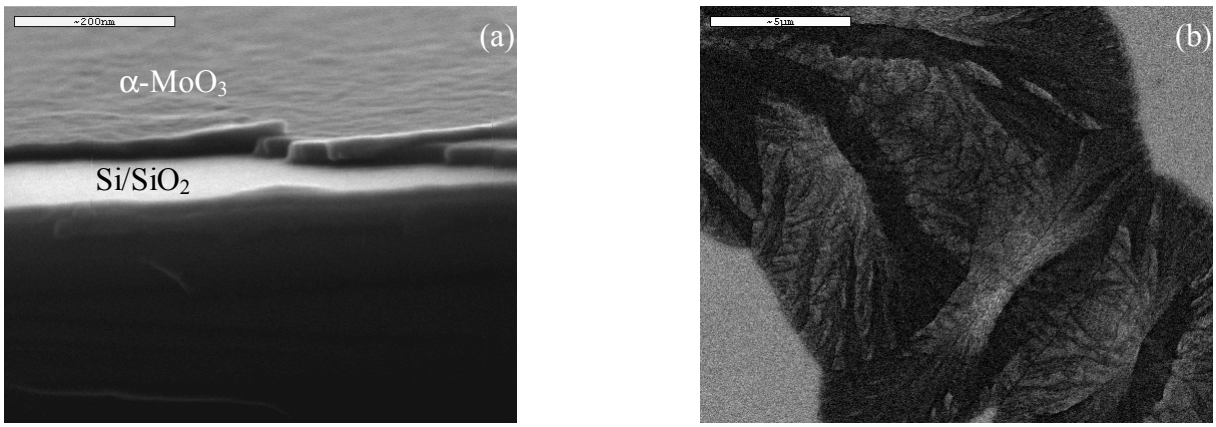

Figure 2. SEM images demonstrating the effect of different AHM to gelatin gel compositions on the morphology of the resulting α-MoO_3. (a) Smooth ~ 25 nm thick α-MoO_3 film on silicon via spin-coating (scale bar is 200 nm); (b) helical α-MoO_3 morphology of (Ø = ~15 µm) obtained by spin-coating gelatin composite fibres on silicon (scale bar is 5 µm).

We have observed a strong interaction between some of the used polyoxometalate precursors and the gelatin leading to gummy masses, which at specific concentrations could be used to extract fibers out of the gelatin-polyoxometalate mixture. From the mixture of AHM and gelatin fibers were spun on the silicon wafers and calcined at 573 K in air. As a result α-MoO_3 particles with helical morphology were obtained (*Figure 2b*). However, we were able to obtain smooth

thin films, which could be varied in thickness from a few nanometers to several microns, by simply increasing the concentration of gelatin in the gel at constant amount of polyoxometalate (*Figure 2a*).

Based on our observations and considering the few examples found in the literature, it seems worth to further investigate the potential of gelatin-inorganic mixed gels for the synthesis of materials such as organic-inorganic hybrids.

Selective oxidation of propene.

Before starting the catalytic tests, several blind tests were carried out, which proved the reactor system containing an uncoated silicon wafer to be inactive for propene oxidation below 723 K. Reactions were therefore performed at different temperatures but never higher than 713 K. Additional temperature limitations were imposed due to the apparently lower sublimation temperature of the thin films compared to the powder pellets. While for the pellets sublimation was observed to start at around 713 K, in the case of the thin films first deposits on the reactor cover plate were observed at around 673 K (*see below*).

The catalytic data for the thin film is displayed in *Figure 3*. Since it was impossible to measure the activity of the thin films with an ordinary quadrupole mass spectrometer, a PTR-MS (*see experimental part*) was used for product analysis. The major drawback of this analytic technique is that the products of total oxidation (CO_x) can not be detected, thus permitting only a qualitative analysis of the data. However, the observed temperature dependence and the distribution of the partial oxidation products shown in *Figure 3* for the thin film, and in *Figure 4* for the powder pellet, provide valuable information about the characteristics of the catalysts.

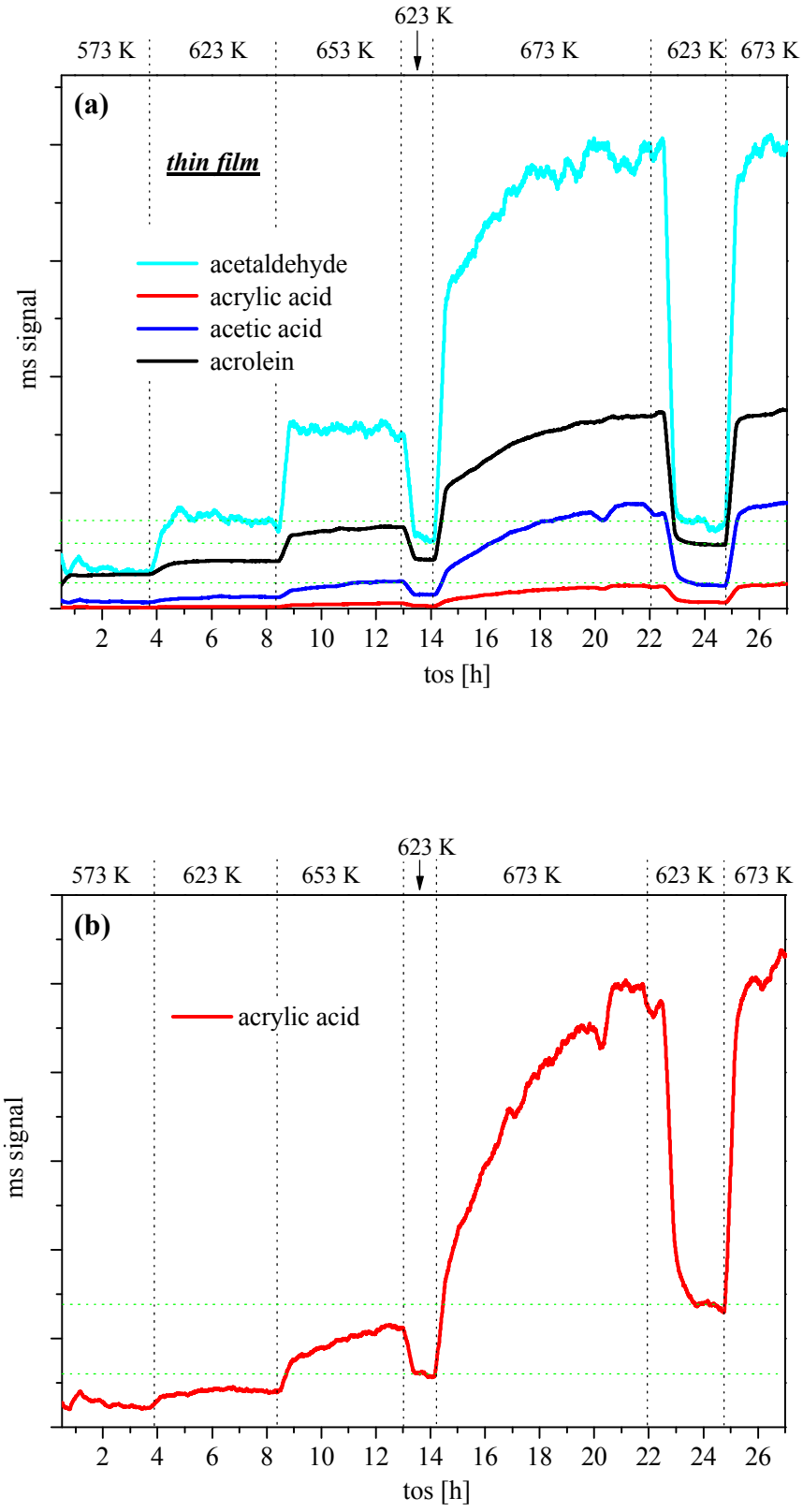

Figure 3. Course of the different products from partial oxidation of propene over the Mo-V-W mixed oxide **thin film**. Temperatures are displayed at the top of the graphs. (a) Main selective oxidation products, overview; (b) magnification of the course for acrylic acid.

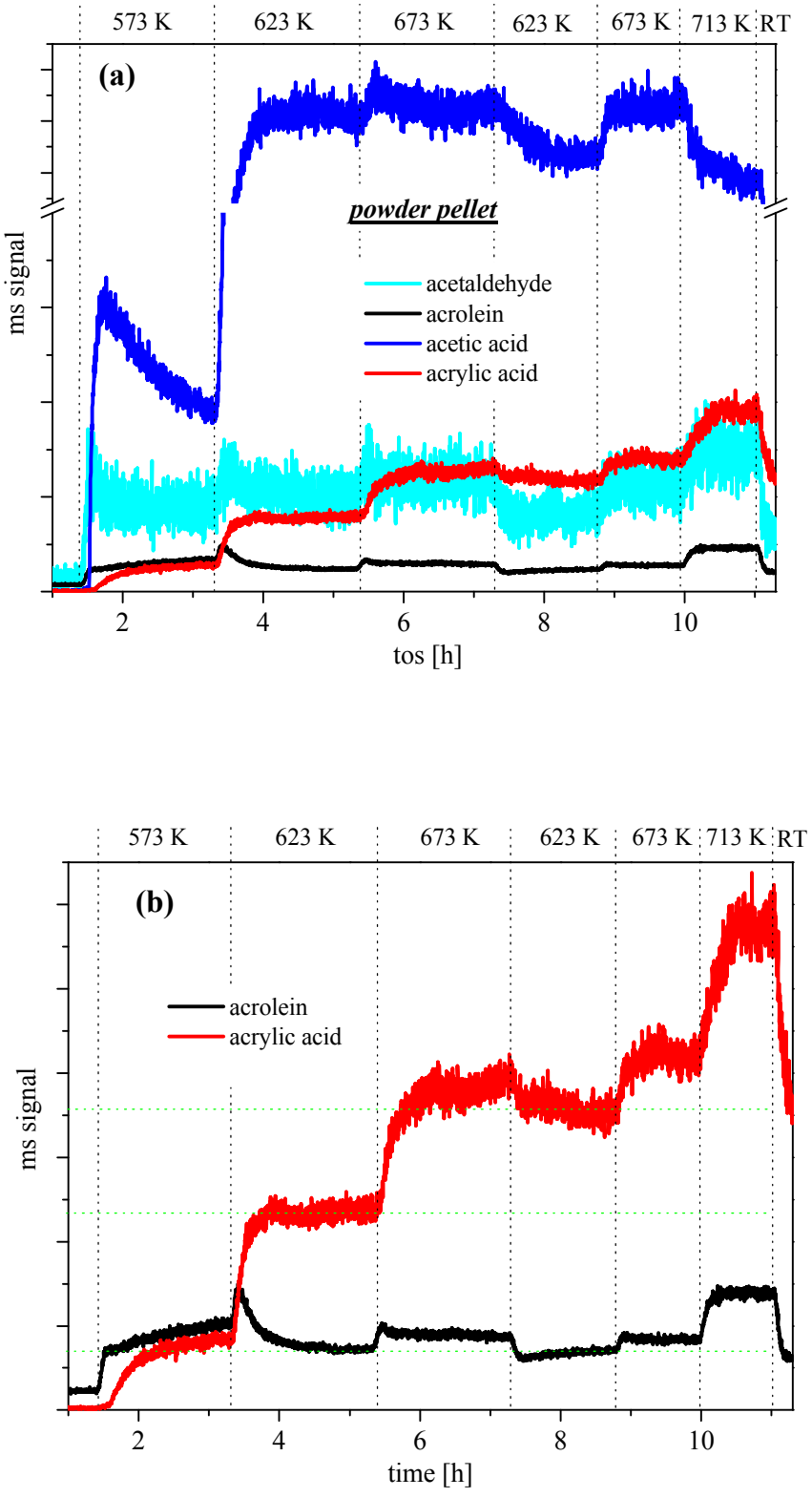

Figure 4. Course of the different products from partial oxidation of propene over the Mo-V-W mixed **powder pellet**. Temperatures are displayed at the top of the graphs. (a) Main selective oxidation products, overview; (b) magnification of the course for acrylic acid (red) and acrolein (black).

On the thin film propene is converted to selective partial oxidation products, namely acetaldehyde, acrolein, acetic acid and acrylic acid (*Figure 3a*). In order to detect a possible activation of the film during reaction, a comparison of the activity for the selective oxygenates at 623 K was performed repeatedly. Activation is observed for all partial oxidation products but is especially large in the case of acrylic acid (*Figure 3b*). After 7 h time on stream at 673 K the activity of the thin film towards acrylic acid at 623 K has been doubled!

For the powder pellet the catalytic data under the same reaction conditions in the same reactor is shown in *Figure 4*. The same selective oxidation products as for the thin film are observed. However, it is obvious that the relative amounts of oxygenates is markedly different for the two catalyst systems. Whereas for the thin film the order of decreasing product amount after the first hours in the feed is acetaldehyde > acrolein > acetic acid > acrylic acid, for the powder pellet the order of decreasing product amount goes acetic acid > acrylic acid > acetaldehyde > acrolein. The main product on the powder pellet, acetic acid, is further oxidized at 713 K and decreases rapidly (*Figure 4a*). Conversely, the amount of acrylic acid increases further at 713 K. Acrolein and acetaldehyde are not affected that drastically by the increased temperature. It is interesting to note that the two aldehydes behave rather similar during the reaction steps and no activation is observed for them, whereas the two acids show contrary mass signals.

Important for the information transfer between thin film and powder pellet is that both show a very strong enhancement of the selectivity towards acrylic acid as compared to the other oxygenates (*Figures 3b, 4b*).

Microstructure.

Unfortunately the XRD and TEM investigations on the thin films was still in progress and only available for the powder catalysts at the end of the thesis. In addition to the Raman data (*next section*), SEM images of the thin film before and after the catalytic test reaction were performed (*Figure 5*). During the test reaction the smooth and about 20 nm thick film (height verified from

SEM cross-section) transforms into a dense arrangement of randomly orientated nanometer sized clusters.

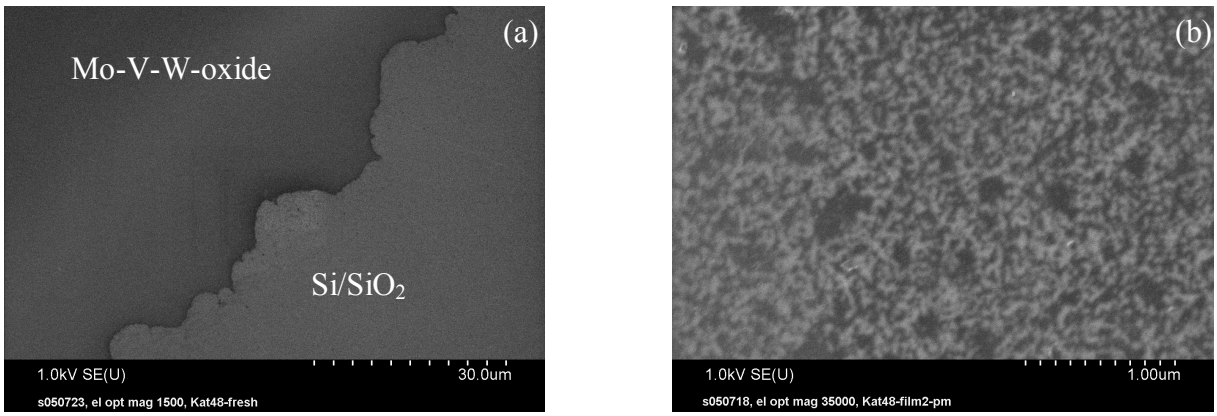

Figure 5. Scanning electron micrographs showing a top view on the thin film catalyst before (a) and after (b) test reaction in propene and oxygen at 673 K. For the image of the thin film before reaction an area at the border of the silicon substrate was selected to show the smoothness of the precalcined film compared to the silicon substrate.

In *Figure 6* the XRD patterns of the powder catalyst before and after reaction are shown. The most intense reflex at $2\theta = 22.29°$ is not distinctive enough, since a reflex around 22° (2θ) is observed in many molybdenum suboxides (*e.g.* Mo_5O_{14}, Mo_4O_{11}, Mo_8O_{23}, Mo_9O_{26}).[11] Other reflexes of the pre-calcined powder are too broad to be used for a unequivocal structure assignment. Various studies from our institute on the thermal behavior of the $Mo_{0.68}V_{0.23}W_{0.09}$ mixed oxide catalyst under different gases revealed that the thermal pre-treatment of the spray-dried precursor at 623 K in air or at 673 K in nitrogen results in a poorly nanocrystalline Mo_5O_{14} type structure, containing sometimes small amounts of nanocrystalline α-MoO_3.[3, 12, 13] As the XRD pattern in *Figure 6a* is not explicit but resembles the patterns presented by the cited authors, a similar mixture of products was supposed to be present in our powder samples. The SEM and HRTEM images shown in *Figure 7* support the existence of nanometer sized crystalline areas but additionally indicate that great part of the pre-calcined sample remains amorphous at this stage. Part of the spray dried, spherical particles have

smooth morphology but some of them are riddled with elongated nanometer sized flat needles, which grow perpendicularly out of the surface of the spheres.

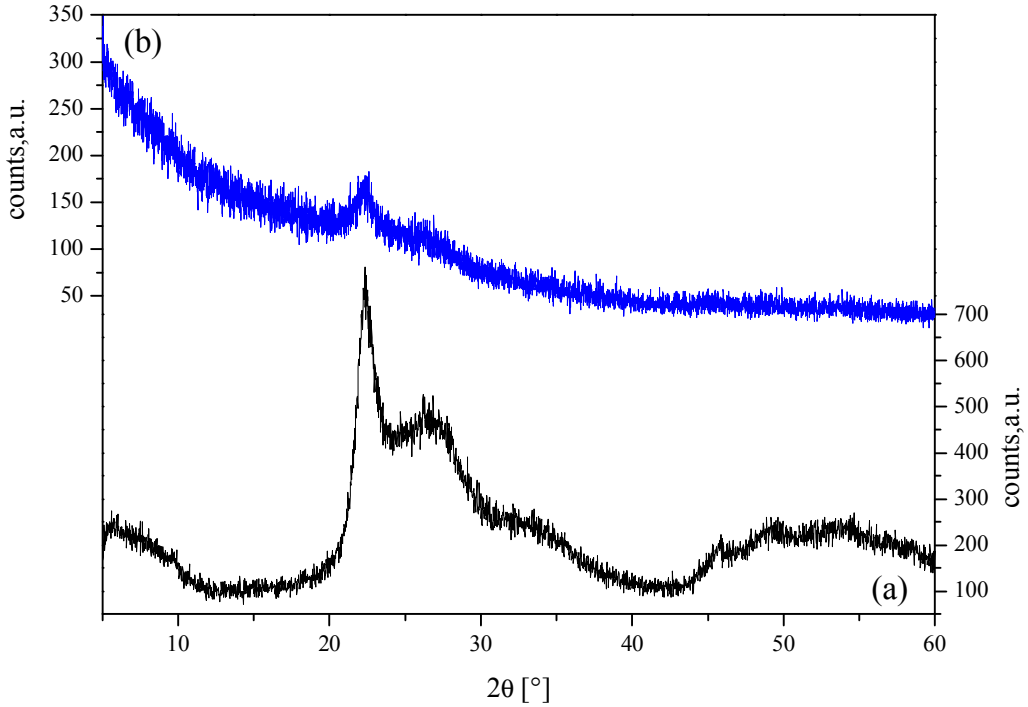

Figure 6. XRD pattern of the powder pellet catalyst before (a) and after (b) the catalytic test. Before the catalytic test the powder was pretreated for 2h at 623 K in air.

The size of the needles is relatively large, reaching up to 50 nm in length and about 15 nm breadth wise. However, lots of defects are observed resulting in the rather poor crystallinity of the needles (*Figure 7c, d*).

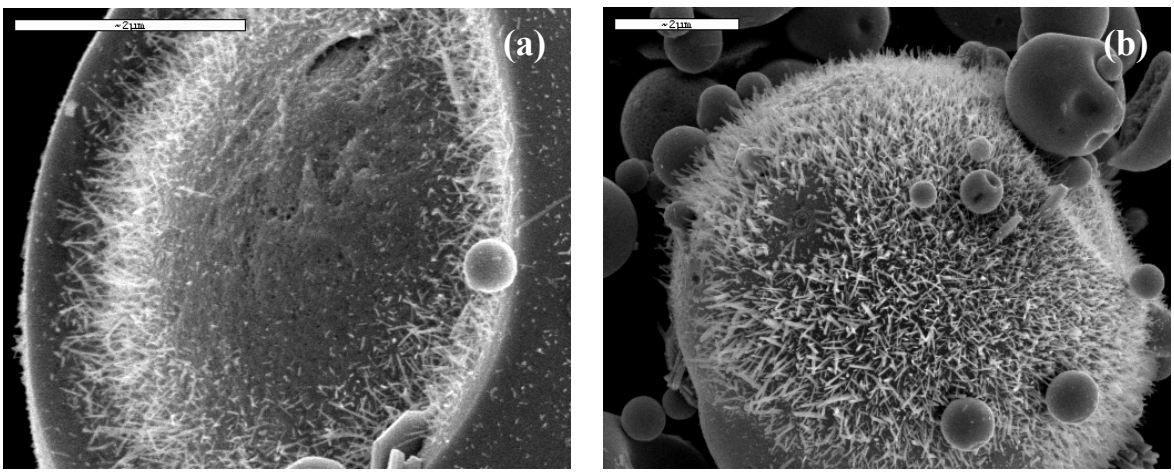

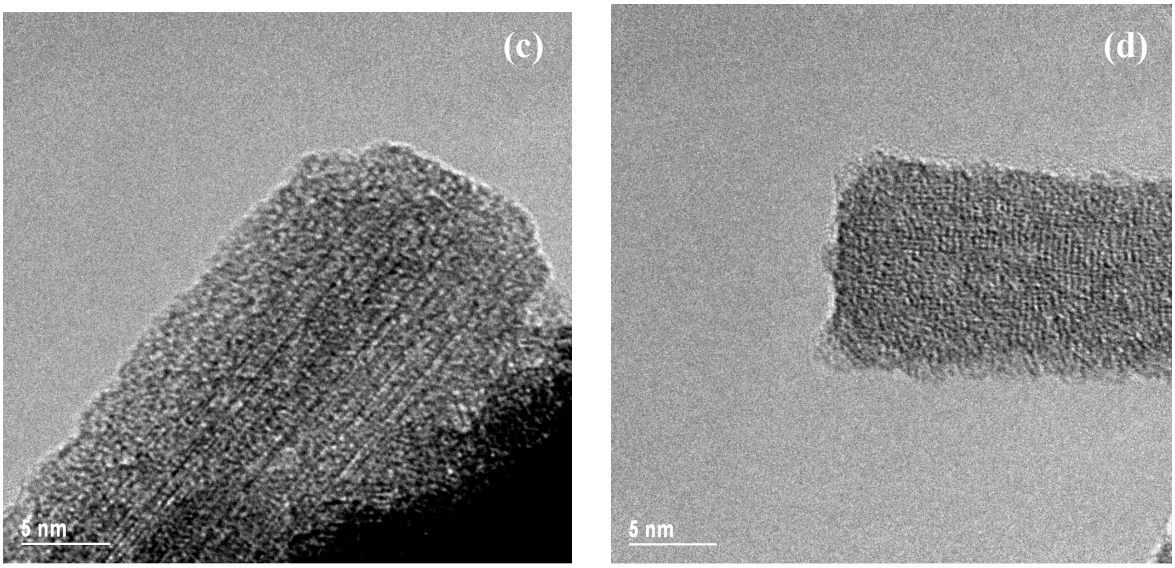

Figure 7. SEM (a, b) and HRTEM (c, d) images of precalcined sample before reaction.

For the structural evolution of the Mo-V-W oxide system at higher temperatures contrary results were found in the literature. Dieterle *et al.* found that for a $Mo_{0.64}V_{0.27}W_{0.09}$ composition the Mo_5O_{14} type structure crystallizes in a nanocrystalline form at 803 K, being the major crystalline phase in the narrow temperature range from 803 to 818 K.[14] The decomposition into MoO_3 and MoO_2 started at temperatures higher than 823 K.[14] Knobl *et al.* observed the formation of a single-phase compound of Mo_5O_{14}-type structure after heating a catalyst of the composition $Mo_{0.68}V_{0.23}W_{0.09}$ first at 623 K in air (pre-treatment) and then in helium at 713 K.[3] Both authors confirm that crystallization to the Mo_5O_{14} structure is enhanced under reaction conditions of selective oxidation of acrolein. Recent investigations in our department have shown that calcination parameters as gas flow conditions, heating rate, partial gas pressure and even calcination-tube design have large effects on the crystallinity of the final product.[15]

As the highest temperature for the pellet during the catalytic testing was 713 K, the crystallinity of the sample was expected to increase only moderately during reaction. Surprisingly, the XRD pattern of *Figure 6b* suggests that the crystallinity is even reduced during reaction. This is remarkable since the catalyst has been treated for over 10 h at elevated temperatures.

Nevertheless, one has to keep in mind, that the experimental conditions were quite different from the ones applied in the literature since no water vapor was added in the feed and propene instead of acrolein was used.

SEM and HRTEM were applied to reveal the structural changes that occurred during the reaction and to explain the unusual XRD pattern for the powder pellet after reaction (*Figure 8*). From the SEM images it appears that the total amount of structured material has increased probably due to the crystallization of the former amorphous parts of the sample. The HRTEM images give an indication for the unexpected changes in the XRD pattern after reaction (*Figure 8c-f*). Some of the typical needle shaped crystals can still be found but much less in abundance. Instead, very small spherical crystals of 5-10 nm in diameter were grown (*Figure 8c, d*) which, to some extent, condense to form larger aggregates (*Figure 8e, f*).

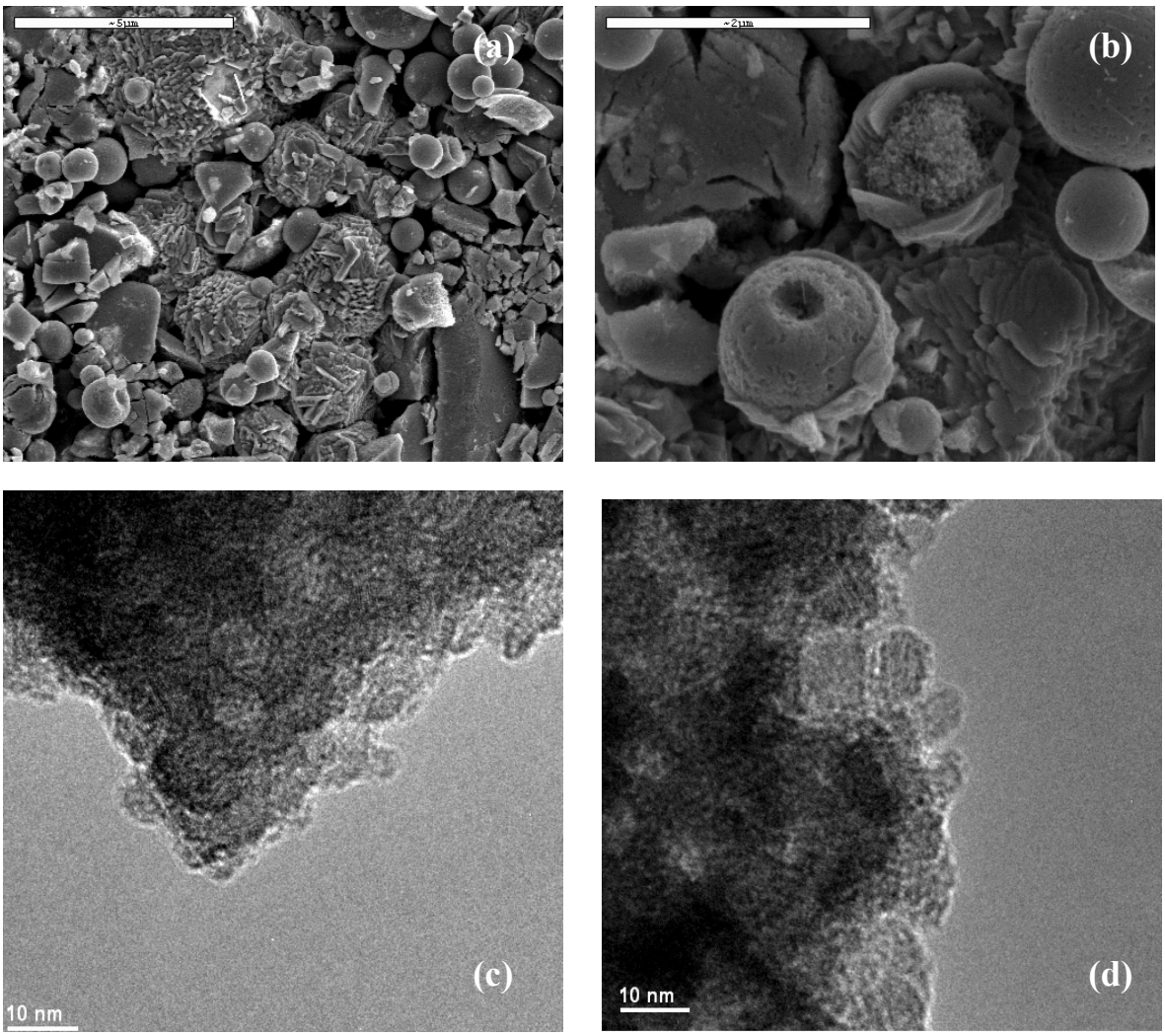

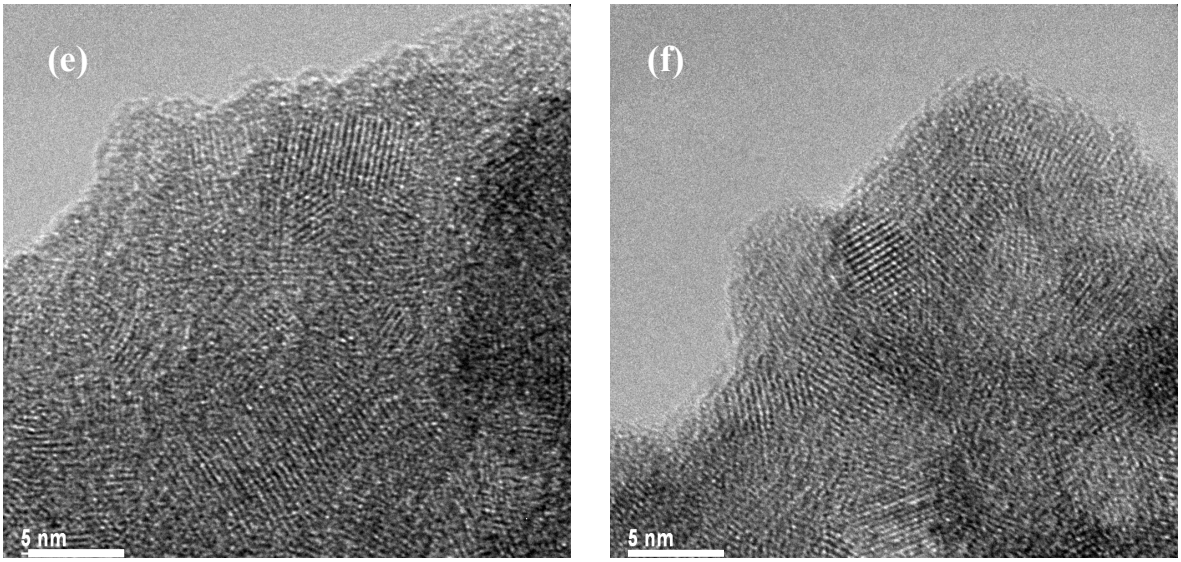

Figure 8. SEM (a, b) and HRTEM (c-f) images of powder pellet sample after reaction.

The spherical nanoparticles are composed of fairly well defined crystal planes. In fact, the *in situ* Raman spectroscopy results indicate that the local ordering of the sample is enhanced after reaction (*see below*). The small crystallite size is probably the reason for the poor XRD pattern after reaction and not, as suggested before, a decrease in crystallinity.

In situ Raman spectroscopy.

In *Figure 9* the *in situ* Raman spectra of the powder pellet catalyst at different temperatures are displayed. For each temperature interval from 5 to 10 spectra at different points on the sample were measured to check the homogeneity of the sample. The spectra for one temperature interval were almost identical and only differing in their absolute intensities which was explained by small deviations when focusing the laser (due to the confocal operation mode of the Raman Microscope). Therefore the displayed spectra in *Figure 9* are representative for the spectra of each interval. The presence of crystalline α-MoO_3 in the catalyst was excluded since α-MoO_3 has a large Raman cross section and typically shows a resonance effect when interacted with the 632 nm of a He/Ne laser, used in the experiments.[16, 17] From *Figure 9* it can

be seen that the spectrum of the catalyst changes reversibly indicating two types of structures in the temperature range from 623 to 713 K.

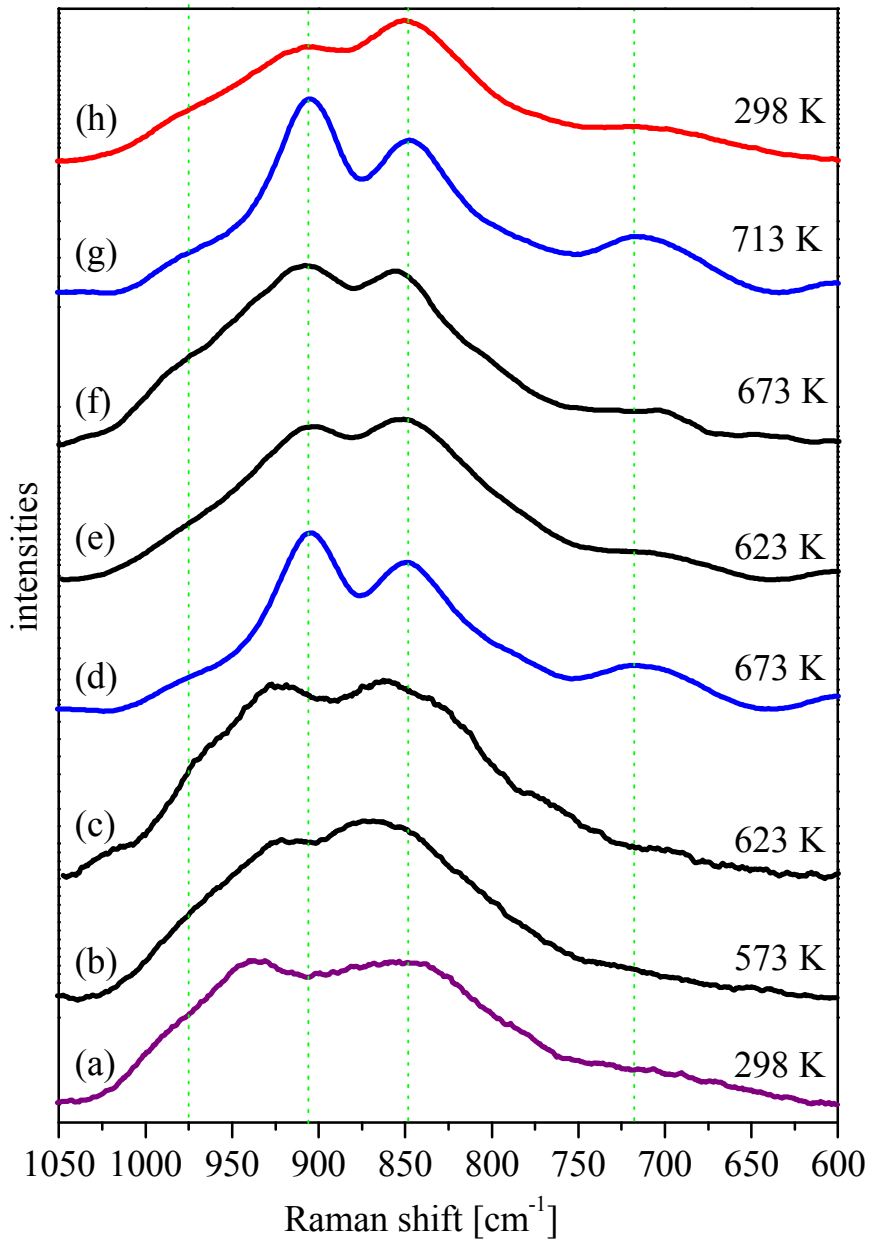

Figure 9. In situ Raman spectra during the selective oxidation of propene over a mixed $Mo_{0.68}V_{0.23}W_{0.09}O_x$ powder catalyst. The catalyst powder was pretreated for 2 h at 623 K in air. Spectra were smoothed by a five point average method.

The similarity of the two types of spectra (*9d, g vs. 9h*) point out, that both structures are closely related. However, the high intensity and the narrow bandwidths of the *in situ* Raman spectra at 673 and 713 K (*9d, g*) not only indicate the presence of a modified structure, but also evidence

the higher local order of this structure compared to the structure at lower temperatures. To prove if this reversible structure formation correlates to the activity of the powder catalyst we have to compare *Figure 9* with *Figure 5*.

It was already mentioned before that heating to 673 K under reaction conditions activates the catalyst, which is confirmed after subsequent cooling to 623 K (*Figure 5b*). However, the Raman spectrum of the sample at 623 K (*9e*) has changed during the cooling step and is closer to the Raman spectrum after reaction (*9h*) at 298 K. Even more interesting is, that after the second heating step to 673 K (*9f*) the spectrum does not return to the initially observed spectrum at the same temperature (*9d vs. 9f*). To achieve the "higher ordered" structure the temperature needs to be increased until 713 K (*9g*). The *second* increase in temperature from 623 (*9e*) to 673 K (*9f*) is accompanied by an increase in activity towards acrylic acid, but has not the expected effect of an activated catalyst and seems to be related mainly to the increase in temperature (*Figure 5b*). However, the next heating step to 713 K involves the structural transformation (*9g*) and is associated with a large increase in acrylic acid formation (*Figure 5b*). It is difficult to speculate about the information depth of the *in situ* Raman experiments, but we can exclude that the observed changes in the spectra are limited to surface restructuring, since the He/Ne laser certainly penetrates at least some tens of nanometers into the oxide bulk. The fact that the activated catalyst at 623 K exhibits a Raman spectrum that is in between the two types of structural ordering (*9e*) gives evidence that there are additional effects besides the two structures that determine the catalyst activity and selectivity. Most probably these are related to the top surface layers and the information should become available with the thin film model applying surface sensitive methods. Nevertheless, the presence of the local higher ordered structure seems to be beneficial for both activity and selectivity (*Figure 5b*).

Until now we have only talked about two *types* of structures observed in the *in situ* Raman experiments, but in order to correlate the Raman spectra to a certain structure we have to compare the spectra to some reference data. The literature reports on Raman spectra of Mo_5O_{14}-

type oxides are rather scarce. During their investigation of the $Mo_{0.64}V_{0.27}W_{0.09}$ mixed oxide, Dieterle and Mestl applied a variety of analytic methods to reveal the structure of the catalyst, including Raman spectroscopy.[13, 18] In *Figure 10b* the *ex situ* fingerprint Raman spectrum of the nanocrystalline Mo_5O_{14} type mixed oxide catalyst from Mestl together with the *in situ* spectra of the powder catalyst at 713 K (*Figure 10a*) and after reaction at 298 K (*Figure 10c*) are shown.[19]

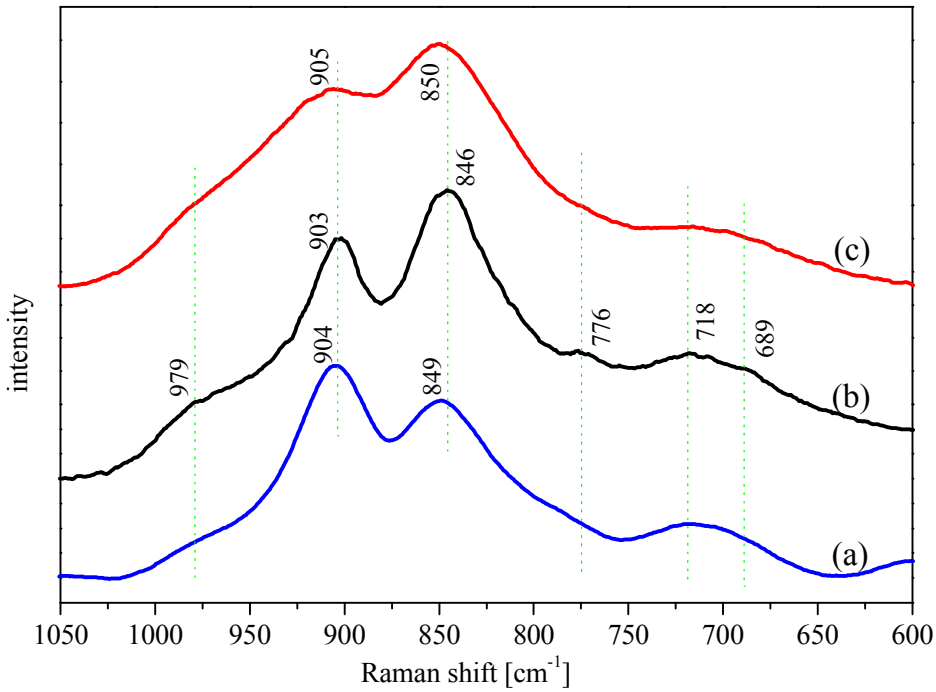

Figure 10. Comparison of Raman spectra. (a) *in situ* spectrum of powder catalyst at 713 K; (b) reference "fingerprint" Raman spectrum of the nanocrystalline Mo_5O_{14}-type mixed oxide catalyst from Mestl; (c) *in situ* spectrum of powder catalyst after reaction at 298 K .

The major band positions of all three spectra coincide, but the relative intensities of the two bands at 846 and 904 cm^{-1} are reversed in case of the high temperature spectrum (*Figure 10a*). The nanocrystalline reference Mo_5O_{14}-type oxide from Mestl and the spectrum after reaction at 298 K (*Figure 10c*) only differ in their relative bandwidths. Therefore, one might conclude that the nanoparticles after reaction are indeed of the Mo_5O_{14} type structure. However, since most of the nanoparticles are in the size range of 5 nm and the unit cell parameter of the tetragonal Mo_5O_{14} structure in a-direction is 2.3 nm, it may be more precise if we say that the

nanoparticles are composed of the main structural motifs of the Mo_5O_{14} structure! There are several explanations for the differences in between the two Raman spectra shown in *Figure 10a* and *10c*. The main structural motifs of the Mo_5O_{14} type structure must be retained because the band positions do not change and the bandwidth are even reduced. A possible transformation mechanism could be the reversible formation of an ordered superstructure. In many molybdenum sub-oxides ordered shear defects induce the formation of superstructures.[11] However, the formation of an apparent superstructure could also be induced by the growth of the nanoparticles via inter-particle condensation.

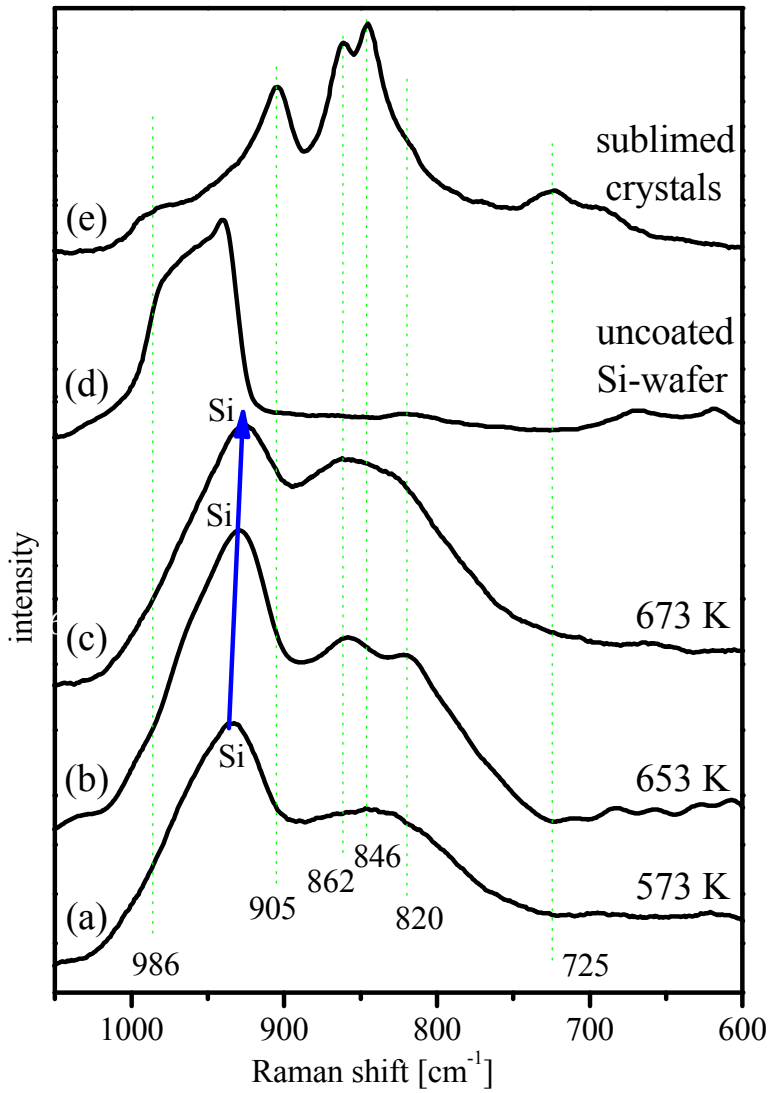

Figure 11. *In situ* Raman spectra of the thin films during catalytic reaction at different temperatures (a-c); *ex situ* Raman spectrum of an uncoated silicon wafer at 298 K (d); *ex situ* Raman spectrum of sublimed crystals during reaction on thin films serve as a reference (e).

A prerequisite for the condensation is a spatial reorientation or alignment of the particles and this alignment can form something like a superstructure. Until the actual the condensation has not taken place the alignment is weak and reversible. As the temperature is not high enough for an appropriate growth of the Mo_5O_{14} structure the final state of the powder is the one observed by TEM in *Figure 8*, which is characterized by randomly orientated nanoparticles.

It should be emphasized, that the *in situ* Raman spectra of the thin film give – in contrast to the powder pellet – only information about the ~20 nm thick coating. Therefore, differences in the spectral features of the thin film and the powder pellet should also be related to the differences in information depth. A drawback of using the He/Ne laser for the *in situ* Raman spectra of the thin films is the deep penetration depth (~2 µm) of the laser beam into the silicon wafer.[22] As the catalyst film is about 20 nm thick, its Raman signal is very low compared to the signal of the Si-wafer (*Figure 11*).

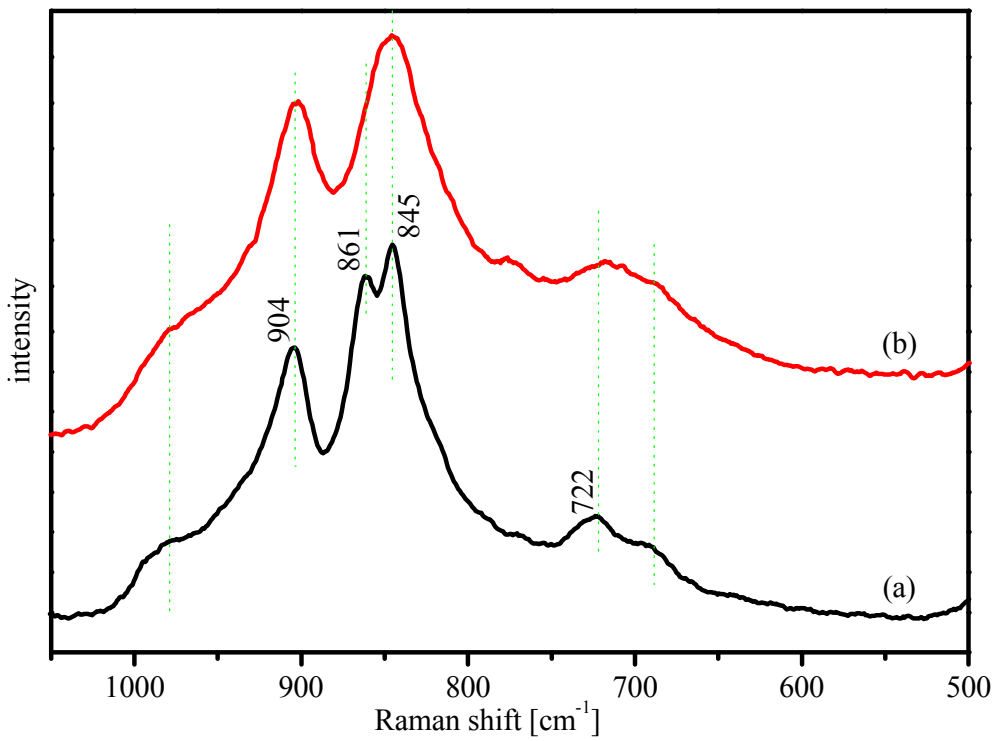

Figure 12. The Raman spectrum of the needle shaped crystals sublimed from the thin film (a) is compared with the fingerprint spectrum of the reference Mo_5O_{14}-type structure from Mestl (b).

A further difficulty emerged at higher temperatures. The broad band of the silicon wafer at 940 cm^{-1}, deriving from symmetry forbidden phonons, shifts to 926 cm^{-1} at 673 K (*Figure 11*).[20, 21] This shift has the negative effect to move exactly into the fingerprint region of the Mo_5O_{14}-type structure. It was thus very difficult to compare the thin film spectra with the powder spectra. However, the bands deriving unambiguously from the thin film could be analyzed and related to the powder pellet spectra (*see below*).

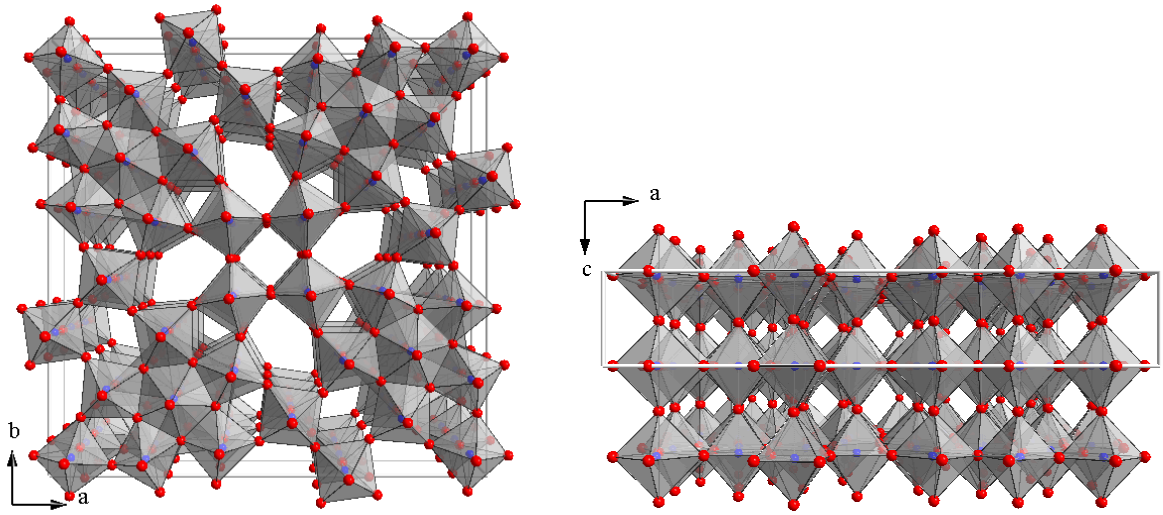

Figure 13. The tetragonal Mo_5O_{14}-type structure representation (*P*4/*mbm*) taken from [9] . Red spheres indicate oxygen atoms and blue spheres are metal atoms (Mo, W).

At this point it is useful to remind that the films started to sublime under reaction conditions at 673 K, which is – as already mentioned at page 85 – a considerably lower sublimation temperature as compared to the powder pellets. As the distance from the film surface to the reactor cover is only 125 µm, the sublimation products were trapped at the cover plate. After the reaction the sublimed micro-crystals were investigated *ex situ* under the Raman microscope. Along with some of the expected crystals of α-MoO_3, fine needle shaped crystals of about 0.5 to 1 µm length were found. The Raman spectrum of the needles is compared in *Figure 12* with the fingerprint reference spectrum of the Mo_5O_{14}-type structure from Mestl. The two spectra are

identical only differing in that the spectrum of the sublimed needles resolves the band at 845 cm^{-1}, possibly due to the higher crystallinity as compared to the reference sample of Mestl. Unfortunately it was not possible to get enough material of the sublimed crystals to make any further structural and elemental analysis.

The fact that the Mo_5O_{14}-type structure sublimes from the thin films establishes a basis for the structural comparison between the thin film and the powder catalysts. The spectrum of the sublimed crystals is introduced as a new "reference" Mo_5O_{14}-type spectrum for the *in situ* spectra of the thin films in *Figure 10*.

At 573 K the *in situ* spectrum of the thin film is dominated by the high intensity of the silicon band at 935 cm^{-1} and a broad unresolved band originating from the mixed oxide which is centered at 847 cm^{-1} (*Figure 11a*). The position matches exactly the most intense band of the reference Mo_5O_{14}-type spectrum but the band is too broad to make any useful assignment. At 653 K the broad band resolves to give two distinct bands at 821 and 859 cm^{-1}. The band at 821 cm^{-1} coincides with a shoulder of the reference while the slightly broad band at 859 cm^{-1} covers the two strongest bands of the reference at 860 and 846 cm^{-1}. The band at 821 cm^{-1} could be an indication for the formation of nanocrystalline α-MoO_3 which has its strongest band occurring at 820 cm^{-1}. This is supported by the fact that sublimed α-MoO_3 crystals were also found at the reactor cover. It is interesting that the reference band at 725 cm^{-1} is specially pronounced for the sublimed crystals and also for the *in situ* spectra of the "higher ordered" structure, but not present in any of the thin film spectra. Having in mind that the tetragonal Mo_5O_{14} structure crystallizes strongly anisotropic in the shape of fine needles this could be an explanation for the appearance of bands depending on the exposed crystal planes. The band at 725 cm^{-1} is probably related to interactions along the c-axis, which are also present in the "higher ordered" structure but apparently not in the thin films. At 673 K the thin film spectrum changes again and instead of the two resolved bands at 821 and 858 cm^{-1} observed at 653 K, the bands overlap to from one broad band with a maximum at around 860 cm^{-1}. At this temperature the film sublimes and the

broad band is probably related to an overlap of many bands due to a continuously changing structure.

Conclusions

We have presented a new synthetic method for the preparation of complex oxide thin films. As already mentioned in the text, the method seems not only promising for the preparation of mixed oxide films but could also be useful for the synthesis of organic-inorganic hybrid materials currently widely investigated. A new type of micro-reactor has been tested successfully in the partial oxidation of propene at elevated temperatures and has shown to be suited for the application of *in situ* Raman spectroscopy. The reactor could be used for other optical spectroscopies, as for example uv-vis spectroscopy, as well.

From an experimental point of view the use of a laser line with shorter wavelength (*e.g.* 514 nm) would be very useful to enhance the Raman signal of the thin film with respect to the underlying substrate. The silicon substrate has the advantage of low reactivity and the possible use in Raman experiments as a surface sensitive temperature indicator (*not discussed*), but in the special case of the Mo_5O_{14} type structure the coincidence of the silicon bands and the fingerprint bands of the thin film inhibited a more detailed analysis of the structural aspects of the thin film.[20] However, for other catalytic systems this might be different.

We believe that the concept of developing more realistic model systems for complex mixed oxide catalysts by the preparation of complex mixed oxide thin films is promising. The combination of *in situ* Raman spectroscopy and *ex situ* HRTEM gave a detailed view of the structural dynamics occurring during reaction. The possibility to directly compare thin film data and powder data has the great advantage to obtain information about bulk and surface structure under the same conditions. The observed structural changes during reaction clearly indicate, that the active surface of the investigated $Mo_{0.68}V_{0.23}W_{0.09}O_x$ catalysts is actually a very dynamic one and not to describe as a stiff crystal structure. For the catalyst to be active in the

selective oxidation of propene there is no need for a crystalline Mo_5O_{14} structure since the mere presence of the main structural motifs is sufficient. However, activity and selectivity seem to be enhanced when an ordered superstructure is present. This is further supported by the different product distribution over the two catalysts, which is associated to the absence or poor defined three dimensional structural ordering in the thin films. More information about the composition of the catalytically active surface species will hopefully be gained in the near future by using the presented model for *in situ* XPS investigations.

Acknowledgments

Dr. G. Mestl is thanked for providing us the reference Raman data of the nanocrystalline Mo_5O_{14}-type oxide.

References

[1] M. Hävecker, A. Knop-Gericke,T. Schedel-Niedrig, R. Schlögl, *Angew. Chem. Int. Ed.* **37** (1998) 1939.

[2] J.W. Niemantsverdriet, A.F.P. Engelen, A.M. de Jong, W. Wieldraaijer, G.J. Kramer, A*ppl. Surf. Sci.* **84** (1995) 339.

[3] S. Knobl, G.A. Zenkovets, G.N. Kryukova, O. Ovsitser, D. Niemeyer, R. Schlögl, G. Mestl, *J. Catal.* **250** (2003) 177.

[4] W. Lindinger, A. Hansel, A. Jordan, *Öster. Phys. Ges*. **2** (1998**)** 7.

[5] W. Lindinger, A. Hansel, A. Jordan, *Int. J. Mass Spectrom. Ion Proc.* **173** (1998**)** 191.

[6] S. Busch, U. Schwarz, R. Kniep, *Chem. Mater.* **13** (2001), 3260.

[7] O. Grassmann, G. Mueller, P. Loebmann, *Chem. Mater.* **14** (2002), 4530.

[8] T. Corradin, S. Bah, J. Livage, *Colloids Surf. B* **35** (2004) 53.

[9] A. Blume, *Thesis*, Technical University Berlin, 2004.

[10] M. M. Lin*, Appl. Catal. A* **250** (2003) 287.

[11] L. Kihlborg, *Acta Chem. Scand.* **13** (1959) 954.

[12] H. Werner, O. Timpe, D. Herein, Y. Uchida, N. Pfaender, U. Wild, R. Schlögl, H. Hibst, *Catal. Lett.* **44** (1997) 153.

[13] G. Mestl, Ch. Linsmeier, R. Gottschall, M. Dieterle, U. Wild, R. Schlögl, *J. Mol. Catal. A* **162** (2000) 463.

[14] M. Dieterle, G. Mestl, J. Jäger, Y. Uchida, H. Hibst, R. Schlögl, *J. Mol. Catal. A* **174** (2001) 169.

[15] *E. Rödel, private communication.*

[16] M. Dieterle, G. Weinberg, G. Mestl, *Phys. Chem. Chem. Phys.* **4** (2002) 812.

[17] M. Dieterle, G. Mestl, *Phys. Chem. Chem. Phys.* **4** (2002) 822.

[18] G.Mestl, Ch. Linsmeier, R. Gottschall, M. Dieterle, J. Find, D. Herein, J. Jäger, Y. Uchida, R. Schlögl, *J. Mol. Catal. A* **162** (2000) 455.

[19] G. Mestl, *J. Raman Spectrosc.* **33** (2002) 333.

[20] T. R. Hart, R. L. Aggarwal, B. Lax, *Phys. Rev. B* **1** (1970) 638.

[21] R. Tsu, J. G. Hernandez, *Appl. Phys. Lett.* **41** (1982) 1016.

[22] Raman and Luminescence Spectroscopy for Microelectronics. Catalogue of optical and physical parameters "Nostradamus" project SMT4-CT-95- 2024, EC, EIR 18595, Ed. De Wolf I., Jimenez J., Landesman J-P, Frogeri C., Braun P., Da Silva E., Calvet E., 1995.

Zusammenfassung

In der vorliegenden Arbeit wurden verschiedene Syntheseansätze zur Herstellung von auf Molybdänoxid basierenden Modellkatalysatoren untersucht. Die Katalysatoren wurden dabei zum einen als Pulver, zum anderen als dünne Filme auf Silizium Einkristallen präpariert. Die hergestellten dünnen Schichten sollten als realistische Modellsysteme dienen, um sowohl oberflächensensitive, als auch volumensensitive Festkörpercharakterisierungs-methoden für deren Untersuchung anwenden zu können. Wichtig war dabei, dass die hergestellten Filme die chemische und strukturelle Komplexität besitzen, die Voraussetzung für katalytische Aktivität ist. Andererseits, sollten die Filme dünn und homogen genug sein, um den Anforderungen der Oberflächenanalytik zu genügen.

Im ersten Kapitel wurde die Synthese von Polyoxomolybdaten durch Hydrolyse von Molybdänalkoxiden in Gegenwart eines Amins beschrieben. Auch hier stand der Modellcharakter im Vordergrund. Die gezielte Synthese von strukturell unterschiedlichen Polyoxomolybdaten sollte zeigen ob und wenn, welche Strukturmerkmale bereits in der Katalysatorvorstufe eine positive Auswirkung auf den späteren Katalysator haben. Die dabei verwendeten Alkoxide wurden über die sogenannte „Amidsynthese“ selbst hergestellt. Der Einfluß verschiedner Hydrolysegeschwindigkeiten, sowie der Einfluß des verwendeten Amins auf die strukturellen Eigenschaften der Polyoxomolybdate, wurde mittels Raman-, IR-Spektroskopie und Pulverdiffraktometrie untersucht. Außerdem wurde die thermische Zersetzung mittels Thermogravimetrie und dynamischer Kalorimetrie untersucht. Abschließend wurde die Reaktivität der Polyoxomolybdate hinsichtlich der selektiven Oxidation von Propen zu Acrolein und Acrylsäure mittels temperaturprogrammierter Reaktionsspektroskopie analysiert. Dabei stellte sich heraus, dass die Hydrolysegeschwindigkeit einen entscheidenden Einfluß auf die Struktur des Polyoxomolybdates hat. Das hergestellte γ-Oktamolybdat zeigte das größte Potential für die

Herstellung eines aktiven Katalysators. Da sich auch das Heptamolybdat im Laufe der thermischen Behandlung in ein Oktamolybdat umwandelt, und nicht die gleiche Reaktivität besitzt, scheint nicht nur das Vorhandensein eines Oktamolybdats entscheidend, sondern wahrscheinlich sogar welches der möglichen Strukturisomere des Oktamolybdats genau vorliegt.

Das zweite Kapitel beschäftigt sich mit den strukturellen Vorgängen in der Lösung von den in Kapitel 1 vorgestellten Alkoxiden. Da die Hydrolyse der Molybdänalkoxide an Luft bis zu drei Stunden dauert, stellt die Reaktion ein ideales Modellsystem dar um Hydrolyse und Kondensation mittels *in-situ* Raman und *in-situ* IR-Spektroskopie zu untersuchen. Das schwierige Thema der schwingungsspektroskopischen Analyse von Metallalkoxiden wurde anhand von zahlreichen Literaturangaben diskutiert. Es wurde erstmals überhaupt ein Bildungsmechanismus für die sogenannten *Primärprodukte* der Polyoxometallate postuliert, der mit dem allgemein akzeptierten *Additions-Mechanismus* von K.-H. Tytko und O. Glemser im Einklang steht.

Im dritten Kapitel wurde mit der aus Kapitel 1 und 2 untersuchten Alkoxidlösung ein Molybdänoxidfilm durch *Spin-Coating* hergestellt. Anhand von Raman und TEM Untersuchungen zeigte sich, dass der Film nach thermischer Behandlung nanostrukturiert vorliegt. Diskutiert wurde vor allem das außergewöhnliche Raman Spektrum, bei dem eine, sonst bei α-MoO_3 nicht beobachtete, Bande bei 1006 cm^{-1} auftrtitt. Die Bande wird einer extrem kurzen Molybdän-Sauerstoff Bindung zugeordnet, welche durch die starke Verzerrung der Polyedergeometrie entsteht. Abschließend wurde die Bande als ein mögliches allgemeines Identifizierungsmerkmal für Nanopartikel diskutiert.

Im vierten und letzten Kapitel wurde ein interessanter neuer Syntheseweg gefunden, um extrem dünne Schichten aus wässrigen Übergangsmetalllösungen herzustellen. Dabei wurde ein bereits untersuchter Mo-V-W-Mischoxidkatalysator als Pulver in einer Gelatinelösung gelöst, und anschließend mittels *Spin-Coating* auf einen 10x10x0,7 mm

großen Silizium Einkristall aufgebracht. Nach der thermischen Behandlung wird ein etwa 20 nm dünner homogener Film des Mischoxids auf dem Silizium erhalten. Der Film wurde dann in einem eigens entwickelten Quarzglasreaktor hinsichtlich der selektiven Oxidation von Propen zu Acrolein und Acrylsäure untersucht. Der gleiche Reaktor wurde benutzt, um den Filmkatalysator mit dem Pulverkatalysator zu vergleichen. Da der Reaktor eine *in-situ* Charakterisierung des Katalysators mittels Raman Mikroskopie erlaubt, wurden Katalysedaten und Strukturdaten von Film und Pulver bei gleichen Reaktionsbedingungen erhalten. Es konnte gezeigt werden, dass der hergestellte Film in der Lage ist aus Propen Acrolein und Acrylsäure zu machen, und somit den anfangs genannten Aktivitätsanforderungen entspricht. Weiterhin konnte gezeigt werden, dass der Katalysator bei 673 K eine strukturelle Umwandlung durchmacht welche mit einer verbesserten Aktivität korreliert. Diese Umwandlung war unter den gewählten Bedingungen reversibel und kann somit nur mittels *in situ* Methoden beobachtet werden. Bei der aktiven Volumenstruktur handelt es sich vermutlich um strukturell definierte Domänen, die sich von der Mo_5O_{14}-Struktur ableiten lassen. Allerdings müssen noch weitere Faktoren einen Einfluß auf die Aktivität und Selektivität haben, die wahrscheinlich direkt mit der dynamischen Oberflächenstruktur zusammenhängen. Mit dem vorgestellten Modell sollte es möglich sein mittels oberflächensensitiver Methoden diese Faktoren zu bestimmen.

Die Anforderungen, die zu Begin an ein realistisches Modellsystem für komplexe Mischoxidkatalysatoren gestellt wurden, konnten somit vor allem durch die in Kapitel 4 vorgestellte Gelatinesynthese-Methode zufriedenstellend erfüllt werden.